

Institute of Polar Studies

Report No. 27

Seismic Investigation of Ice Properties and Bedrock Topography at the Confluence of Two Glaciers, Kaskawulsh Glacier, Yukon Territory, Canada

by

Gilbert Dewart

Institute of Polar Studies

September 1968



**GOLDTHWAIT POLAR LIBRARY
BYRD POLAR RESEARCH CENTER
THE OHIO STATE UNIVERSITY
1090 CARMACK ROAD
COLUMBUS, OHIO 43210 USA**

**The Ohio State University
Columbus, Ohio 43210**

INSTITUTE OF POLAR STUDIES

Report No. 27

**SEISMIC INVESTIGATION OF ICE PROPERTIES AND BEDROCK
TOPOGRAPHY AT THE CONFLUENCE OF TWO GLACIERS,
KASKAWULSH GLACIER, YUKON TERRITORY, CANADA**

by

Gilbert Dewart

**Institute of Polar Studies
The Ohio State University**

September 1968

**The Ohio State University
Columbus, Ohio 43210**

ABSTRACT

The purpose of this study is twofold: (1) to investigate seismic velocity inhomogeneity and anisotropy in strongly deformed glacier ice; and (2) to determine the form and dimensions of that part of a sub-glacial valley where two large temperate glaciers merge. The field investigations were carried out during the summers of 1964 and 1965 at the confluence of the North and Central Arms of the Kaskawulsh Glacier in the St. Elias Mountains, Yukon Territory, Canada.

Continuous seismic noise interfered with the measurements. It is attributable chiefly to wind. Individual pulses of noise were also recorded. They are apparently associated with the process of ice deformation and changes in air temperature.

According to the results of wide-angle seismic reflection measurements, the mean vertical P-wave velocity in the glacier is 3.70 km./sec. At depths of 10-100 meters the mean P-wave velocity is 3.63 km./sec., S-wave velocity is 1.74 km./sec. and Poisson's ratio is 0.350. From 10 m. depth to the surface the velocities of P- and S-waves decrease markedly to approximately 3.0 km./sec. and 1.5 km./sec., respectively. The low velocities near the glacier surface are apparently due to melting, fracturing, and relatively high porosity of the ice.

Where foliation and preferred orientation of ice crystal optic-axes are strong the velocity of P-waves perpendicular to the S-planes of the foliation is smaller than the velocity of P-waves parallel to the S-planes. It is concluded that velocity anisotropy is mainly caused by the foliation structure of alternating layers of clear and bubbly ice. When foliation is strong velocity anisotropy from this cause predominates over velocity anisotropy due to crystallographic fabric. Crystallographic fabrics are seldom strong enough to cause significant velocity anisotropy.

Velocity anisotropy also occurs where the surface ice has a strong fracture pattern. P-wave velocity perpendicular to the trend of the fractures is smaller than parallel to it.

In no case does P- or S-wave velocity vary with direction of propagation by more than a few percent.

Seismic measurements of ice thickness and of strike and dip of the bed of the glacier were made along transverse

profiles above and below the confluence. Locations had to be corrected for glacier movement, which varies with position and time, and was appreciable during the period of seismic shooting.

The greatest depth of ice in the Central Arm, which is 3000 m. wide, and in the combined glacier, which is 5000 m. wide, is about 1000 m. The North Arm is somewhat less deep. The base of the ice is lower than the glacier terminus, 40 km. down-glacier, but no bedrock depression was found at the confluence. Both glacier arms are roughly parabolic in cross-section. There is no break in the slope of the valley wall where the glacier surface meets it. The valleys of the two arms merge at approximately the same distance down-glacier from the point of confluence that the surface movements of the two glaciers merge into a uniform flow of ice.

The acoustic impedances of the rocks found in the vicinity of the confluence were determined and the reflection coefficients at interfaces between ice and these rocks were calculated. The field data agree well with calculated values except for some totally non-reflecting regions which may contain pockets of debris between ice and rock. Impedances of the rocks were too close to one another for sub-glacial contacts to be delineated.

It is concluded that only under especially favorable circumstances can seismic measurements be used practically in the study of crystallographic fabrics in glacier ice. However, strong foliation involving clear and bubbly ice layers is potentially subject to such investigation.

ACKNOWLEDGMENTS

The problems studied here were suggested by Dr. Colin Bull, Director of the Institute of Polar Studies of The Ohio State University, and Dr. Albert P. Crary, Deputy Director, Division of Environmental Sciences, National Science Foundation.

The field investigations were carried out as part of the Icefield Ranges Research Project, which is a joint operation of the American Geographical Society and the Arctic Institute of North America. The cooperation of Dr. Walter A. Wood, Director, Richard Ragle, Field Leader, and Phillip Upton, Chief Pilot, and other members of the Project is gratefully acknowledged.

Special thanks are due to field assistants Peter Simoni, Phillip Muehrcke and Fred Erdmann, and to Dr. Colin Bull and Dr. Peter Anderton, who also helped with the field work.

Financial assistance was provided by the Institute of Polar Studies and the Department of Geology of The Ohio State University, the Arctic Institute of North America, and the Explorer's Club of New York.

Generous loans of exploration seismic equipment were made by the Office of Antarctic Programs of the National Science Foundation. The station seismographs were lent

by the Seismological Laboratory of the California Institute of Technology, where special thanks are due to Mr. Francis Lehner.

The Department of Welding Engineering of The Ohio State University very kindly permitted the use of its ultrasonic testing facilities and Matthew J. Golis and other members of the Department staff gave valuable assistance. The base map of the study area was prepared by John Weng of the Department of Geodetic Science, which provided the plotting equipment.

Many helpful suggestions were made by Dr. Colin Bull and Dr. Howard J. Pincus of the Department of Geology. Much essential information was provided by Dr. Peter Anderton, who carried out a related glaciological investigation of the Kaskawulsh Glacier at the time of the present study.

Dorothy Amrine typed the final copy of this dissertation and Richard L. Jolley drafted the line drawings.

CONTENTS

	Page
Acknowledgments	v
List of Symbols	xiil
General Introduction	1
Chapter I, Preliminary Material	3
1.1 Physiography	3
1.2 Tectonics	5
1.3 The Kaskawulsh Glacier	7
1.4 Local Geology	10
1.5 Glacial History	12
1.6 Climate	13
1.7 Physical Concepts and Definitions	14
Stress, strain and elastic constants	16
Elastic constants of crystals	18
Elastic wave velocity	20
1.8 Historical Background	28
Chapter II, Equipment and Operations	33
2.1 Station Seismograph	33
2.2 Exploration Seismograph	34
2.3 Drilling	37
2.4 Explosives	38
2.5 Communications	41
2.6 Logistics	41
2.7 Field Operations	42
2.8 Safety	44
Chapter III, Seismic Noise Sources and Related Topics	46
3.1 Introduction	46
3.2 Continuous Noise	47
3.3 Impulsive Noise	59
Measurement	59
Thermodynamic relations	67
Elastic constants	72
Mechanical sources	75
3.4 Earthquakes	82
3.5 Avalanches	83
3.6 Summary	83

CONTENTS (CONTINUED)

	Page
Chapter IV, Wide-Angle Reflection Survey	86
4.1 Introduction	86
4.2 Direct P-Waves	90
4.3 Direct S-Waves	93
4.4 Surface Waves	94
4.5 Elastic Constants	96
4.6 Reflected Waves	97
4.7 Amplitude of Reflected Waves	105
4.8 Conclusions	108
Chapter V, Anisotropy of Seismic Wave Propagation . .	110
5.1 Introduction	110
5.2 Crystal Orientation	111
5.3 Field Experiment	118
5.4 Foliation	124
5.5 Fractures	138
5.6 Conclusions	141
Chapter VI, Reflection Survey	143
6.1 Introduction	143
6.2 Procedure for Determining Depth and Strike and Dip of Glacier Bed	144
6.3 Corrections to Seismic Reflection Data . . .	146
6.4 Interpretation of Seismic Reflection Data .	156
6.5 Laboratory Studies	161
6.6 Conclusions	169
Chapter VII, Discussion	172
7.1 General Remarks	172
7.2 Factors Affecting the Elastic Constants . .	174
Temperature	174
Stress	177
Other effects	179
7.3 Seismology and Structural Analysis	180
7.4 Symmetry Considerations	183
7.5 Additional Non-crystallographic Fabrics . .	185
7.6 Conclusions	190
7.7 Suggestions for Further Work	191
Appendix I, Mapping	195
References	196

LIST OF TABLES

Table		Page
1	Meteorological data for the Kaskawulsh confluence area, 1964 and 1965	15
2	Seismic wave velocities and isotropic elastic constants in the ablation zones of temperate glaciers of Europe and Asia	31
3	Mean cross-spread velocities of direct compressional waves in glacier ice	92
4	Transverse isotropic elastic constants for different types of foliated ice	133
5	Computed velocities for propagation directions parallel and perpendicular to the foliation planes	134
6	Velocity of compressional waves at locations on the surface of the Kaskawulsh Glacier compared with the orientation and intensity of local fractures	140
7	Vertical ice thickness and strike and dip of the ice-rock interface at points on the Kaskawulsh Glacier	153
8	Acoustic impedances and reflected signal amplitude ratios for ice and rocks found in the Kaskawulsh Glacier confluence area	166

LIST OF FIGURES

Figure		Page
1	Map of southwest Yukon Territory and vicinity, showing location of Kaskawulsh Glacier	4
2	Map of portion of the St. Elias Mountains . .	9
3	Study area at confluence of the North and Central Arms, Kaskawulsh Glacier, Yukon Territory	11
4	Character of the deformations corresponding to elastic moduli C_{ij} in the hexagonal crystal .	21
5	Polarization of particle motion for shear waves	25
6	Section (meridional plane) of velocity surface of V_1 for a hexagonal crystal such as ice . .	26
7	Block diagram of exploration seismograph system	35
8	Principle of the Munroe effect (shaped charge)	40
9	Background noise, wind speed, and temperature at 3-hourly intervals, July 23, 1965	49
10	Number of impulsive noise events and time rate of change of temperature at Kaskawulsh Camp at 3-hourly intervals	52
11	Section of moulin	54
12	Ice rupture between air bubble and atmosphere.	57
13	Amplitude distribution of impulsive events . .	60
14	The proportion of total impulsive energy as a function of amplitude level	61
15	Power law relationship between number and amplitude of impulsive events	52
16	Percentage distribution of impulsive events according to pulse length at intervals of 0.2 second	63

LIST OF FIGURES (continued)

Figure		Page
17	Temperatures at 3-hour intervals averaged for August 5, 6, 12, 1965 at Kaskawulsh Camp, "Ice," and "Knoll" weather stations	65
18	Thermo-elastic strains between two crystals in contact	68
19	Strain-time curves for long-term and short-term creep	77
20	Time-distance plots of wide-angle reflection profile	89
21	Geometry of Pflueger's method of obtaining apparent dip of a reflecting interface	100
22	Geometry of Favre's method of obtaining apparent dip of a reflecting interface	101
23	Minimum reflection time when shooting up-dip	103
24	Map of glacier confluence showing foliation trends and fabric types	112
25	Equal-area contour diagram of 4-maxima optic-axis fabric	114
26	Spread geometry at point IB, showing crystallographic fabric, foliation, flow and strain rate	119
27	Velocity-depth curves at point IB for waves traveling parallel and perpendicular to the crystallographic axis of symmetry	122
28	Photographs of sections of bubbly ice	129
29	Map of glacier confluence, showing surface fractures	139
30	Geometrical relationship between dipping reflecting interface and spreads on the glacier surface	145
31	Azimuth correction for relative movement of survey markers	148

LIST OF FIGURES (continued)

Figure		Page
32	Position correction for slope of glacier surface	150
33	Contour map of sub-glacial topography	154
34	Transverse sections at glacier confluence	155
35	Seismogram at point 38	157
36	Interpretation of seismogram at point 38	158
37	Seismogram at point 106	159
38	Geometry of the ultrasonic experiment for determining the velocity of elastic waves in rock specimens	163
39	Examples of superposed fabrics	189
40	Photograph of seismic shooting on the Kaskawulsh Glacier	194

LIST OF SYMBOLS

A = amplitude

A_1, A_3, A_f = anisotropy factors

a = attenuation constant

a_1, a_2, a_3, c = crystallographic axes

$\alpha_1, \alpha_2, \alpha_3$ = temperature coefficients of expansion

$\alpha_x, \alpha_y, \alpha_z$ = direction cosines of strain components

α, β, γ = direction cosines of normal to the reflecting
interface

B = amplitude in Andrade Law

b = wave direction vector

β = exponent in Glen's flow law for ice

$\beta_x, \beta_y, \beta_z$ = direction cosines of wave vector

C = reflection coefficient

C' = center of symmetry

C_{1j} = elastic modulus (stiffness)

C_p = specific heat at constant stress

D = creep parameter in steady-state flow law

D_{nh} = Schoenflies symmetry symbol: axis of n -fold symmetry
with plane of symmetry perpendicular to it

d = thickness or diameter

δ = azimuth correction angle

δ_{ij} = Kronecker delta

e = instrumental amplification

E = strain

LIST OF SYMBOLS (continued)

E_i = strain matrix component

E_{ij} = strain tensor component

\dot{E} = strain rate

η_s = slope correction angle

θ = dip

θ_A = apparent dip

θ_s = azimuth correction angle

F = force

f = wave frequency

f_t = critical frequency for non-laminar flow

G = Gibbs Function

g = acceleration of gravity

g_s = creep parameter in steady-state flow

h = depth

K = compressibility

k_b^∞ = isotropic symmetry

k = wave equation constant

k_i = function of wave direction vector and elastic moduli
in velocity equation

k_b = Boltzmann constant

L = long period surface wave

ℓ = length

λ = Lamé's constant

M = Poisson's ratio

m = mass

LIST OF SYMBOLS (continued)

μ = rigidity (shear modulus)

N = number

\bar{n} = normal vector

n = exponent in Griggs' power law

ν = viscosity

ξ, η, ζ = displacements along the X, Y, Z axes

ξ_s = slope correction angle

P-wave - compressional (longitudinal) elastic wave

PP = P-wave reflected as a P-wave

PS = P-wave reflected as an S-wave

P = projected distance

p = pressure

p, q, r = direction cosines of wave displacement vector
= heat energy

R = amplitude ratio

ρ = density

S = entropy

S-plane = plane parallel to a planar metamorphic structure

S-wave = shear (transverse) elastic wave

S_H = horizontally polarized S-wave

SP = S-wave reflected as a P-wave

SS = S-wave reflected as an S-wave

S_{ij} = elastic coefficient (compliance)

σ = stress

σ_i = stress matrix component

LIST OF SYMBOLS (continued)

σ_{ij} = stress tensor component

T = temperature

T_0 = natural period of seismometer pendulum

T_g = natural period of galvanometer

t = time (used with various subscripts)

U = internal energy

u, v, w = components of wave displacement

ϕ = angle between basal plane of crystal and wave normal

ϕ_d = dip direction azimuth

v = velocity (general)

V_I = seismic wave velocity in medium I

V_{II} = seismic wave velocity in medium II

V_a = seismic wave velocity in upper layer

V_b = seismic wave velocity in lower layer

V_r = Rayleigh wave velocity

V_s = S-wave velocity

V_p = P-wave velocity

V_1, V_2, V_3 = velocities of anisotropic wave modes

V' = computed velocity based on foliation parameters

$V(A)$ = mean glacier velocity at the ice surface

$V(B)$ = mean summer glacier velocity at the ice surface

W = potential energy

W_0 = explosion energy per unit area

W_x = energy per unit area at distance X from origin

LIST OF SYMBOLS (continued)

w = creep activation energy

X = distance

x, y, z = Cartesian coordinates

Z = acoustic impedance

ψ = angle between fracture trend and normal to reflection
profile

GENERAL INTRODUCTION

This investigation was undertaken in order to determine some of the physical properties of glacier ice and the nature of the sub-glacial topography at the confluence of two large temperate valley glaciers. The factors influencing the velocity of seismic waves are of particular interest. The problem of the sources of seismic noise in a glacier is also treated. The confluence of the North and Central Arms of the Kaskawulsh Glacier in the St. Elias Mountains, Yukon Territory, Canada, was chosen as a suitable site for the field studies.

The major parts of the research program, in order of treatment, are as follows:

- (1) Studies of seismic noise sources in the glacier and its surroundings with a continuously recording seismograph station.
- (2) Seismic refraction and wide-angle reflection measurements.
- (3) Investigation of the relationship of seismic wave velocity to ice crystal orientation, foliation, and fracture, and the velocity distribution near the upper surface of the glacier.
- (4) Seismic reflection survey, including the problems presented by glacier movement.

These problems are interrelated. Seismic noise affects the collection of data for all the other investigations. The wide-angle reflection observations provide mean velocity values necessary for the interpretations of vertical reflection survey data. The validity of assumptions of homogeneity and isotropy that are made in the reflection survey is examined under topic (3). The primary interest in topic (3), however, is the use of seismological methods in petrological and structural studies.

CHAPTER I

PRELIMINARY MATERIAL

1.1 Physiography

The Kaskawulsh Glacier lies on the northeastern slope of the Icefield Ranges (Map, Fig. 1). These mountains form the core of the St. Elias Mountains, which straddle the boundary between Canada and the northern part of the Alaska panhandle. They constitute the largest range of high peaks and contain the greatest number of glaciers and icefields in North America. Physiographically, the St. Elias Mountains belong to the outer mountain area of the western system of the Canadian Cordillera (Bostock, 1948). They are about 300 km. long by 150 km. wide and bordered by the Yukon Plateau on the northeast, the Pacific Ocean on the southwest, the Coast Mountains of British Columbia on the southeast and the Chugach, Wrangell and Nutzotin mountains of Alaska on the northwest.

Between the Yukon Plateau and the high mountains of the Icefield Ranges a series of elongate physiographic subdivisions parallels the northwest trend of the mountains and is traversed by the Kaskawulsh Glacier and its drainage in the following order:

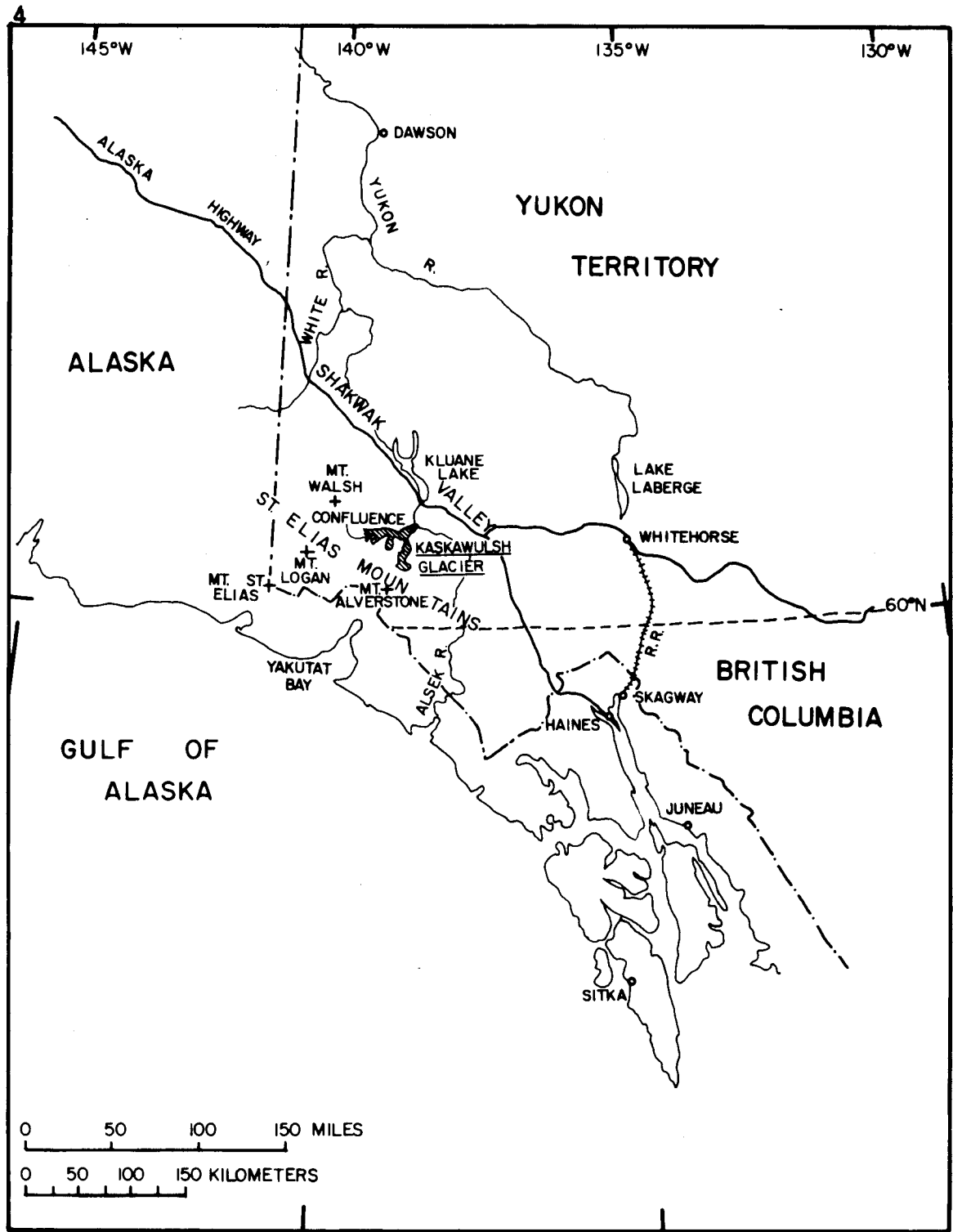


Figure 1. Map of southwest Yukon Territory and vicinity, showing location of Kaskawulsh Glacier.

(1) border ranges, a deeply dissected complex of ridges 20-30 km. wide, with peaks reaching 2500-3000 m. They are composed of mid-Paleozoic to Mesozoic sedimentary and metamorphic rocks and granitic intrusives. These rocks underlie the Kaskawulsh Glacier and debris from them forms the moraines that in part cover, and in part underlie, the ice.

(2) Duke Depression, a plateau-like strip of subdued relief in which the Kaskawulsh Glacier terminates.

(3) Kluane Ranges, the front ranges of the St. Elias Mountains, several kilometers wide, with rugged topography and peaks reaching 2000-2500 m.

(4) Shakwak Valley, one of the great Cordilleran trenches, more than 300 km. long by 15 km. wide, trending north 50° - 60° west. It forms a border between the St. Elias Mountains and the Yukon Plateau and contains Kluane Lake, which receives part of the Kaskawulsh Glacier drainage.

1.2 Tectonics

The trend of the ranges and of such major structural features as the Shakwak Valley and the valleys of the Hubbard and Logan glaciers is northwest-southeast. Several major transcurrent faults and fault zones with the same general strike have been traced or hypothesized in the region. A fault postulated to run along the Shakwak Valley-Kluane Range front may link up with the Denali fault of the Alaska Range (St. Amand, 1957). Sporadic seismic activity

near Kluane Lake may be associated with this fault. South of the valley and paralleling it is a fault zone that may extend from Glacier Bay to the head of Cascade Glacier, a major tributary of the Kaskawulsh. Northwest-striking thrust faults have been mapped by Wheeler (1963) in the latter region.

A northwest-striking fault near Lituya Bay may be continuous with one that appears several hundred kilometers to the northwest in the Chitina River valley and possibly in the great trough of the Hubbard and Logan glaciers. The Chugach-St. Elias fault parallels the coast. Several large earthquakes that occurred northwest of Yakutat Bay during 1954-64 have been attributed to movement on this fault (Tobin and Sykes, 1966).

The sector of the Circum-Pacific belt between central Alaska and Central America is of relatively low seismicity compared to most of the rest of the belt. The pattern in this region has been continuous minor activity with large shocks at comparatively long time intervals. All the earthquakes in the St. Elias region are shallow, producing high intensity motion over a relatively small area (Gutenberg and Richter, 1949).

There has been speculation about possible relations between the glaciers and the seismicity of the region (Miller, 1958). Large changes in accumulation, such as appear to have occurred during the 19th Century, may have resulted in

widespread secondary results when an earthquake occurs. The seismic noise effects of earthquakes and avalanches will be considered in Chapter III.

1.3 The Kaskawulsh Glacier

The glaciers of the St. Elias Mountains cover more than 25,000 sq. km. and form part of a continuous icefield extending 350 km. from the Alsek River to the Chugach Mountains. The transection glaciers in the center of the range slope outward and separate into broad valley glaciers. The glacier system extends through a great range of elevation from the flanks of the mountains to the névé fields at 2000-3000 m. to the coastal piedmont glaciers which reach sea level. Meltwater from the outlet glaciers flows directly into the Pacific Ocean in the south, indirectly to the Pacific in the east and west via the Alsek and Copper River systems, respectively, and into the Yukon River system in the north.

Most of the ice flows toward the Pacific Ocean. The divide between this ice and that moving toward the Yukon Plateau lies roughly along a line between Mt. Alverstone and Mt. Steele, i.e., northeast of the axis of the mountain range.

The divide between ice moving toward the Yukon River and the Alsek River drainage lies between Mt. Alverstone and the Kaskawulsh Glacier. Meltwater from the Kaskawulsh

Glacier contributes to both the Yukon and Alsek River systems, via the Slims and Kaskawulsh Rivers, respectively. The Kaskawulsh River flows through the Duke Depression.

The Kaskawulsh is one of a group of large valley glaciers which flow northeastward through the border ranges toward the Yukon Plateau. The icefield that supplies most of the ice in the Kaskawulsh Glacier covers about 500 sq. km. between the border ranges and the first row of major peaks of the Icefield Ranges. This icefield has an elevation of about 2500 m. and is punctured by many nunataks. In addition to feeding the Kaskawulsh Glacier, it also drains northward into Kluane Glacier and westward and southward into the Hubbard Glacier (Pacific Ocean drainage). A seismic traverse has been made across this icefield (Clarke, 1964).

The Kaskawulsh Glacier is formed by two converging outlet glaciers, the Central and North Arms (Fig. 2). The icefield funnels into the Central Arm at 2000 m. elevation (just above the firn limit), about 10 km. west-southwest of the confluence. The Central Arm maintains a fairly constant gradient and a width of about 3.5 km. from its head to the confluence. There is no real icefall, though the glacier is severely crevaased in its upper reaches. It receives many small, steep feeder glaciers from both sides. A large glacier joins it from the southeast about 3 km. above the confluence with the North Arm.

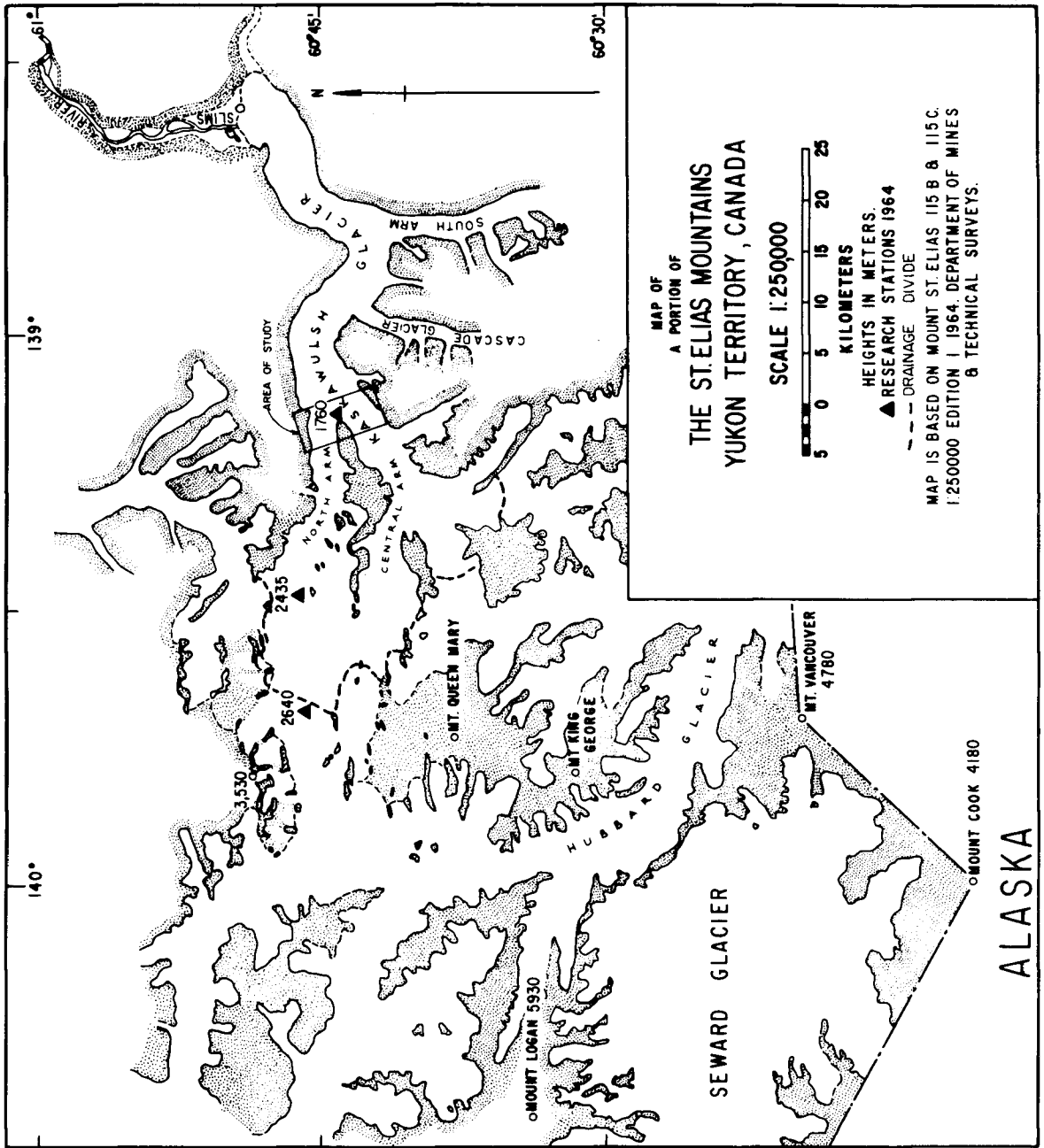


Figure 2. A portion of the St. Elias Mountains, Yukon Territory, Canada, showing the area of the present study.

The North Arm emerges from the icefield at about 2300 m. elevation, approximately 16 km. west-northwest of the confluence. This arm of the glacier descends in a series of icefalls and narrows to a width of about 2 km., then widens abruptly as it slopes down steeply to the confluence. The North Arm receives many small glaciers from the north slope of the ridge that separates it from the Central Arm.

At the confluence (elevation 1770 m.) the combined glacier is 5-6 km. wide (Fig. 3). It narrows to a width of 4-5 km. and maintains this width throughout most of its lower course. The glacier terminates 40 km. below the confluence after receiving several more tributaries, the largest of which are the Cascade Glacier and the South Arm. The moraine-covered terminus spreads out to a width of more than 6 km. at an elevation of about 850 m.

The term "point of confluence," as used below, refers to that point at the upper surface of the glacier where the margins of the two arms and the dividing ridge come together (Fig. 3).

1.4 Local Geology

The St. Elias Mountains form part of the Nevadan orogenic belt. Large-scale intrusion and intense folding occurred in the Jurassic and Cretaceous Periods. Complex igneous and metamorphic structures are characteristic of the bedrock exposures in the valley of the Kaskawulsh Glacier.

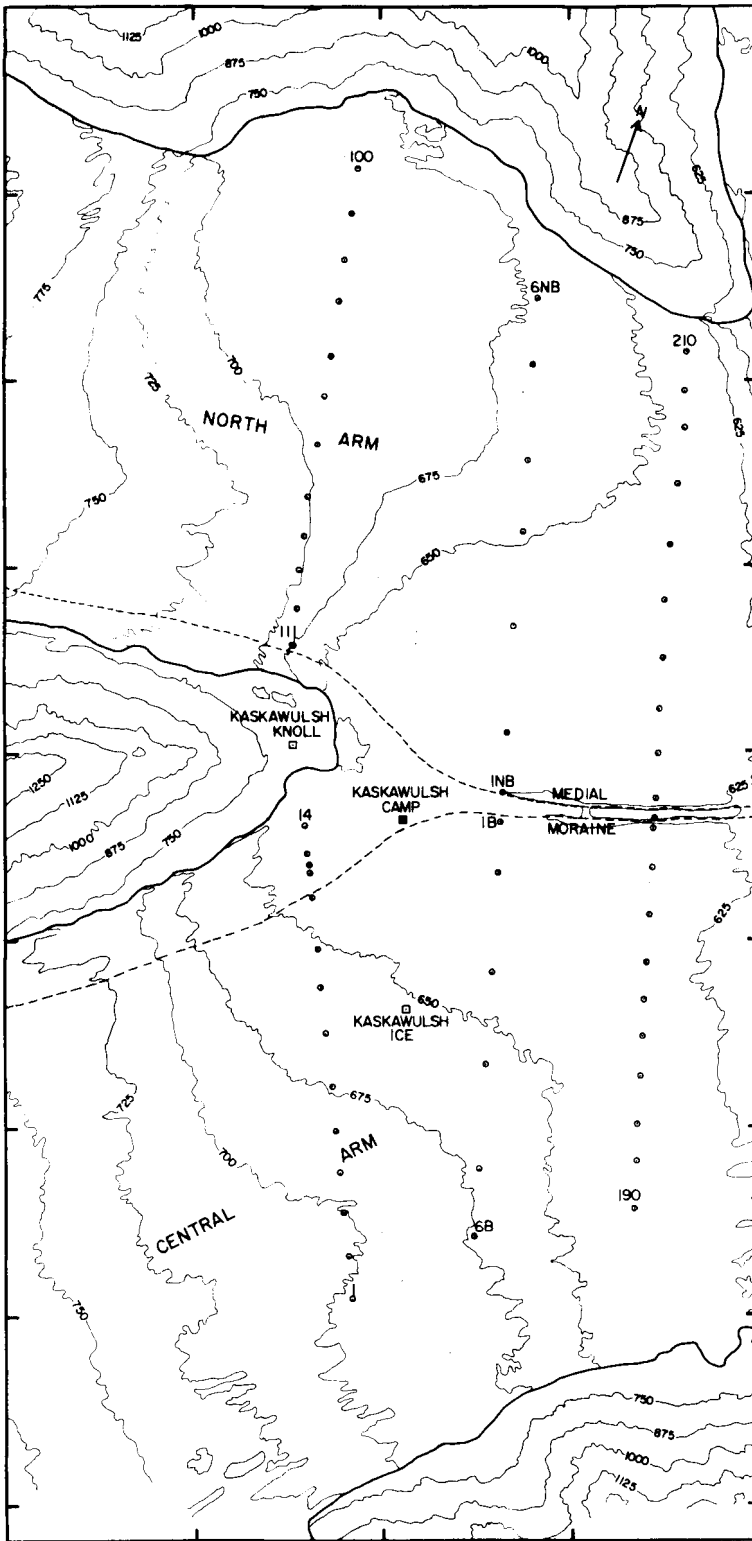
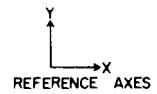
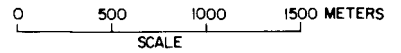


FIGURE 3
STUDY AREA AT
CONFLUENCE OF NORTH
AND CENTRAL ARMS.
KASKAWULSH GLACIER,
YUKON TERRITORY

- SURVEY MARKER
- CAMPSITE AND MET STATION
- OTHER MET STATIONS



CONTOUR INTERVAL:
 25 METERS ON ICE
 125 METERS ELSEWHERE
 REFERRED TO ARBITRARY DATUM



Greywacke, slate, greenstone and quartzite are exposed in the mountains north of the North Arm and on the dividing ridge just above the confluence. There is a sharp north-striking contact between these rocks and a massive Devonian limestone about 4 km. west of the point of confluence. The lateral moraines which receive debris from the dividing ridge and the medial moraine which forms from their merger at the confluence consist largely of limestone fragments. Slate, greywacke and limestone crop out on the south side of the Central Arm above the confluence. Farther downstream the valley walls consist largely of granodioritic rocks (Wheeler, 1963; Muller, 1967). During the present study it was observed that the lateral moraines on the south side of the Central Arm contain large amounts of quartz and basic igneous rocks.

1.5 Glacial History

During the Pleistocene epoch the icefields of the St. Elias Mountains were thicker than at present and the outlet glaciers were much more extensive. They filled the Shawkak Valley and covered part of the western Yukon Plateau. The late Pleistocene upper limit of ice appears to be at about 1800 m. in the Kluane Ranges. During this time the Kaskawulsh Glacier forked at its present terminus and one branch flowed down the Slims Valley while the other flowed through the Duke Depression and dammed the Alsek River (Denton, 1965; Krinsley, 1965; Denton and Stuiver, 1966).

According to Goldthwait (1966) and Borns and Goldthwait (1966), the Kaskawulsh Glacier has fluctuated greatly during the last 10,000 years. Prior to Hypsithermal Time (7100-2200 B.C.), it was retreating rapidly after the last major advance. Hypsithermal climate was drier and about 1° C. warmer than today and the glacier retreated until its terminus was about 20 km. up the valley from the present terminus. During this period outwash may have been deposited on the valley floor, and it may now underlie much of the lower Kaskawulsh Glacier.

A cooler period began around 1400 B.C., and Neoglaciation reached its peak between 1500 and 1850 A.D., when the mean annual temperature was probably about 2° C. lower than at present. In the last 100 years the Kaskawulsh, like most of the neighboring glaciers, has retreated. The terminus now is about 1.6 km. from its position 100 years ago (Borns and Goldthwait, 1966).

1.6 Climate

Climatological data for the St. Elias Mountains are scanty. Precipitation is very heavy near the coast, but on the leeward side of the mountains it diminishes greatly. There is very little precipitation at the North Arm-Central Arm confluence of the Kaskawulsh Glacier during the summer, but there is frequent overcast and fog is common. A pit dug in the middle of the Central Arm near the confluence

before the melt season began revealed 3 m. of snow accumulated during the winter of 1964-1965 (Marcus, 1965a).

The confluence is just below the firn limit, and mean air temperature at the surface of the glacier is probably not far from 0° C. The penetration of the winter cold wave has an effect on seismic wave velocities which will be treated in the final discussion (Chapter VII). Near-surface temperature in the ice appears to have reached 0° C. by the time seismic shooting started in June.

One of the most striking features of the weather is the wind that usually blows strongly down the valley all day, but diminishes at night. The seismic noise effects of this wind are considered in Chapter III.

Meteorological data for parts of the summers of 1964 and 1965 at instrument shelters in the confluence area are given in Table 1 (Marcus, 1965b; Marcus, Rens and Taylor, 1966).

1.7 Physical Concepts and Definitions

The basic concepts presented in this section were developed largely by Christoffel (1877) and Voigt (1928). Other references for this brief review will be given at the head of each sub-section.

Table 1. Meteorological data for the Kaskawulsh confluence area, 1964 and 1965. These data are based upon 3-hourly observations.*

(a) Mean daily values at Kaskawulsh Camp, on the medial moraine, elevation 1770 m. (see map, Fig. 3).

Time Interval	Air Temperature		Air Pressure	Relative Humidity	Wind Velocity Km./hr.	Cloudiness
	Mean	Mean Max. Mean Min.				
<u>1964</u>						
8-31 July	4.6	8.3 0.9				
1-21 Aug.	4.2	7.6 0.8				
Summer mean	4.4	8.1 0.9				
<u>1965</u>						
28-31 May	2.6	5.7 -2.8	820.4	76.6	18.0	11.2 4.1
1-30 June	0.4	2.9 -3.7	825.2	76.2	16.4	10.2 5.9
1-25 July	3.7	6.4 0.1	855.7	81.6	15.0	9.3 6.6

NOTE: Wind came almost entirely from the 210°-300° quadrant. Total precipitation for the summer of 1964 was 3.0 cm., water equivalent. Precipitation for the summer of 1965 was 0.76 cm. rain, 1.1 cm. snow, water equivalent.

(b) Mean daily values at Kaskawulsh Ice (elevation 1770 m.) and Kaskawulsh Knoll (1830 m.) weather shelters.

Station	Time Interval	Air Temperature	Relative Humidity
Kaskawulsh Ice	8-26 July 1965	3.0	85.1
Kaskawulsh Knoll	1-26 July 1965	5.8	62.4

NOTE: Kaskawulsh Ice weather shelter was located about one kilometer south of Kaskawulsh Camp, on the Central Arm of the glacier. Kaskawulsh Knoll weather shelter was about 700 m. northwest of Kaskawulsh Camp on the ridge between the North and Central Arms of the glacier.

Units: Air Temperature: Centigrade degrees Wind Velocity: kilometers per hour (and m.p.h.)
 Air Pressure: millibars Cloudiness: tenths of sky covered by clouds
 Relative Humidity: per cent Precipitation: centimeters of water equivalent

*Ref.: Marous, 1965; Marcus, Rens and Taylor, 1966.

Stress, strain, and elastic constants

(Love, 1944; Nye, 1957).

In a Cartesian coordinate system with axes X, Y, Z, numbered 1, 2, 3, respectively, the stress components are written, in tensor form:

$$\begin{array}{ccc} \sigma_{11} & \sigma_{12} & \sigma_{13} \\ \sigma_{21} & \sigma_{22} & \sigma_{23} \\ \sigma_{31} & \sigma_{32} & \sigma_{33} \end{array} = [\sigma_{ij}] \quad (i, j=1, 2, 3) \quad \dots (1)$$

Here the first subscript refers to the axis normal to the plane upon which the force acts, and the second subscript refers to the axis parallel to the direction of the force. This is a symmetric tensor, $\sigma_{ij} = \sigma_{ji}$, so there are six stress components.

In matrix form, they are:

$$\begin{array}{ccc} \sigma_1 & \sigma_6 & \sigma_5 \\ \sigma_6 & \sigma_2 & \sigma_4 \\ \sigma_5 & \sigma_4 & \sigma_3 \end{array} = (\sigma_i) \quad (i=1, \dots, 6) \quad \dots (2)$$

The strain tensor is:

$$\begin{array}{ccc} E_{11} & 2E_{12} & 2E_{13} \\ 2E_{21} & E_{22} & 2E_{23} \\ 2E_{31} & 2E_{32} & E_{33} \end{array} = [E_{ij}] \quad (i, j=1, 2, 3) \quad \dots (3)$$

Here the first index refers to the coordinate axis normal to the plane perpendicular or parallel to which displacement takes place; the second index refers to the axis parallel to the direction of displacement. $E_{ij} = E_{ji}$, so there are six strain components. In matrix form they are:

$$\begin{array}{ccc}
 E_1 & E_6 & E_5 \\
 E_6 & E_2 & E_4 \\
 E_5 & E_4 & E_3
 \end{array}
 = (E_i) \quad (i = 1, \dots, 6.) \quad (4)$$

The generalized Hooke's Law relating the stress and strain matrices is:

$$\sigma_1 = C_{11} E_1 + C_{12} E_2 + C_{13} E_3 + C_{14} E_4 + C_{15} E_5 + C_{16} E_6$$

$$\sigma_2 = C_{21} E_1 + C_{22} E_2 + C_{23} E_3 + C_{24} E_4 + C_{25} E_5 + C_{26} E_6$$

$$\sigma_3 = C_{31} E_1 + C_{32} E_2 + C_{33} E_3 + C_{34} E_4 + C_{35} E_5 + C_{36} E_6$$

$$\sigma_4 = C_{41} E_1 + C_{42} E_2 + C_{43} E_3 + C_{44} E_4 + C_{45} E_5 + C_{46} E_6$$

$$\sigma_5 = C_{51} E_1 + C_{52} E_2 + C_{53} E_3 + C_{54} E_4 + C_{55} E_5 + C_{56} E_6$$

$$\sigma_6 = C_{61} E_1 + C_{62} E_2 + C_{63} E_3 + C_{64} E_4 + C_{65} E_5 + C_{66} E_6$$

$$\text{or, } \sigma_i = \sum_{j=1}^6 C_{ij} E_j \quad i = 1, \dots, 6. \quad (5)$$

The matrix of constants, (C_{ij}) , is called the "stiffness matrix." It is symmetric, so in the most general case there are 21 independent elastic constants. In the tensor notation the two-index constant, C_{ij} , is expressed by a four-index constant, C_{klmn} , for which the first two indices refer to the corresponding stress tensor component and the last two indices refer to the corresponding strain tensor component. Thus, $C_{44} = C_{2323}$; both expressions refer to the constant that relates the σ_4 (σ_{23}) stress component to the E_4 (E_{23}) strain component. Generally in this treatment the matrix notation will be used.

Conventionally, a constant defined by the partial derivative of a generalized force with respect to a generalized displacement is called a "modulus," while the constant

defined by the inverse relationship is called a "coefficient."

C_{ij} is the elastic modulus, and the elastic coefficient,

s_{ij} , is defined by the relation:

$$E_i = \sum_{j=i}^6 s_{ij} \quad i = 1, \dots, 6 \quad \dots (7)$$

C_{ij} and s_{ij} are also called the "stiffness" and "compliance," respectively, and (s_{ij}) is called the "compliance matrix."

The two constants are related to each other as follows:

$$\sum_{k=i}^6 C_{ik} s_{jk} = \alpha_{ij} \quad \dots (8)$$

where δ_{ij} is the Kronecker delta: $\delta_{ij} = \begin{matrix} 1 & \text{for } i = j \\ 0 & \text{for } ij \end{matrix}$

Elastic constants of crystals (Cady, 1964).

In the generalized Hooke relationship there are 21 independent elastic constants. This is the case for a completely non-symmetric medium, e.g., a triclinic hemihedral crystal. The introduction of symmetry elements reduces the number of independent constants: some are repeated, and some vanish. The highest symmetry is isotropic, for which there are only two elastic moduli, the Lamé constants λ and μ . In elastically isotropic media the elastic constants and the velocities of elastic waves do not vary with respect to direction at a fixed point. In media of lower symmetry, i.e., anisotropic media, the elastic constants depend upon the direction of application of stress and the velocities of elastic waves depend upon the direction of wave propagation.

This study is concerned with the ice crystal, which belongs to the hexagonal system of symmetry. In the hexagonal system there is one crystallographic axis of six-fold rotational symmetry (there may be other crystallographic symmetry elements; the elastic constants are defined by the rotational symmetry). Elastically the hexagonal axis is an axis of ∞ -fold rotational symmetry. This type of symmetry is also referred to as transverse isotropy because the elastic properties are the same in any direction perpendicular to the axis of symmetry.

In the hexagonal symmetry system there are five independent elastic moduli. The matrix of moduli is:

$$(C_{ij}) = \begin{matrix} C_{11} & C_{12} & C_{13} & 0 & 0 & 0 \\ C_{12} & C_{11} & C_{13} & 0 & 0 & 0 \\ C_{13} & C_{13} & C_{33} & 0 & 0 & 0 \\ 0 & 0 & 0 & C_{44} & 0 & 0 \\ 0 & 0 & 0 & 0 & C_{44} & 0 \\ 0 & 0 & 0 & 0 & 0 & C_{66} \end{matrix} \dots (9)$$

where $C_{66} = \frac{1}{2} (C_{11} - C_{12})$.

The axis of elastic symmetry coincides with the crystallographic C-axis, i.e., the optic axis. The a_1 , a_2 , a_3 axes which define the basal plane of the hexagonal crystal are consequently normal to the axis of elastic symmetry and the basal plane of the crystal coincides with the X, Y (or 1, 2) plane of the elastic coordinate system. The a_1 crystallographic axis is usually taken to coincide with the elastic X-axis, but this choice is arbitrary.

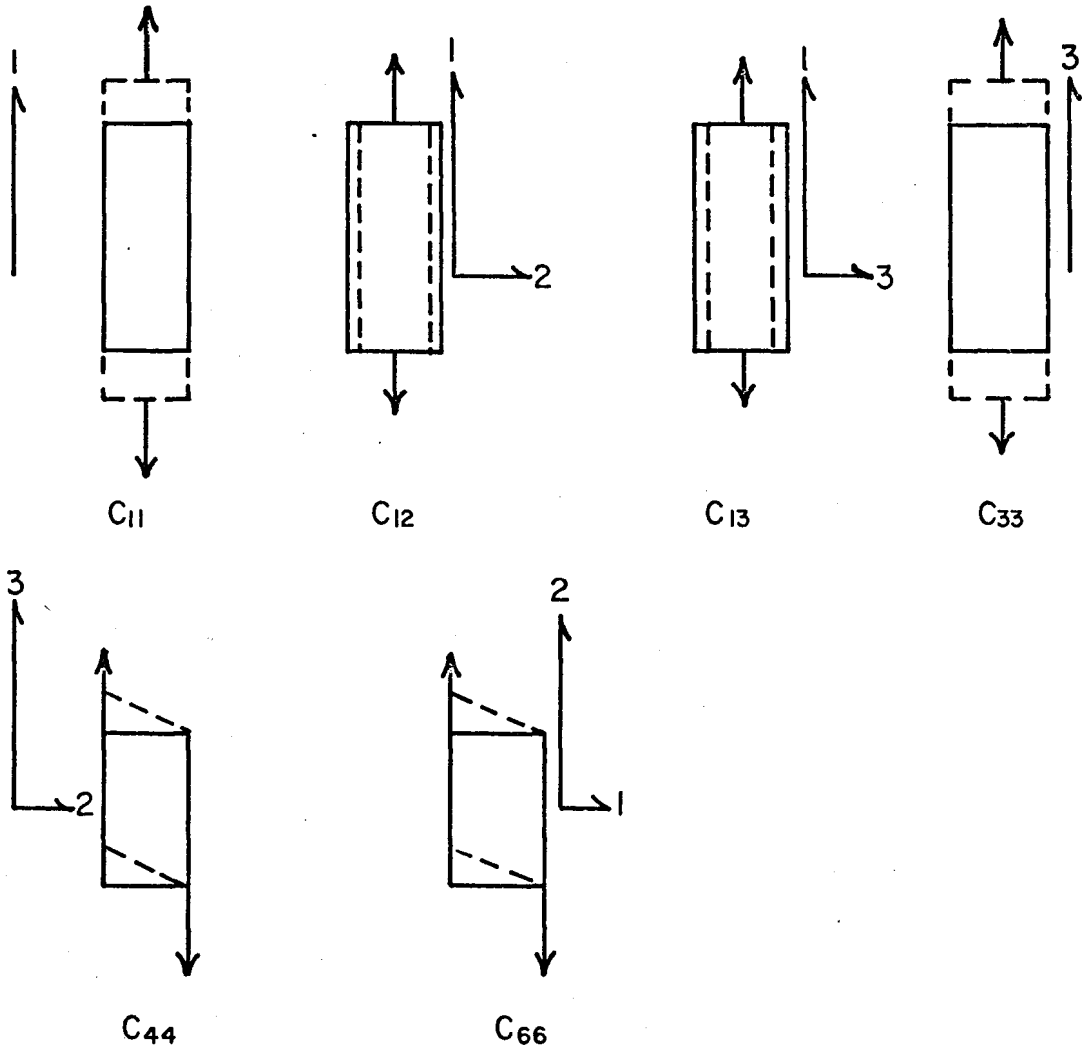
The physical meaning of the hexagonal moduli is illustrated in Figure 4. C_{11} and C_{33} represent longitudinal response to tension (or compression) in the directions perpendicular and parallel to the symmetry axis, respectively. C_{12} and C_{13} are "cross-constants" representing transverse shortening (or thickening) in response to longitudinal tension (or compression). Thus, the ratio $\mu_{21} = C_{12}/C_{11}$ is analogous to Poisson's ratio in an isotropic substance. C_{44} and C_{66} represent response to shearing stress parallel and perpendicular to the symmetry axis, respectively.

The elastic constants of single ice crystals have been determined theoretically by Penny (1948) and experimentally by Jona and Scherrer (1952), Green and Mackinnon (1956), and Bass, Rossberg and Ziegler (1957). Determinations of the constants of polycrystalline ice with strongly preferred orientation of the C-axes were made by Brockamp and Querfurth (1964). The results of the latter workers will be utilized in the present study.

Elastic wave velocity (Musgrave, 1959; Kraut, 1963).

The propagation of elastic waves can be represented in a cartesian coordinate system, by the equations:

$$\begin{aligned} \rho \frac{\partial^2 u}{\partial t^2} &= \frac{\partial \sigma_{11}}{\partial x} + \frac{\partial \sigma_{12}}{\partial y} + \frac{\partial \sigma_{13}}{\partial z} \\ \rho \frac{\partial^2 v}{\partial t^2} &= \frac{\partial \sigma_{21}}{\partial x} + \frac{\partial \sigma_{22}}{\partial y} + \frac{\partial \sigma_{23}}{\partial z} \\ \rho \frac{\partial^2 w}{\partial t^2} &= \frac{\partial \sigma_{31}}{\partial x} + \frac{\partial \sigma_{32}}{\partial y} + \frac{\partial \sigma_{33}}{\partial z} \end{aligned} \quad \dots (10)$$



—→ DIRECTION OF THE APPLIED STRESS
 - - - OUTLINE OF A DEFORMED PARALLELEPIPED
 —→ 1, 2, OR 3 REPRESENTS DIRECTION OF THE
 X, Y, OR Z COORDINATE AXIS

Figure 4. Character of the deformations corresponding to elastic moduli C_{ij} in the hexagonal crystal.

where ρ is the density of the medium, u, v, w are the components of displacement of the medium along the coordinate axes X, Y, Z , and σ_{ij} are the components of stress, which are related to the components of strain by equation (6).

For isotropic media these equations lead to the two familiar relationships for compressional and shear wave velocities:

$$V_p = \frac{\lambda + 2\mu}{\rho}^{\frac{1}{2}} \quad \dots (11)$$

$$V_s = \frac{\mu}{\rho}^{\frac{1}{2}} \quad \dots (12)$$

For anisotropic media consider a wave traveling in an arbitrary direction defined by the vector b . $b = \beta_x X + \beta_y Y + \beta_z Z$, where $\beta_x, \beta_y, \beta_z$ are direction cosines. The displacement components, u, v, w , are functions of the direction of propagation b , so the strain components become:

$$\begin{aligned} E_1 &= \alpha_x \frac{\partial u}{\partial b^2}, \quad E_2 = \alpha_y \frac{\partial v}{\partial b^2}, \quad E_3 = \alpha_z \frac{\partial w}{\partial b^2} \\ E_4 &= \alpha_y \frac{\partial w}{\partial b} + \alpha_z \frac{\partial v}{\partial b} \\ E_5 &= \alpha_x \frac{\partial w}{\partial b} + \alpha_z \frac{\partial u}{\partial b} \\ E_6 &= \alpha_x \frac{\partial v}{\partial b} + \alpha_y \frac{\partial u}{\partial b} \end{aligned} \quad \dots (13)$$

Substituting (13) into (6) and (6) into (1), the wave equations become:

$$\begin{aligned} \rho \frac{\partial^2 u}{\partial t^2} &= \Gamma_{11} \frac{\partial^2 u}{\partial b^2} + \Gamma_{12} \frac{\partial^2 v}{\partial b^2} + \Gamma_{13} \frac{\partial^2 w}{\partial b^2} \\ \rho \frac{\partial^2 v}{\partial t^2} &= \Gamma_{21} \frac{\partial^2 u}{\partial b^2} + \Gamma_{22} \frac{\partial^2 v}{\partial b^2} + \Gamma_{23} \frac{\partial^2 w}{\partial b^2} \\ \rho \frac{\partial^2 w}{\partial t^2} &= \Gamma_{31} \frac{\partial^2 u}{\partial b^2} + \Gamma_{32} \frac{\partial^2 v}{\partial b^2} + \Gamma_{33} \frac{\partial^2 w}{\partial b^2} \end{aligned} \quad \dots (14)$$

where $\Gamma_{kl} = \Gamma_{lk}$, the Christoffel moduli, are functions of the elastic moduli, C_{ij} , and the direction cosines α_x , α_y , α_z ,

The displacement is defined by a vector ξ that is a function of the displacement components and their direction cosines, p , q , r .

$$\xi = pu + qv + rw \quad \dots (15)$$

$$\text{so } u = p\xi, v = q\xi, w = r\xi \quad \dots (16)$$

Substituting (16) into (14), the wave equation can be written in terms of the wave propagation direction b and the displacement ξ :

$$\frac{\partial^2 \xi}{\partial t^2} = k \frac{\partial^2 \xi}{\partial b^2} \quad \dots (17)$$

$$\text{where } pk = p\Gamma_{11} + q\Gamma_{12} + r\Gamma_{13}$$

$$qk = p\Gamma_{21} + q\Gamma_{22} + r\Gamma_{23} \quad \dots (18)$$

$$rk = p\Gamma_{31} + q\Gamma_{32} + r\Gamma_{33}$$

Equations (18) can be solved if the determinant of the coefficients vanishes:

$$\begin{vmatrix} \Gamma_{11} - k & \Gamma_{12} & \Gamma_{13} \\ \Gamma_{12} & \Gamma_{22} - k & \Gamma_{23} \\ \Gamma_{13} & \Gamma_{23} & \Gamma_{33} - k \end{vmatrix} = 0 \quad \dots (19)$$

This equation has three real, positive roots, indicating the propagation of three wave modes with velocities:

$$v_i = \sqrt{\frac{k_i}{\rho}} \quad i = 1, 2, 3 \quad \dots (20)$$

The k_i are generally rather complicated polynomial functions of the direction cosines, $\beta_x, \beta_y, \beta_z$, and the elastic moduli, C_{ij} .

In isotropic media the two modes of vibration, compressional and shear, are distinct. In anisotropic media the three modes are mixed except when wave propagation is in a direction perpendicular to a plane of symmetry or to an axis of rotational symmetry. In a hexagonal crystal pure modes are propagated parallel to the C-axis and in any direction perpendicular to it. In these directions V_1 is the velocity of a pure compressional wave and V_2 and V_3 are the velocities of pure shear waves. The latter have different displacement polarizations and velocities when propagated perpendicular to the C-axis and hence exhibit double refraction analogous to that of light waves in crystals. When propagated parallel to the C-axis, V_2 and V_3 merge. The directions of polarization are illustrated in Figure 5.

Consider a surface that represents the loci of endpoints of velocity vectors from a seismic source (Fig. 6). In a medium of hexagonal or transverse isotropic symmetry this is a surface of revolution about the axis of rotational symmetry. There is a different surface for each of the three modes, corresponding to V_1 , V_2 , V_3 . In the ice crystal V_1 is greater parallel to the C-axis ($\phi = \pi/2$ in Fig. 6) than perpendicular to it. This type of figure will be referred to as "prolate" (this does not imply that the velocity figure is ellipsoidal). V_2 is the same at $\phi = 0$ and $\phi = \pi/2$ and reaches a maximum at $\phi = \pi/4$. V_3 is greater

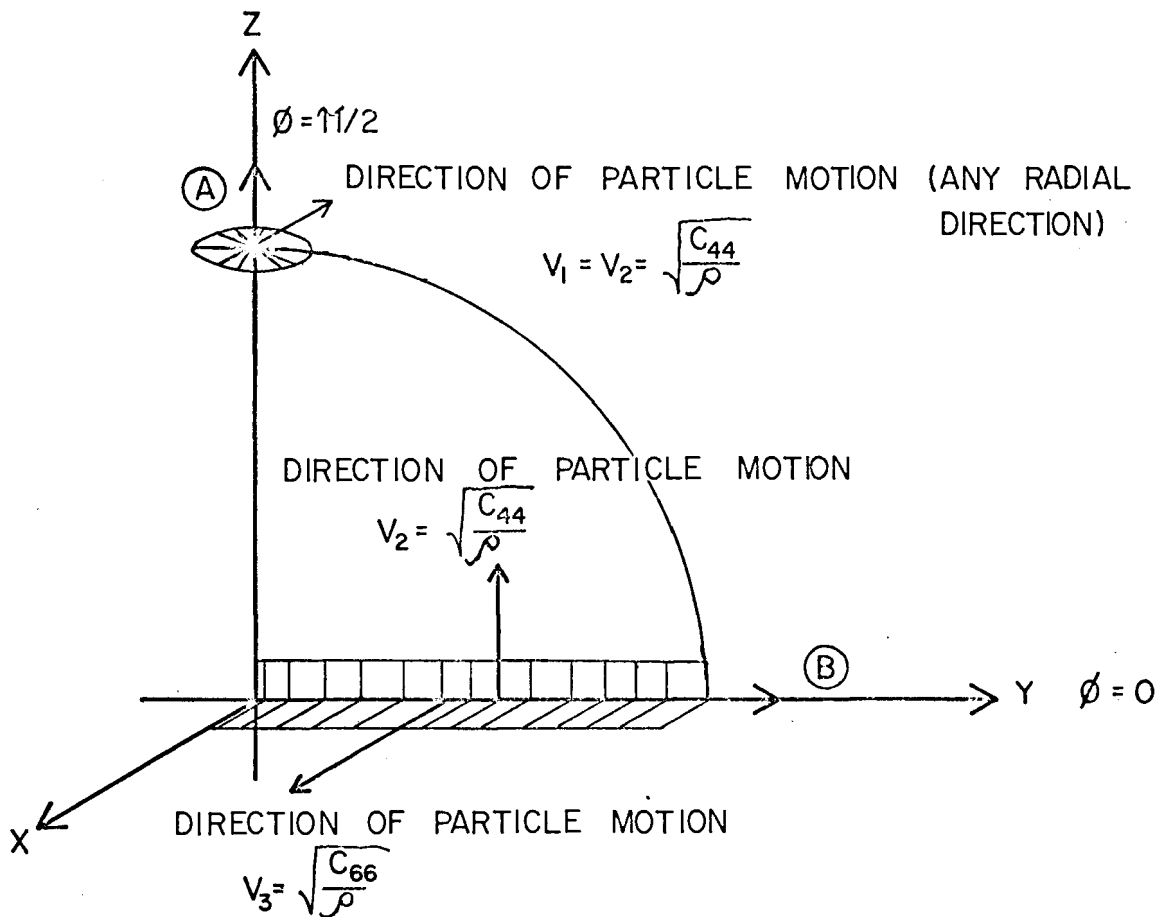


Figure 5. Polarization of particle motion for shear waves. Particle motion is shown for waves traveling parallel to the C-axis (a) and perpendicular to the C-axis (b) of a hexagonal crystal. ϕ is the angle between the direction of wave propagation and the basal plane of the crystal.

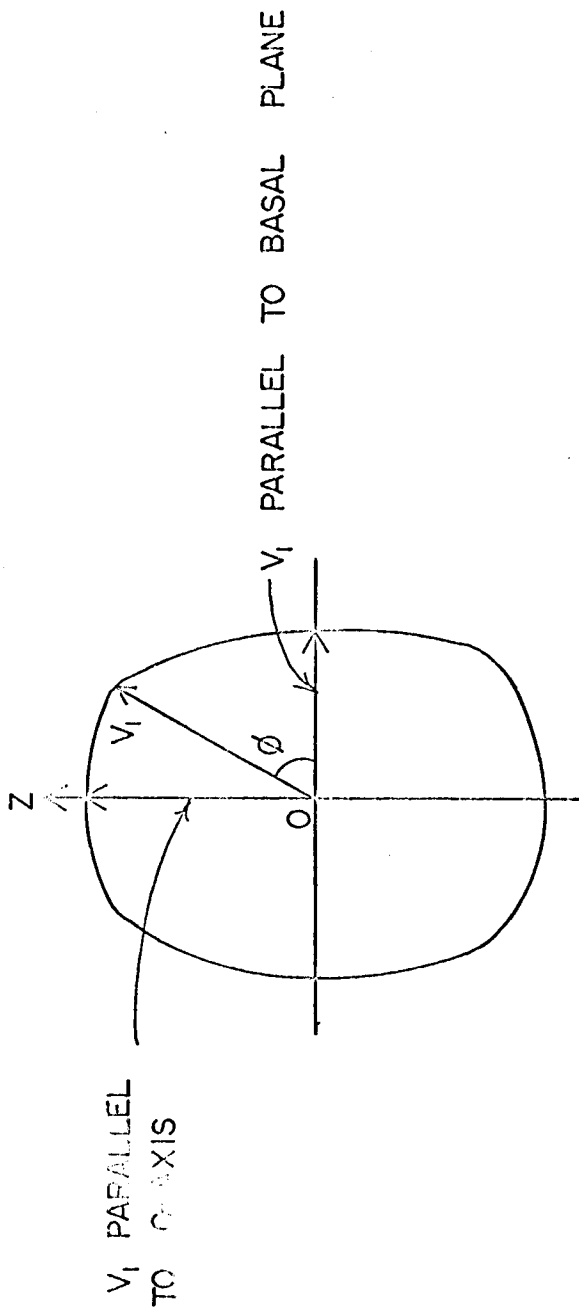


Figure 6. Section in the meridional plane of the velocity surface of V_I for a hexagonal crystal such as ice.

at $\phi = 0$ than at $\phi = \pi/2$ and this type of velocity surface will be called "oblate." The ratio of the velocity at $\phi = 0$ to the velocity of the same mode at $\phi = \pi/2$ is called the "anisotropy factor" (Uhrig and Van Melle, 1955).

As an illustration of these principles, it will be noted in Figure 5 that for V_2 at $\phi = 0$, the wave displacement is parallel to the C-axis and perpendicular to an arbitrary axis which lies in the basal plane and hence is orthogonal to the C-axis. In the tensor notation the C-axis corresponds to the 3-axis. The arbitrary orthogonal axis can be called the 2-axis. The wave displacement represents the response of a shear strain in the plane normal to the 2-axis, in the direction of the 3-axis, to a shear stress in the same plane and in the same direction. The modulus relating shear strain and stress in this case is C_{2323} in the tensor notation, or C_{44} in the matrix notation. In this case the wave is purely in the shear mode and its velocity is $V_2 = \sqrt{\frac{C_{44}}{\rho}}$.

In this study compressional (longitudinal) waves will be referred to as P-waves and shear (transverse) waves will be referred to as S-waves. A P-wave that is reflected from an interface as a P-wave will be called a PP reflected wave. A P-wave converted to an S-wave upon reflection at an interface will be called a PS reflected wave. SP and SS have analogous definitions.

1.8 Historical Background

Extensive seismological investigations have been made in recent years on polar ice sheets and caps, e.g., in Antarctica, Greenland, Iceland, and Novaya Zemlya, and on firn fields and the accumulation zones of temperate glaciers. The literature on seismological studies of the ablation zones of valley glaciers is relatively limited.

The use of seismic wave propagation in measurements of ice thickness began in the Alps in the 1920's, shortly after the development of practical methods of seismic prospecting. Mothes (1927), Brockamp and Mothes (1930, 1931), and their colleagues made several such studies on the Pasterze and Hintereis Glaciers and their work was continued after World War II by Förtsch and Vidal (1956, 1958) and others on the Hintereis and the nearby Gurgler Glacier. The Commission Helvatique des Glaciers made seismic soundings on the Grosser Aletsch (Renaud and Mercanton, 1950), the Rhone, and the Unteraar Glaciers (Jost, 1954). Ice thickness has also been determined by seismic means on the Gorner Glacier (Süsstrunk, 1951) and on the Mer de Glace (Renaud and Mercanton, 1950). Italian workers, including Cassinis and Carabelli (1953), Carabelli (1961), and De Visintini (1963) have made seismic explorations on the Miage, Forni and Belvedere Glaciers.

Soviet seismological work on valley glaciers was begun in 1956 by Kravtsov and Terent'eva (1959) on the Maliy Aktru Glacier in the Altai Mountains. This was followed by the

investigations of Berzon, Bokanenko and Isasv (1959) and Borovinskii (1963) on the Tuyuksu Glacier complex near Alma Ata, seismic studies during the expedition to the Fedchenko Glacier in the Pamir Mountains (Berzon, Pak and Yakovlev, 1960), and work in the Caucasus Mountains (Bokanenko and Isaev, 1960). Kravtsov (1960) pioneered in seismological determination of physical properties of ice in his research in the Altai.

During 1934-35 Goldthwait (1936) made a series of seismic observations near the termini of the South Crillon and the much smaller Klooch Glaciers in southeast Alaska. In 1951 Allen and Smith (1953) made seismic soundings on the ice piedmont of the Malaspina Glacier and the following year Allen carried out similar measurements on the Saskatchewan Glacier, the major outlet of the Columbia Icefield in the Rocky Mountains (Meier, 1960). The neighboring Athabaska Glacier was explored later (Kanasewich, 1963). Allen followed his Rocky Mountain work with seismic soundings on the Blue Glacier in the Olympic Mountains (Allen, Kamb, Meier and Sharp, 1960) and his work there has been continued by others (e.g., Westphal, 1965).

In 1956 detailed glaciological studies were made on the Salmon Glacier in the Coast Mountains of British Columbia. The work included seismic depth measurements (Doell, 1963). Redpath (1965), working on Axel Heiberg Island in the Canadian Archipelago, extended seismic profiles down from the ice cap to the ablation zone of one of the major outlets.

the Thompson Glacier, and to the smaller White Glacier, a more clearly defined valley glacier.

A few salient results obtained by these investigators are presented in Table 2. Most of these workers also found that, neglecting the transient snow cover, the glacier ice in the ablation zone is nearly homogeneous in regard to seismic wave velocities. There are exceptions. Goldthwait (1936) found indications that there are three layers of different seismic velocity on the South Crillon Glacier: an upper layer about 30 m. thick, in which the average P-wave velocity, V_p , is 3.23 km./sec.; an intermediate layer, at 30-60 m. depth, with V_p ranging from 3.20 to 3.60 km./sec.; and a deep layer, extending from a depth of 60 m. to the bottom of the glacier, with $V_p \approx 4.00$ km./sec.

Borovinskii (1963) reports that on the Central Tuyuksu Glacier V_p varies along a longitudinal profile from 3.62 ± 0.08 km./sec. near the firn line to 3.795 ± 0.085 km./sec. near the terminus. However, the variation is not continuous and the scatter of observed values is large.

The shapes of sub-glacial valleys, as determined by seismic methods, show great variations. The bed of the Malaspina Piedmont Glacier is nearly flat, with a rim at the terminus. Most of the Soviet glaciers have steep sides and nearly flat beds, but the Mer de Glace has a non-classical V-shaped transverse profile in its lower reaches.

Table 2. Seismic wave velocities and isotropic elastic constants in the ablation zones of temperate glaciers of Europe and Asia.

Glacier	Range	Investigator	ρ	V_p	V_s	σ	E	μ
Kesselwand	Alps	Förtsoh, Schneider, Vidal (1955)		3600				
Hintereis	Alps	Förtsoh and Vidal (1956)		3600	1730	0.36		
Gurgler	Alps	Förtsoh and Vidal (1958)		3510	1630	0.36		
Tuyuksu: Seismic	Tien Shan	Berzon, Bokanenko, Isaev (1959)						
(1)			0.90	3810	1905	0.334	8.93	3.34
(2)			0.90	3700	1830	0.338	8.22	3.08
Ultrasonic								
(1)			0.895	3530	1700	0.350	7.25	2.69
(2)			0.895	3840	1770	0.365	7.79	2.88
Elbrus: Seismic	Caucasus	Bokanenko and Isaev (1960)						
(3)			0.90	3650	1780	0.343	7.87	2.92
(4)			0.90	3540	1820	0.324	8.06	3.04
Ultrasonic								
(3)			0.87	3420	1760	0.320	7.34	2.74

Notes: (1) Lower profile, near terminus of glacier.

(2) Upper profile, near firn line.

(3) Near terminus

(4) Near terminus, higher than (3).

Frequencies of ultrasonic waves used:

Tuyuksu Glacier, 35 kHz.; Elbrus Glacier, 100-150 kHz.

Ice temperature in each case was approximately 0°C.

Symbols:

ρ = density (g./cm.³)

V_p = compressional wave velocity (meters/sec.)

V_s = shear wave velocity (meters/sec.)

σ = Poisson's Ratio

E = Young's Modulus (10¹¹ dynes/cm.²)

μ = Rigidity (10¹¹ dynes/cm.²)

Sometimes a bedrock depression is found at the confluence of glaciers. The Grosser Aletsch Glacier, in the Bernese Alps, is formed by the convergence of three glaciers of nearly equal size. At the confluence, which, like that of the Kaskawulsh Glacier, lies just below the firn limit, there is a level region, the Konkordia Platz, which is underlain by a bedrock depression. However, on the Highway Glacier, a polar glacier that drains the Penny Ice Cap on Baffin Island, there is no significant depression at a similar major glacier confluence (Röthlisberger, 1955).

CHAPTER II

EQUIPMENT AND OPERATIONS

2.1 Station Seismograph

A set of continuously recording station seismographs was operated on the Kaskawulsh Glacier during the 1965 field season. Its primary purpose was to register noise generated in and near the glacier. The instrumentation consisted of two horizontal motion torsion seismometers ($T_o = 1.0$ sec.)⁽¹⁾ mounted at right angles to each other, a vertical motion seismometer-galvanometer combination ($T_o = 0.5$ sec.; $T_g = 0.3$ sec.), and a horizontal "strong-motion" seismometer ($T_o = 1.0$ sec.). These instruments were arranged on a common base and recorded optically on separate strips of 35 mm. film.

The seismograph station was established on the medial moraine near Kaskawulsh Camp. A tent covered by several layers of tarpaulin ensured light-proof conditions during film-changing. Tilting due to differential ablation of

(1) T_o is the natural period of oscillation of the seismometer pendulum or suspension; T_g is the natural period of oscillation of the galvanometer suspension.

the ice under the moraine was a serious problem. No suitable bedrock site adjacent to the glacier was found.

2.2 Exploration Seismograph

A 12-channel commercial seismograph system was used for the reflection and refraction work. A block diagram of this equipment is shown in Figure 7. The geophones were of the moving-coil type and had a natural frequency of 20 Hz. The coupling between the geophones and the ice was usually very good because the geophones melted their way into the ice. During the early part of the field season, when the glacier surface was covered by wet snow and slush, there was some tilting and sinking of the geophones.

The geophone cable was 600 ft. (182.88 m.) long, with 12 takeouts, one every 50 ft. (15.24 m.). Either end could be connected to the seismograph input.

The cable was connected to the amplifiers through a testing unit which contained an ohmmeter for measuring the resistance of the geophone leads and the primary winding of the amplifier input transformer, and a voltmeter measuring the voltages of the test oscillator, amplifier output and batteries. The test oscillator provided a signal which could be varied from 1 V. to 0.1 V. in 10 db. steps.

The amplifiers were of vacuum tube design and were arranged in two banks of six each. Each bank, with the associated filters, was contained in a case weighing about

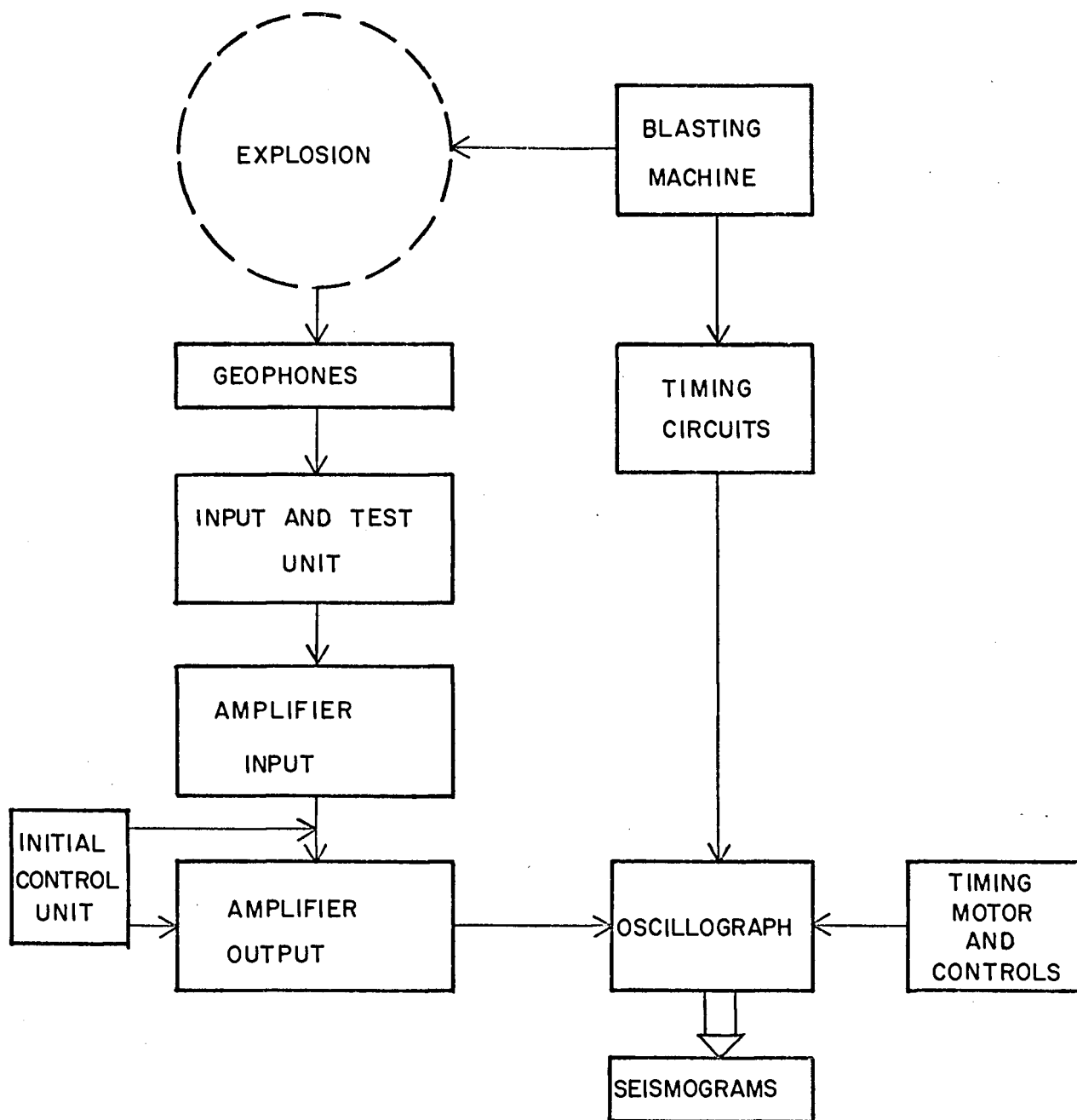


Figure 7. Block diagram of exploration seismograph system.

40 kg. All the seismograph components were arranged in similarly manageable cases.

Automatic gain control, which is of great utility in dealing with a stack of reflecting horizons, was available. In the present study there was essentially one reflecting horizon, at variable orientation, and relative amplitudes of signals were important, so the A.G.C. was infrequently used.

Each amplifier channel passed through high-cut and low-cut filters. The low-cut frequencies were: 18, 21, 48, 60, 70, 90, 120, 210 Hz.; the high-cut frequencies were: 20, 31, 47, 66, 120, 215, 320 Hz. Filters could be cut out, in which case the band spread was from 5 to 500 Hz. Several filter types of increasing sharpness of cut-off could be selected: single section constant K, single section M-derived, K-M combination, double section K, and double section M.

Output was recorded on photographic paper by the oscillograph. The recording paper could be fed at three speeds: high (85 cm./sec.), medium (34 cm./sec.), and low (17 cm./sec.). Medium speed was normally used in reflection work; high speed in short refraction studies. The latter speed permits the records to be read to approximately 0.1 millisecond.

Shot times were recorded by a pulse from the blasting machine. A shot-point seismometer signal could also be recorded. Shot depths were small, so that the uphole times between time break and shot point seismometer pulse were very short.

The system was operated with a minimum of two 12-volt storage batteries. Cathode voltage was taken directly from the terminals and plate voltage (100 V.) from a dynamotor.

The most frequent malfunctions involved the oscillator test unit, A.G.C., oscillograph timing motor, and the recording paper feed. Extreme care was taken to see that fine snow was not blown into the equipment, where it could melt and cause malfunction. Other serious problems were experienced keeping the batteries charged and maintaining proper temperature for the photographic processing solutions.

The operating console, amplifier banks, oscillographs, developing box and dynamotor were secured to a 400 kg. capacity Nansen sledge. Storage batteries, blasting machine, cables, geophones and stove were carried on a 100 kg. capacity 6 ft. (1.8 m.) Akhio sled. Fuel, photographic supplies, explosives and drilling equipment were loaded on another Akhio sled. When fully loaded, the Nansen sledge carried 110 kg. and each of the Akhio sleds about 80 kg. The sleds were man-hauled. Sometimes surface conditions required that the equipment be back-packed or hand-carried.

2.3 Drilling

Shot holes, usually 3 m. deep, were hand-drilled with a SIPRE 3-inch (7.6 cm.) diameter auger. Hand augering on a wet glacier is difficult; auger and core form a plug between

water in the hole and the atmosphere. The driller must lift against atmospheric pressure and when the auger is pulled out, the core is often forced by the pressure back into the hole. All operations were at elevations lower than the firm limit so the holes were drilled directly into solid ice, except for the layer of residual snow at the start of the season.

2.4 Explosives

High-velocity, high-density, gelatinized nitro-glycerin was used as an explosive charge. It was cartridge-ridged in rigid paper shells. The cartridges were $2\frac{1}{4}$ inches (5.7 cm.) in diameter and weighed $2\frac{1}{2}$ pounds (1.14 kg.) or 5 pounds (2.27 kg.). They could be cut easily into smaller sizes and "fast-couplers" were proved for joining cartridges. The gelatin was well suited for the molding of small charges of different shapes and sizes. The density of 1.6 g./cm.^3 permitted easy sinking in a shot hole filled with clean water, but if much slush was present the charge had to be weighted. No. 8 no-lag electric blasting caps, fired by a condenser discharge blasting machine, were used as detonators. The shot holes were usually stemmed by 2-3 meters of water.

The gelatin was rated at 60% strength, with explosion pressure 65-85 kilobars, explosion temperature 4000° K. , and detonation velocity 20,700 ft./sec. (6,310 m./sec.).

This high velocity explosion has a shattering effect on a brittle substance like ice. Unlike the case for shooting in snow and firn, "sprung" holes in ice are less efficient than new ones.

Because shear wave velocities are necessary for complete knowledge of the elastic properties, various methods of enhancing their production were tried. Vertically polarized shear waves are normally produced by internal reflection at a free surface and horizontally polarized shear waves are produced by propagation of vertical fractures near the shot point (Knopoff and Gilbert, 1960; Kisslinger, Mateker, and McEvelly, 1961). Shooting in deep, water-filled boreholes will produce vertically polarized shear waves preferentially directed downward (White and Sengbush, 1963), but deep boreholes were not available in the present investigation.

Asymmetric energy radiation creates shear waves. The common method of generating shear waves at short distances by detonating a blasting cap with or without a small charge beside a plank or sheet of metal buried in the ground was attempted. Alternatively, an embedded plank, in contact with a geophone to provide a time break, was struck with a sledge hammer. For greater asymmetric energy production experiments were made using the principle of the Munroe effect (shaped charge) (Lawrence, 1947; Poulter, 1950). This is illustrated in Figure 8. None of the above methods was entirely satisfactory.

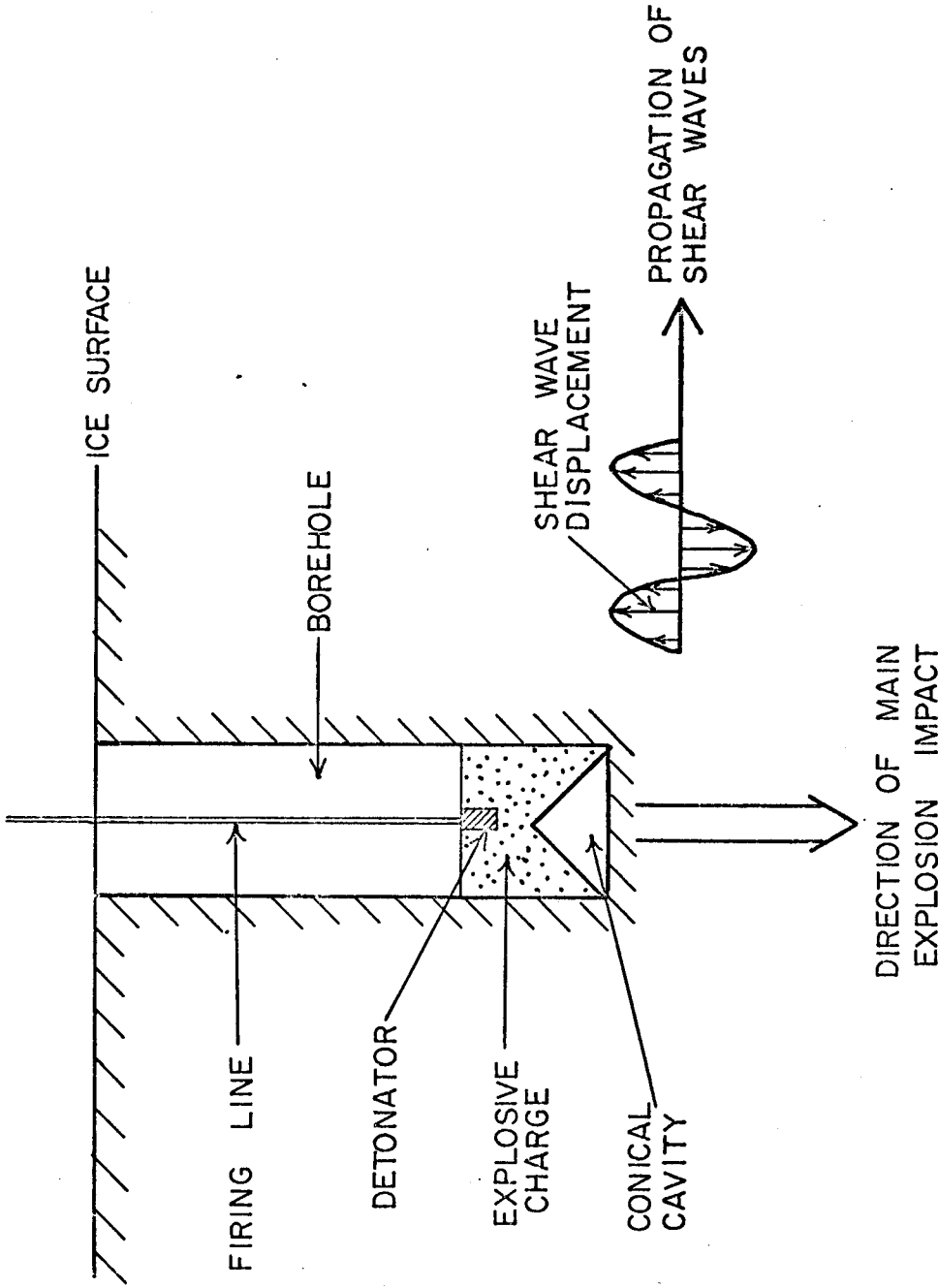


Figure 8. Principle of the Munroe effect (shaped charge). The conical cavity in the base of the charge causes most of the explosion energy to be directed downward. The asymmetry of energy flux results in enriched production of shear waves.

2.5 Communications

Short-wave radio communication was maintained between the field party and the Icefield Ranges Research Project base camp at Kluane Lake. During the wide-angle reflection work, when shooter and recording crew were up to 1000 m. apart, portable radios were used. Telephone wire was used to transmit time break and shot point seismometer signals from the shot point to the seismograph.

2.6 Logistics

The Kaskawulsh Glacier Camp contained several tents for the 5-9 personnel working in the confluence area during the summer. It was established on a level site on the medial moraine central to the work area. Supplies were brought in by air from the base camp. The Helio Courier aircraft operated by the Icefield Ranges Research Project could make ski landings on the snow cover until the middle of June. Thereafter, as the snow line retreated upglacier, uncovering the rough ice surface, landings had to be made progressively farther from the camp.

During the 1964 season supplies were brought in periodically throughout the summer. This resulted in an inordinate amount of time spent hauling sleds over a crevassed, slush-covered surface. To avoid a piecemeal supply operation in 1965, most of the bulk items were

brought in early. Free-fall drops of small items were made occasionally. At the end of the season most materiel was cached and the rest was hauled 8 km. to the nearest landing site.

The geophysical program consumed 200 kg. of explosive, 300 electric blasting caps, 150 gallons of gasoline (mainly for battery charging) and several cases of photographic paper and chemicals. Equipment was normally left in the field overnight, except for the batteries, which were hauled to depots where the generator, charger, fuel, and supplies were placed for convenient servicing of operations. Once a profile had been started it was usually possible to predict the time requirements, size and number of charges, and fuel consumption for battery charging that would be necessary.

2.7 Field Operations

During the 1964 season the seismic exploration program was carried out by one man, sometimes with an assistant. The following year, with a three-man party, it was possible to introduce some division of labor into the procedure.

The seismic spreads were usually lined up by eyesighting and compass: on spreads parallel to the cross-glacier profile direction the cable-layer aimed for the stake marking the next point on the profile. The cross-spreads were oriented with a Brunton compass. Where

greater precision was sought, as in the short refraction profiles, a theodolite was used for locating points.

The 1964 season lasted from mid-July until mid-August. The early part of this period was spent in trials of the effectiveness of various combinations of shot hole depths, charge size and shape, and seismograph parameter settings in obtaining seismic reflections. This work was performed at points on the Central Arm near the medial moraine: the X line, point 10 and points 10 and 11 of the upper line of stakes (Fig. 3). During the latter half of the season reflection shooting was carried out on the upper line of the Central Arm. The rest of the reflection profiles, the wide-angle reflection profile, and the short refraction investigations were carried out in 1965, when the party was in the field from mid-May until late August.

Most of the shots of the exploration program were made at points marked by bamboo poles, which also served as markers for the determination of the movement of the glacier surface (Anderton, 1967). These points were arranged along three profiles which cross the glacier transversely to the direction of ice flow. The "upper line" is about 1.5 km. above the confluence and is divided by the nunatak into two segments, the upper Central Arm line, and the upper North Arm line. The "strain line," whose points are surrounded by quadrilaterals measured for the calculation of strain rate, is about 200 m. below the confluence and

extends across the combined glacier. The "lower line" is about 1.5 km. down-stream from the strain line and also extends across the whole glacier. The strain and lower lines are each divided by the medial moraine.

The numbering of the points is shown in Figure 3. On the upper and lower lines, right angle L-spreads were used, with the cross-spreads generally up-glacier from the upper line and down-glacier from the lower line. Double split-spreads at right angles to each other, where feasible, were used on the strain line. Details of the movements of the seismological party, including supply operations and depot-laying are given in a separate report (Dewart, 1965).

2.8 Safety

Warm clothing and mountaineering equipment were provided, and were frequently necessary. Among the latter were five 30 ft. (9.2 m.) lengths of cable ladder for crevasse rescue and crevasse and moulin exploration. Rules of safety imposed by Alpine conditions had to be observed. The many crevasses and moulins in the confluence area were snow-bridged and difficult to detect in the early part of the season. Skis or snowshoes had to be worn, parties had to be roped, and crevasse-probing was often necessary. The probability of falling into a moulin is less than that of falling into a crevasse, but the probability of the moulin

fall being fatal is much greater. These shafts are wet, smooth-sided, deeper than crevasses and, in contrast to most crevasses, increase in cross-sectional area with depth (see Chapter III).

Meltwater streams and snow swamps abounded from mid-June until mid-July. During this period the party became resigned to ice-water baths. High winds and near-freezing temperatures presented an exposure problem that required extra clothing for quick changes.

The large quantity of fuel used for the generator and the liquified gas used for cooking presented a fire hazard. Inflammable materials were stored at considerable distance from camp behind a natural barrier.

Explosives and blasting caps were stored in dumps separate from the fuel dump. As far as possible preparation of charges (not including priming, of course) was done at a protected work area before leaving for the field. Non-sparking knife and punch were used in this work. Shooting in the vicinity of the Camp was scheduled to obviate the danger of radio energy pickup by the firing line.

Grizzly bears destroyed meteorological equipment and looted food caches near the terminus. A high-powered rifle was kept at Kaskawulsh Camp but, although bear spoor was seen near the confluence, the animals did not make their presence known otherwise.

CHAPTER III

SEISMIC NOISE SOURCES AND RELATED TOPICS

3.1 Introduction

An effort was made to obtain a record of the seismic background-noise prevalent in the glacier area. To this purpose the continuously-recording seismograph station was operated intermittently between June 9 and August 6, 1965. The noise considered here is natural ground oscillation, as distinguished from noise produced by the investigative process itself, such as surface waves and air waves from seismic shots (Olhovich, 1964).

The seismograph records exhibited four types of disturbance which contributed to the background noise:

(1) Continuous oscillations, varying in amplitude from barely perceptible to full-scale deflection of the traces. On the sensitive seismograph components, these deflections correspond to 0.05 and 17 microns, respectively (see section 3.2, below). Frequencies were 3-5 Hz.

(2) Individual pulses of one to three cycles, duration 0.8-1.0 sec., and frequency 2-3 Hz.

(3) Earthquake-like shocks, separable into primary, secondary and sometimes long-period phases. These were of variable duration and frequency, but always more prolonged than (2) and usually of lower frequency (1-2 Hz).

(4) Extended disturbances ($\frac{1}{2}$ -2 minute duration), distinguished from (1) by greater amplitude and lower frequency (1-2 Hz). They are not separable into definite phases. They frequently have a sudden commencement, but invariably fade away gradually.

3.2 Continuous Noise

Experience showed that when the wind speed rose to more than 15 mph (6.7 m./sec.) it was very difficult to obtain good shot records because of the high noise level. Diurnal temperature and wind velocity variations have very similar patterns but the few calm days were reasonably quiet regardless of temperature variations. Wind was a serious problem: velocities over 6.7 m./sec. were recorded on 140 of the 470 3-hour periods (29.8%) of the weather record (May 26 - July 25) at Kaskawulsh Camp in 1965, and an even larger percentage of the hours of good visibility.

On the days with the most complete records continuous noise was measured in the following manner: the peak-to-trough amplitudes of the ten oscillations of greatest amplitude occurring over a 20-minute period from 10 minutes before the hour until 10 minutes after the hour were averaged

arithmetically and the mean value was called the amplitude for that hour. The unit of amplitude was arbitrarily chosen as the average amplitude value, obtained as described above, for the quietest hour of record. With this value as unity, a day of normal noisiness registered average values of about 5 on the scale, and a very noisy day, on which it was difficult to obtain good exploration records, registered 10 or more. When the amplitude reached 7 or 8 the traces overlapped and the amplitudes became hard to measure. At values over 15 on this scale the noise became unreadable.

The value of 1 on the scale corresponded to approximately 0.1 millimeter of trace deflection. Magnification of the strong-motion horizontal seismometer was about 500 and magnification of the seismometer-galvanometer systems was about 2000. Accordingly, deflection of 1 unit on the strong-motion horizontal record corresponded to ground motion of approximately 0.2 microns amplitude; on the more sensitive horizontal and vertical records deflection of 1 corresponded to about 0.05 microns of ground motion. In the following discussion units of deflection will refer to the more sensitive instruments unless otherwise stated.

The 3-hourly noise amplitude record for July 23, 1965, is shown in Figure 9. This day was chosen because the wind and temperature variations do not correlate as closely as they do on most days on which good records were obtained. The hours of the amplitude readings were chosen to coincide with the hours of the meteorological observations. Wind

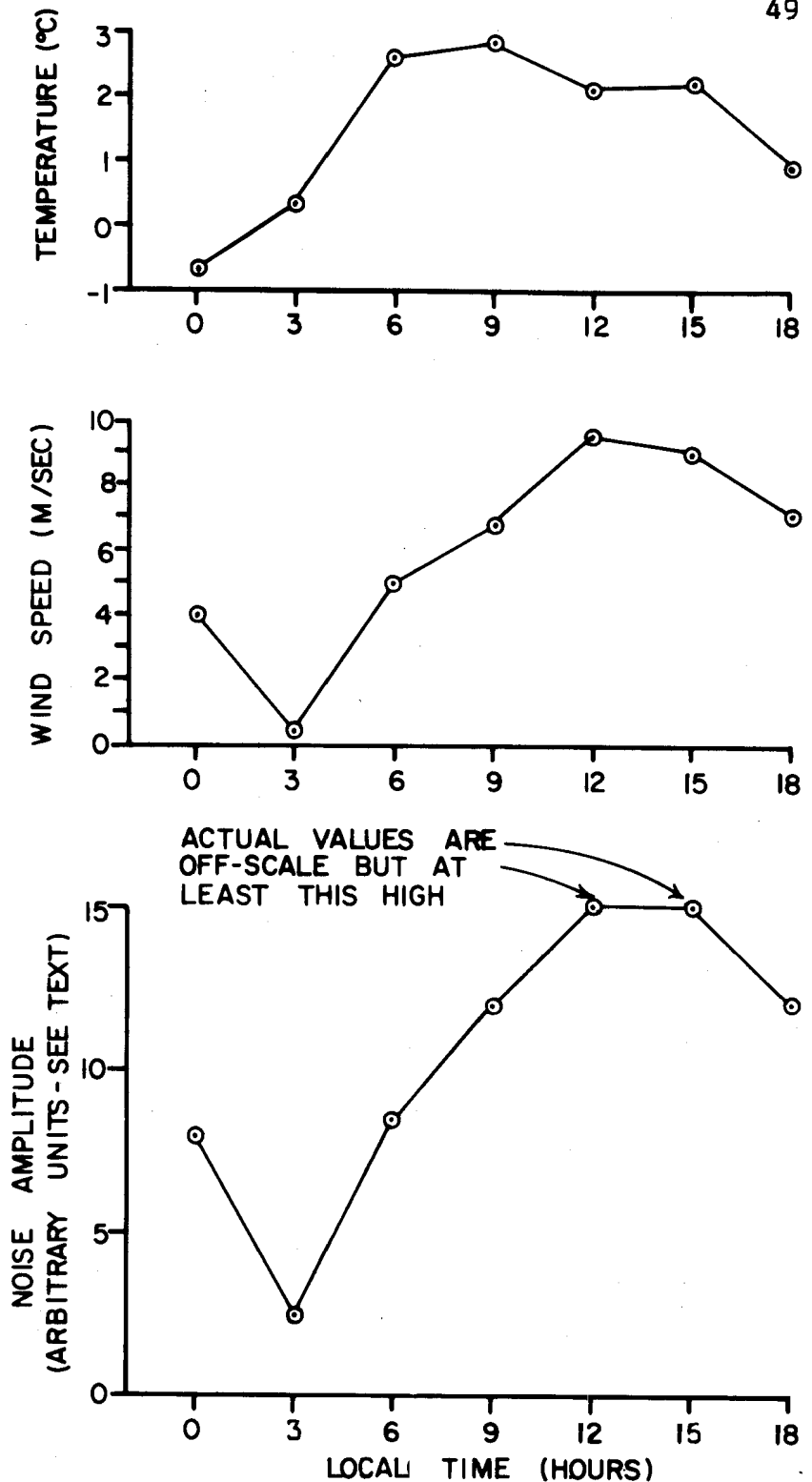


Figure 9. Background noise, wind speed, and temperature at Kaskawulsh Camp at 3-hourly intervals, July 23, 1955.

velocity and temperature values are also plotted and the close correspondence between noise amplitude and wind velocity is apparent.

The extent to which direct thermal effects contribute to continuous noise is not clear. When an ice crystal undergoes a temperature change heat energy is converted into strain energy, which is stored if the crystal is constrained and released suddenly when rupture removes the constraint. After extensional rupture the sides of the fracture accelerate apart, causing the propagation of longitudinal and transverse elastic waves. Energy release resulting from thermo-elastic contraction of ice grains is impulsive individually, but the superposition of impulses from a vast number of grain interactions could have the effect of continuous noise. The formation of thermal cracks depends partly on the rate of temperature change. The effect appears to be greatest when surface temperature drops suddenly. The contraction results in the development of large local stresses which cause rapid opening and expansion of cracks. At the time of a cold "snao" this noise has been reported to be audible (Mellor, 1964).

Gold (1963) observed crack formation in the surface of a smooth ice block produced by contact with a colder ice block. The contact was made instantly and cracks developed within one second. The temperature shock at the surface necessary to generate stresses equal to the ultimate strength of the ice ($30-40 \text{ kg./cm.}^2$) and, hence, produce fracture was

about 6° C. Under these circumstances the ice behaved as a brittle rather than a plastic material. The cracks showed a preference to form parallel to the basal and prismatic planes of the ice crystals.

The situation on the glacier surface is, of course, quite different in regard to rate of change of temperature. Under the conditions of temperature shock in Gold's experiments the rate of change of temperature with respect to time is very large, while on the glacier the rate is seldom greater than 1° C. per hour.

The correlation between seismic noise amplitude and rate of change of temperature is much closer for impulsive energy than for continuous noise (Fig. 10). Impulsive seismic noise will be discussed in the next section.

Running water produces continuous noise in the low frequency range (1-50 Hz). Noise from this source is unavoidable in the ablation zone of a glacier during the melt season. Innumerable streams cross the glacier, ranging in size from trickles to torrents with discharges of several cubic meters per second. Most of the streams drain into nearly vertical shafts -- moulins or "glacier mills" -- which enable them to reach great depth rapidly. Some of the kinetic energy acquired in this manner is converted into acoustic noise when the water strikes the sides or the bottom of the shaft. Exploration of several moulins revealed a series of steps that produce waterfalls in the streams (Dewart, 1965). The moulins received tributary tunnels and

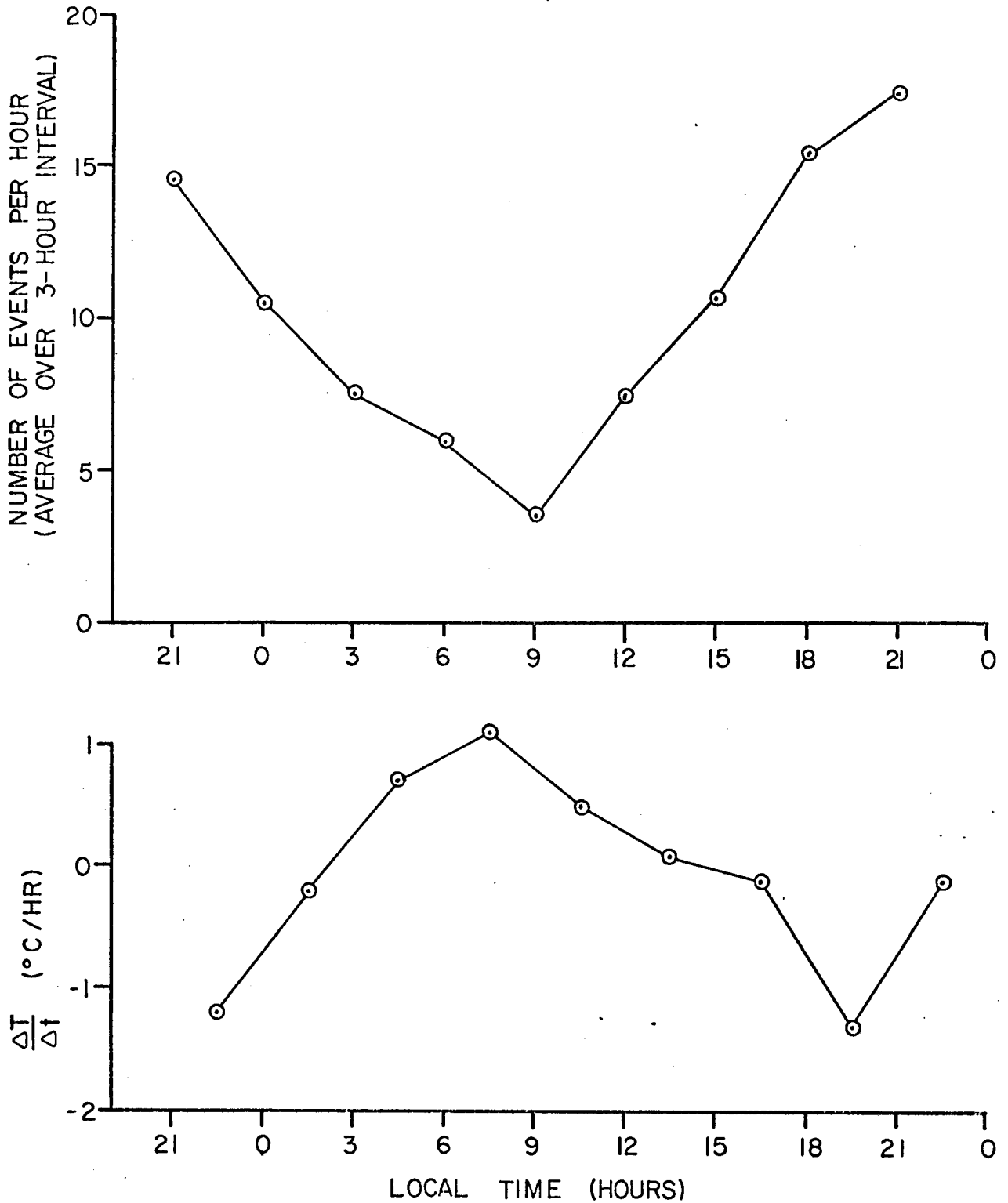


Figure 10. Number of impulsive noise events and time rate of change of temperature at Kaskawulsh Camp at 3-hourly intervals.

became larger in diameter with depth. A schematic section of a moulin is presented in Figure 11.

The moulins contained abundant evidence of highly turbulent flow and large changes of momentum in the water mass, such as corkscrew-shaped passages and plunge pools. Ground vibrations from moulins that were receiving large quantities of water were perceptible to the observer for distances of up to 50 m. from the orifice.

If we assume that acoustic energy radiation is proportional to the kinetic energy, $\frac{1}{2} mV^2$, acquired by the water at the depth where it ends its fall, $X = V^2/2g$, and that the energy received from a source per unit area decreases as the square of the distance from the source, the relationship obtained is that:

$$\frac{\text{energy return}}{\text{energy produced}} \propto \frac{1}{X} \quad . . . (21)$$

Although more energy is released by a high waterfall, less is recorded at the surface than from a lower one of the same volume. The moulins which were investigated all had plunge pools near the surface. If this is generally true, most of the moulin noise comes from near the surface. However, if the shafts unite at depth into a few large waterfalls, these may produce large local noise sources deep within the glacier.

The interaction of atmospheric disturbances with large bodies of water, in particular the oceans near the continental margins, results in the generation of prolonged trains of surface waves, often of Rayleigh type, and generally in

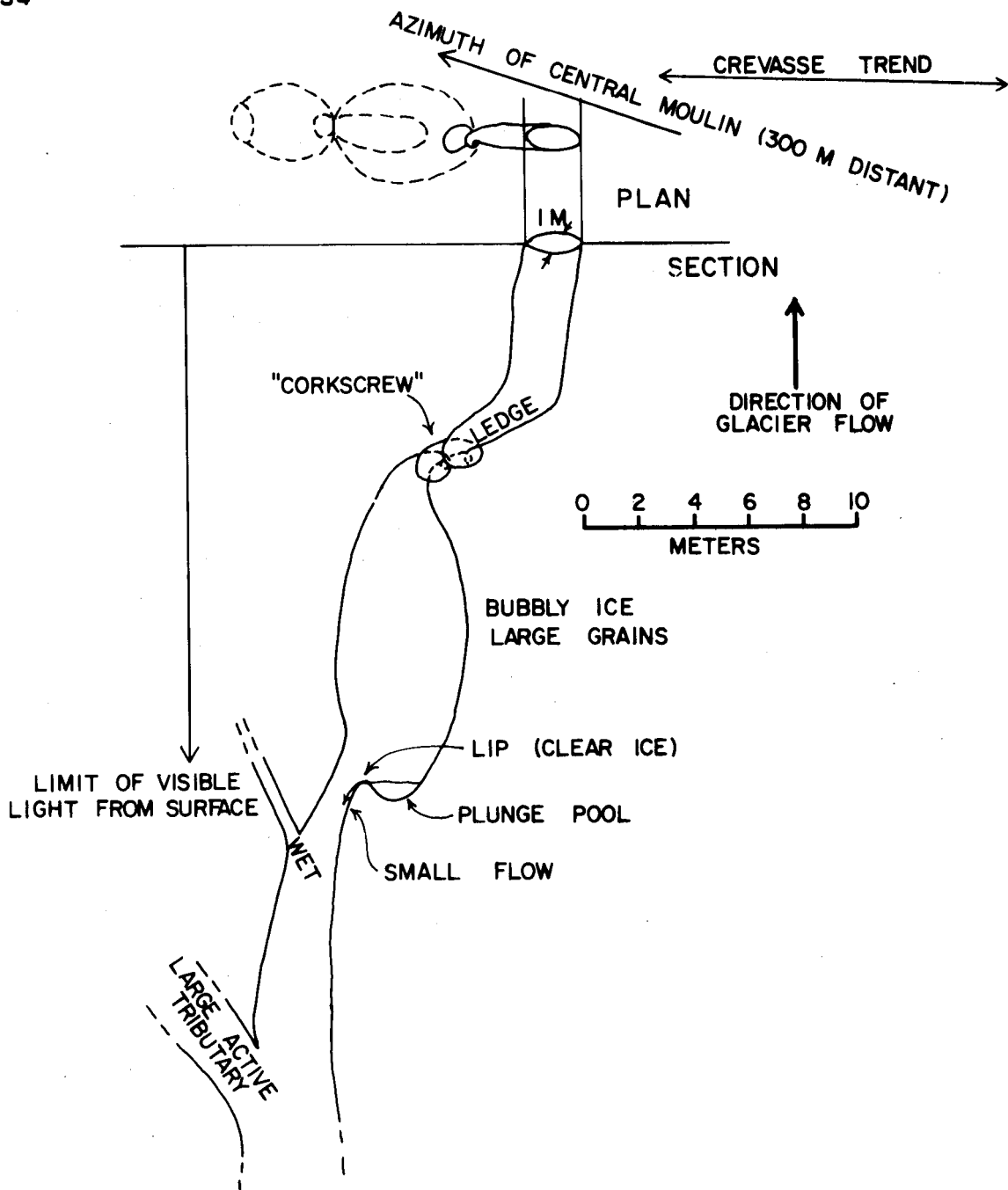


Figure 11. Section of a moulin. The section lies parallel to the planes of the nearby crevasses. The "central moulin" was a large one receiving runoff from several square kilometers of glacier surface.

the low-frequency range from our point of view, i.e., 0.1-1 Hz. These waves can travel hundreds of kilometers under favorable circumstances. Surf-produced noise, which has a higher frequency spectrum is dissipated within a few kilometers of shore. Kaskawulsh Camp is 80 km. from the head and 145 km. from the mouth of Yakutat Bay. The cold fronts which move eastward across the Gulf of Alaska as part of the normal weather circulation at this latitude undoubtedly produce microseisms that travel inland from the coast. However, the absorption rate of microseisms traveling across mountains is high for periods of less than 5 seconds (Carder, 1956).

The same effect occurs with smaller bodies of water. In this case shorter period waves are produced. Kluane Lake may be a source of microseismic noise, especially during stormy periods. Seiches in Kluane Lake would have considerably longer periods than those considered here. The length of the lake is 56 km., mean width about 5.6 km., depth perhaps 100 m. (the latter figure is merely a guess based upon contours in the Shakwak valley). Using the formula $T = 2\ell / \sqrt{gh}$, where T = period, ℓ = length of basin, h = depth of basin, g = acceleration of gravity (Lamb, 1945), the period of oscillation of the longitudinal uninodal standing wave is found to be about 6 minutes. A transverse uninodal wave would have a period of about 36 seconds. Small "self-draining" lakes that form along the margins of the glacier during the melt season could act similarly. A lake

of this nature regularly appears on the North Arm just east of the investigated area. This lake is also a noise-maker by other processes: running-water noise while it is draining and noise accompanying the calving of icebergs, which are prominent on its surface.

During the diagenesis of snow into ice in the accumulation zone of the glacier some of the air in the snow becomes incorporated in the ice because the firn becomes impermeable before the ultimate density of solid ice is achieved. Air pressure in the ice increases during the final stages of diagenesis and during metamorphism, when the bubbles contract because of creep of the ice at depth. Bubble pressures as high as 28 kg./cm.^2 have been measured by Langway (1958) in ice from the Greenland Ice Cap. However, Bader (1950) and other investigators (vide Shumskii, 1964) have found much lower air bubble pressures (e.g., $2\text{-}3 \text{ kg./cm.}^2$) in temperate glacier ice.

The air-laden ice emerges in the ablation zone as the glacier surface melts down. When only a thin film of ice separates the relatively high pressure bubble from the atmosphere, a process somewhat like that illustrated in Figure 12 probably takes place. The shearing stress on the film increases rapidly as the supporting area decreases until the breaking strength of the ice in the film is reached. Then the ice ruptures and the air rushes out of the bubble. Both of these events may be accompanied by the release of acoustic energy, and may account for a seething sound that was noticed

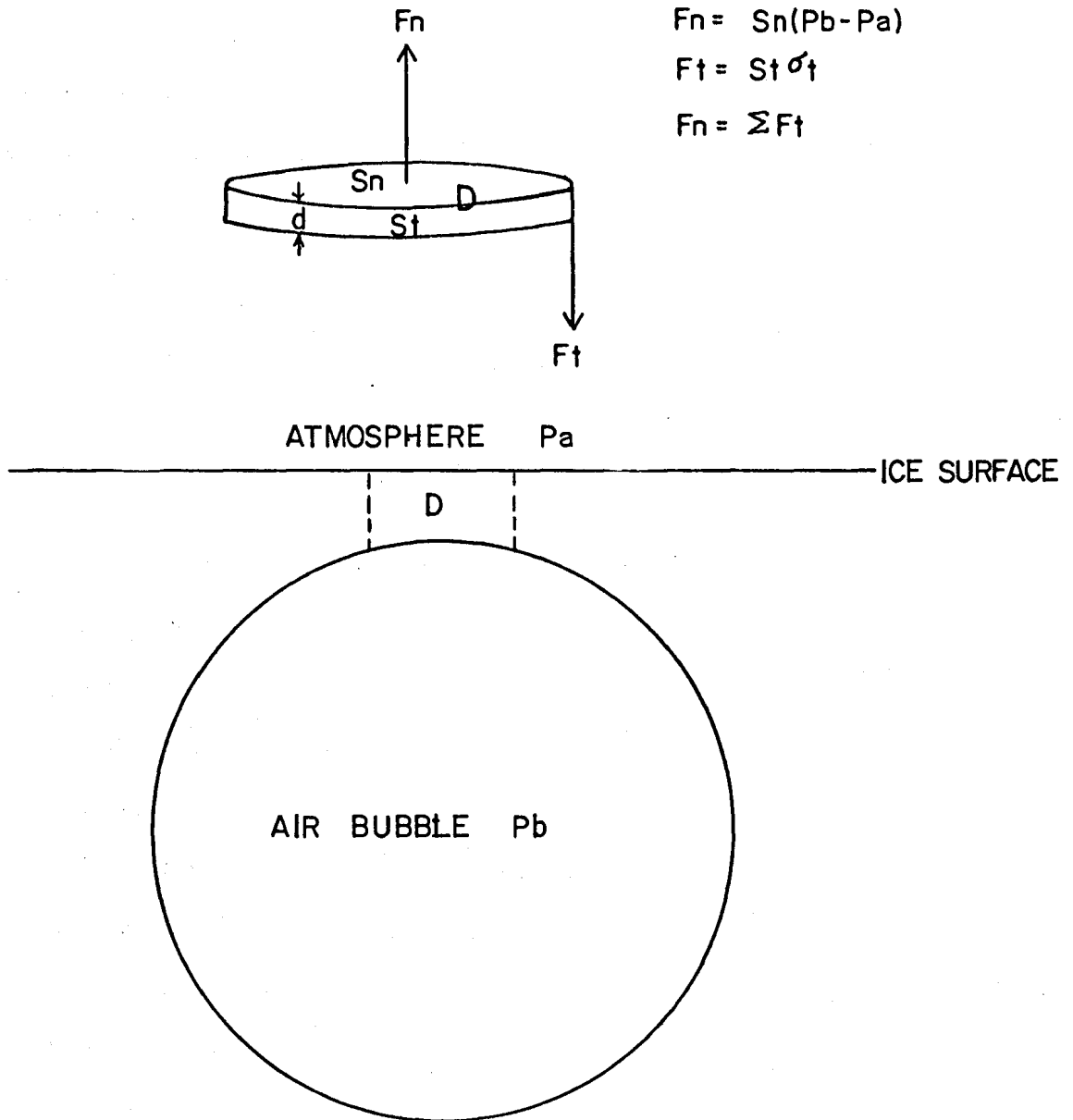


Figure 12. Ice rupture between air bubble and atmosphere. As the ice surface melts toward the bubble the ice in between approaches disc-like shape. The force F_n on the disc D , due to the pressure difference $P_b - P_a$, is balanced by the tangential forces F_t on the side of the disc. As the thickness d of the disc decreases, the area S_t of the side decreases. The forces remain constant, so the shearing stress σ_t increases until the shearing strength of the ice is exceeded and rupture occurs.

in bubbly ice on warm days. However, it does not seem to be an important source of noise.

The intensity of this type of noise must be related to the rate at which bubbles are exposed and hence to the rate of lowering of the ice surface. It tends to reach a maximum when the ice is receiving maximum heat input, whereas thermo-elastic noise tends to reach its peak during the period of maximum heat loss. The relation between the various sources of heat and the rate of ablation at the surface of a glacier has been the subject of much investigation. No simple relationship has been found. Hoinkes (1955) found a good correlation between diurnal variations in ablation rate and heat flux from the air and from solar radiation on Alpine glaciers. Keeler (1964), in the Canadian Arctic, found that glacier surface lowering during the melt season was related to cloud cover, radiation flux, air temperature and wind speed. Air temperature and wind speed were the most important factors. Adams (1966), also working in the Canadian Arctic, found varying time lags between radiation maxima and run-off maxima. There may be a connection between the results of these investigators and the observation that the "seething" described above occurred at times when the altitude of the sun and the temperature of the air were at or near maximum values, but these do not seem to be grounds for any more definite conclusions.

3.3 Impulsive Noise

Measurement

Individual pulses were counted on seven days of relatively quiet continuous noise in order to avoid masking by the latter. The minimum amplitude of a countable impulse was 5 on the noise amplitude scale described in the last section. This amplitude was enough for an impulse to be distinguished from the background during the noisiest parts of the days of observation.

By this qualified definition of a countable "impulse," a mean of 16.1 shocks per hour was registered. The scatter was large, ranging from a minimum of 1 to a maximum of 62 per hour. The percentage distribution with respect to amplitude range is shown in Figure 13. The frequency of events falls off rapidly with increasing amplitude: the curve approximates an inverse square relationship. However, since the energy is proportional to the square of the amplitude, the few high energy shocks contribute a share of the total recorded energy comparable to that of the many low energy shocks (Fig. 14 and Fig. 15). This suggests that the sources were not evenly distributed and of equal energy, for in that case the larger shocks would have a smaller proportion of the total energy, if low attenuation is assumed.

The durations of 100 shocks recorded successively on two days were measured. The distribution of pulse lengths is plotted in Figure 16. The mean length is 0.85 second.

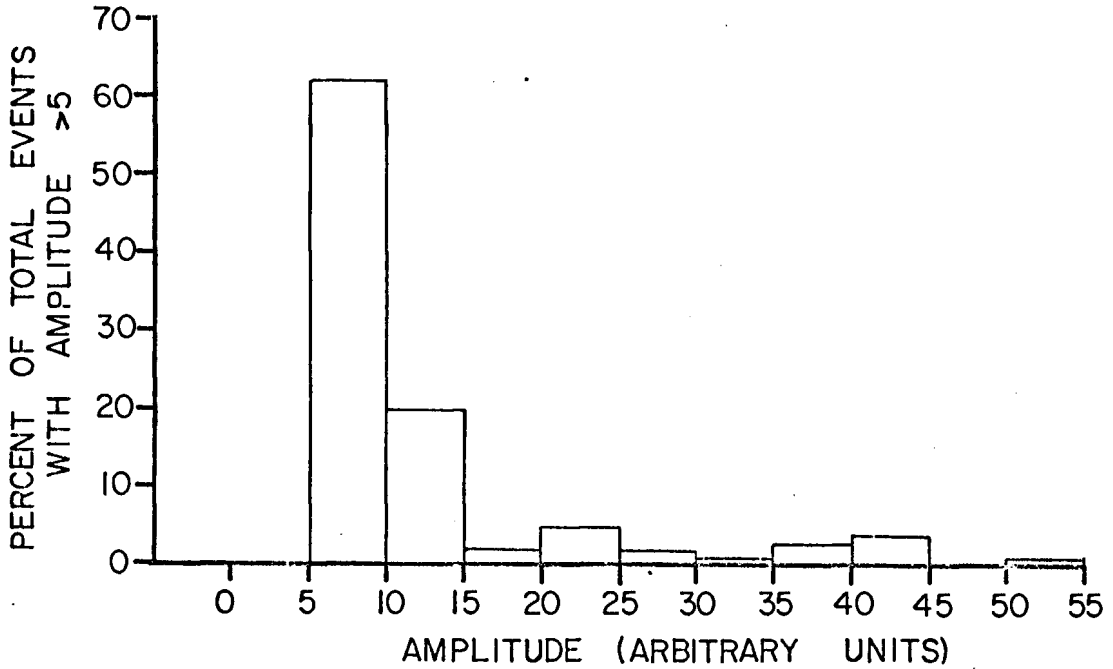


Figure 13. Amplitude distribution of impulsive events. The graph shows the percent of total events with amplitudes between values at intervals of five arbitrary units.

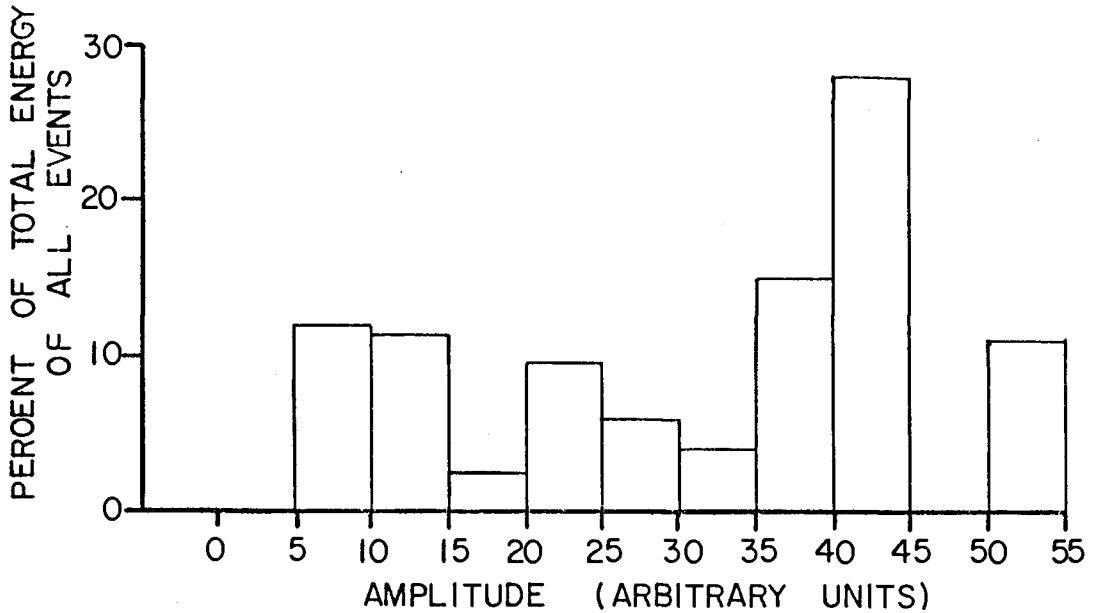


Figure 14. The proportion of total impulsive energy as a function of amplitude level. This graph is based on the data of Figure 13.

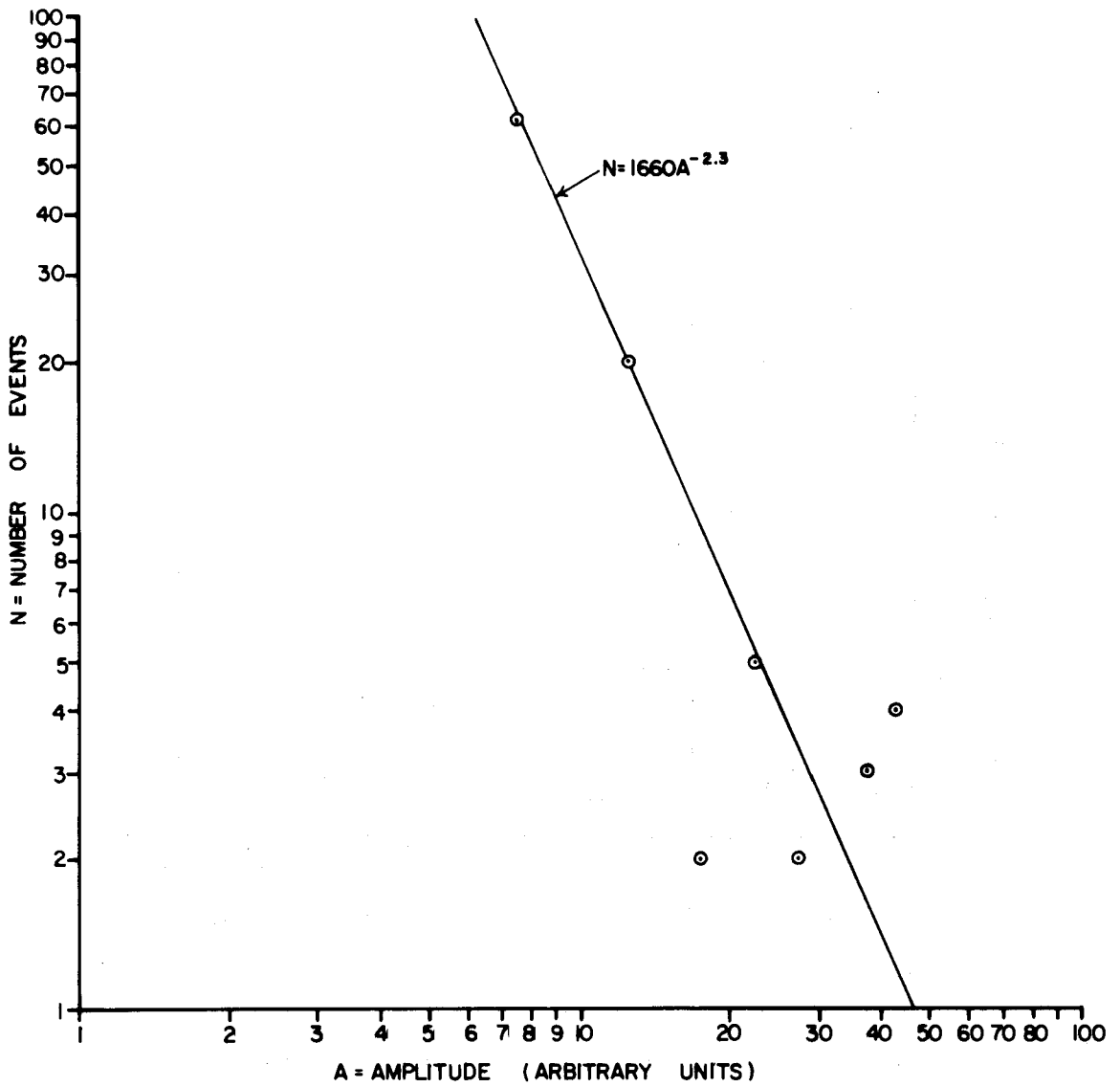


Figure 15. Power law relationship between number and amplitude of impulsive events. The exponent -2.3 gives the best fit.

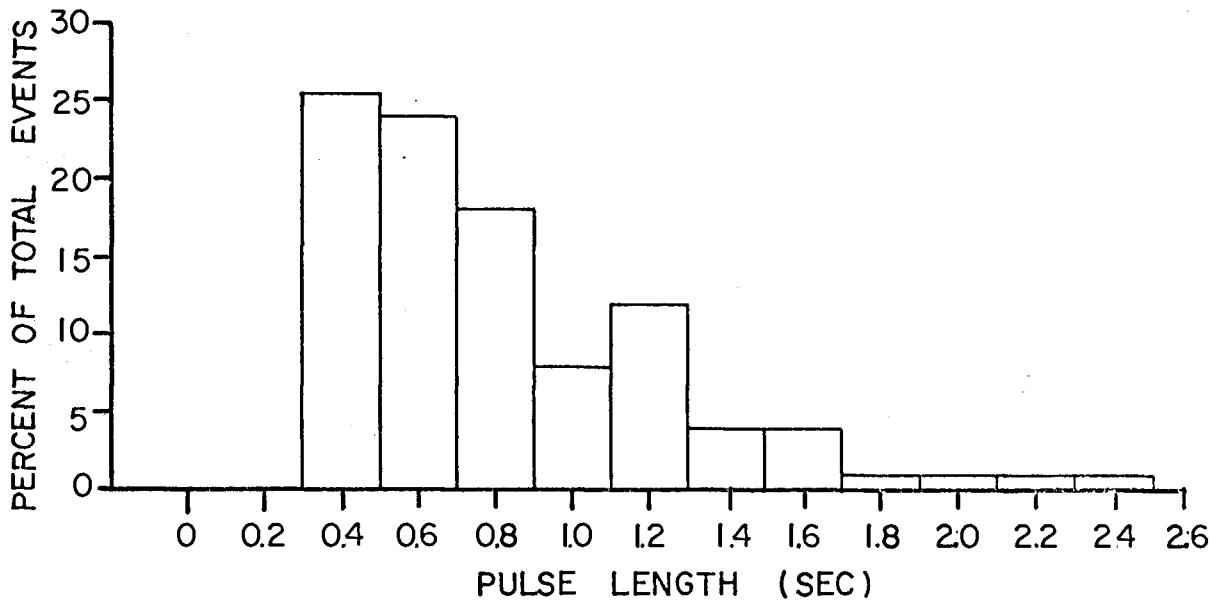


Figure 16. Percentage distribution of impulsive events according to pulse length at intervals of 0.2 second.

If this value is representative of the whole period of seven days, then an average of only 13.7 seconds per hour was occupied by impulsive shocks.

In Figure 10 the rate of impulse occurrence is plotted against time on a 24-hour basis. The values are 3-day averages of the mean number of impulses per hour for 3-hour periods centered about the times of meteorological observations. The three days chosen were good record days for which complete meteorological observations were available. Figure 17 shows the 3-hourly temperatures averaged for the same three days. Data are given for the three weather shelters in the confluence area: Kaskawulsh Camp, about 100 m. from the seismograph station, and "Ice" and "Knoll" stations (Fig. 3). From the data for Kaskawulsh Camp, the mean rates of change of temperature during the periods between observations were calculated and plotted in Figure 10.

The maximum impulse rate occurred in the early evening and lagged six hours behind the temperature and wind velocity peaks. The maximum occurred close to the time of greatest rate of temperature decrease. This suggests a close relation to thermal contraction, as mentioned in the preceding section. However, the impulse rate was moderately high when the temperature was barely changing, so other factors were obviously involved. The minimum impulse rate occurred near the time of temperature minimum.

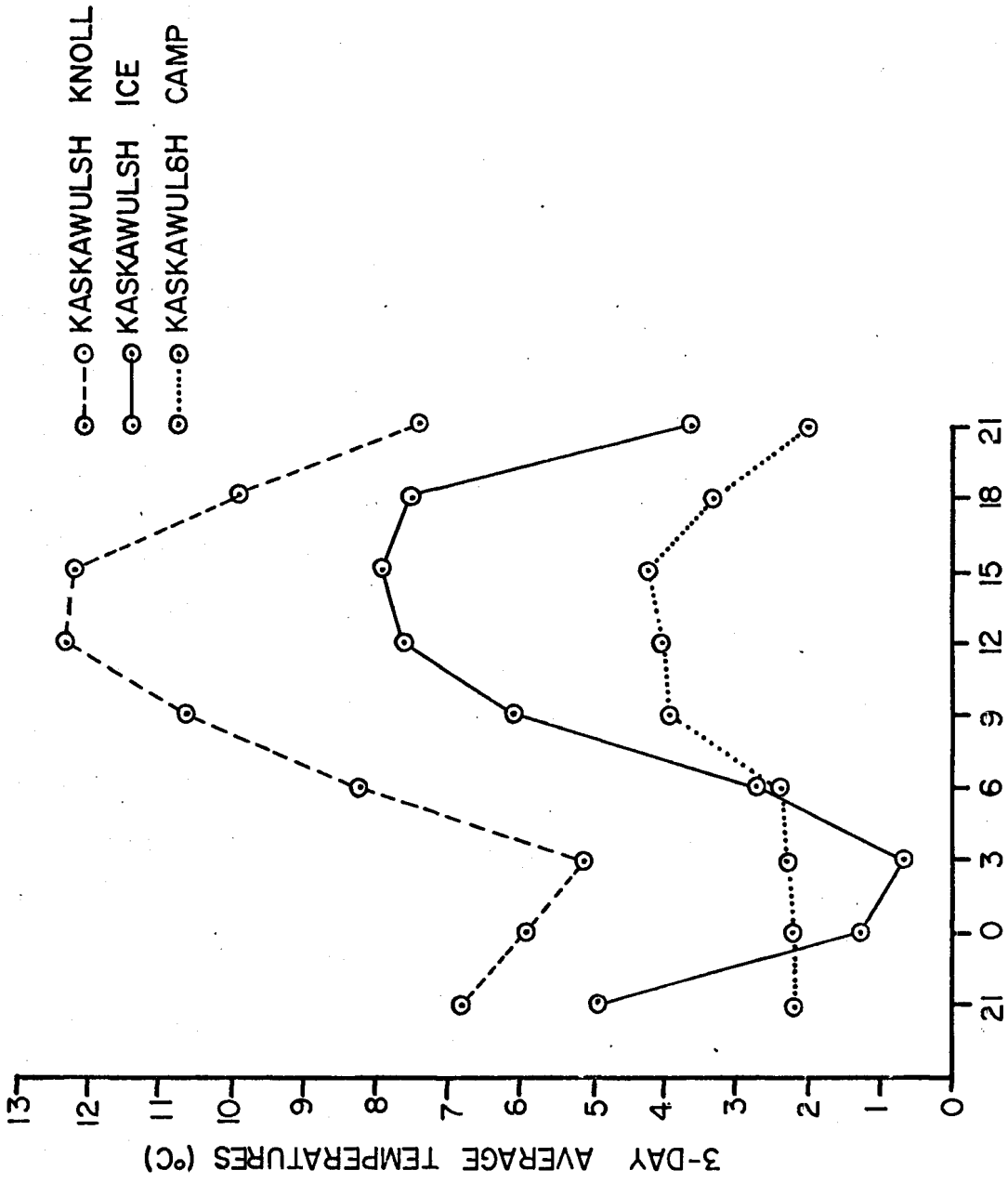


Figure 17. Temperature at 3-hourly intervals averaged for August 5, 6, and 12, 1965 at Kaskawulsh Camp, "Ice," and "Knoll" weather stations.

These data also show that the impulsive noise reached its maximum several hours after the continuous noise started to recede from its maximum. In fact, this was one of the best times for seismic exploration in mid-summer: the wind had abated and light was still adequate.

Delsner (1965) measured acoustic impulses which he termed "eigenimpulses" on the Lovenbreen Glacier in West Spitzbergen during August, 1964. They were recorded at three locations on the terminus and the central part of the glacier by a geophone-amplifier system tuned to the 0-500 Hz. frequency range. The impulse lengths were 0.3 to 0.5 seconds and the dominant frequency was around 60 Hz. The times of maxima varied with location: those on the terminus peaked around midday while those farther up the glacier peaked near midnight. The diurnal temperature variations were much less regular than on the Kaskawulsh Glacier but a 3-hour phase shift was found between temperature and eigenimpulse rate maxima. Atmospheric pressure variations on the Kaskawulsh Glacier had such long periods that comparison with the relatively short time segments of the noise records are not meaningful. However, the Lovenbreen records covered several cycles of pressure fluctuations. Delsner attributed 82 percent of the eigenimpulse power to temperature and pressure fluctuations and the rest to "jerky" movements of the glacier, with a periodicity of 20 to 115 minutes. These were correlated with runoff values and the discontinuous motion was attributed to the influence of a lubricating

water layer in accordance with the ideas of Weertman (1957, 1964).

Delaner's eigenimpulses undoubtedly represent the high frequency components of the same type of disturbance as those observed on the Kaskawulsh Glacier. No stream flow measurements were made on the Kaskawulsh Glacier, but a qualitative estimate would place their maximum late in the afternoon. This is somewhat behind the temperature peak and on the upswing of the impulse rate curve (Fig. 10).

Thermodynamic relations

The fragmentation of an aggregate of ice grains is intensified by the thermoelastic anisotropy of the ice crystal, which changes in shape as well as size in response to temperature change (Fig. 18). The relationship between the temperature coefficients of expansion follows from the first and second laws of thermodynamics, in terms of the strain energy functions. It will be developed at some length here in order to establish some of the principles used in the discussion of elastic constants that follows.

The first law of thermodynamics states that the change in the total internal energy of a body is equal to the change in the potential energy plus the added heat energy:

$$d U = dW + dQ \quad . . . (22)$$

where U is the internal energy, W is potential energy, and Q is heat energy.

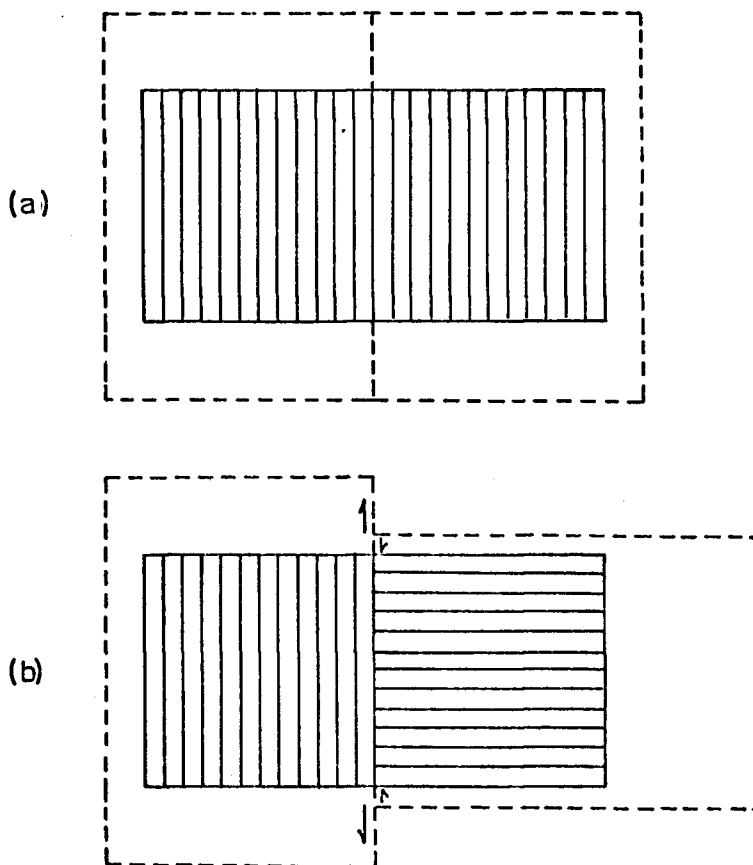


Figure 18. Thermo-elastic strains between two crystals in contact. Parallel lines indicate direction of greater thermal expansion coefficient. Dashed lines indicate crystal outlines after expansion. In (a) there are no shearing strains between the crystals. In (b) shearing strains occur along the boundary because of the different rates of expansion.

The second law defines the entropy relationship between the temperature and the change in heat energy, and can be written in the form:

$$\frac{dQ}{T} \leq S \quad \dots (23)$$

where S is the entropy (2.08 joules/g. °K. at 273° K.), and T is the absolute temperature.

From (22) and (23):

$$dU = dW + TdS \quad \dots (24)$$

The potential energy can be written in terms of elastic strain energy:

$$dW = \sum_{i=1}^6 \sigma_i dE_i \quad \dots (25)$$

so:

$$dU = (\sigma_1 dE_1 + \sigma_2 dE_2 + \sigma_3 dE_3 + \sigma_4 dE_4 + \sigma_5 dE_5 + \sigma_6 dE_6) + TdS \quad \dots (26)$$

To express the strain and entropy in terms of the stresses and temperatures, the Gibbs function, G , is introduced:

$$G = U - \sigma_i E_i - TS \quad dg = -E_i d\sigma_i - SdT \quad \dots (27, 28)$$

then:

$$E_i = \frac{\partial G}{\partial \sigma_i} \quad S = - \frac{\partial G}{\partial T} \quad \dots (29, 30)$$

From the definition of total differential, the differential strains can be written in terms of the differentials of the stresses and temperatures:

$$\begin{aligned} \text{(a)} \quad dE_1 &= \frac{\partial E_1}{\partial \sigma_1} d\sigma_1 + \dots + \frac{\partial E_1}{\partial \sigma_6} d\sigma_6 + \frac{\partial E_1}{\partial T} dT \\ \text{(f)} \quad dE_6 &= \frac{\partial E_6}{\partial \sigma_1} d\sigma_1 + \dots + \frac{\partial E_6}{\partial \sigma_6} d\sigma_6 + \frac{\partial E_6}{\partial T} dT \quad \dots (31) \\ \text{(g)} \quad dS &= \frac{\partial S}{\partial \sigma_1} d\sigma_1 + \dots + \frac{\partial S}{\partial \sigma_6} d\sigma_6 + \frac{dS}{dT} dT \end{aligned}$$

The partial derivatives of the strains with respect to the stresses, at constant temperature, are the isothermal elastic compliances:

$$S_{ij}^T = \frac{\partial E_i}{\partial \sigma_j} \quad \dots (32)$$

The six partial derivatives of the strains with respect to the temperature in the last terms on the right-hand side of equations (31a) through (31f) are the temperature coefficients of expansion:

$$\alpha_1 = \frac{\partial E_1}{\partial T}, \dots, \alpha_6 = \frac{\partial E_6}{\partial T} \quad \dots (33)$$

Each coefficient corresponds to one of the components of the strain tensor. For the purposes of linear measurement the coefficients are defined as:

$$\alpha = \frac{1}{l_0} \left(\frac{\delta l}{\delta T} \right)_\sigma \approx \frac{l_2 - l_1}{l_0(T_2 - T_1)} \quad \dots (34)$$

where l_0 = length of specimen at 0° C.

Using equations (29,30) the temperature coefficients can also be derived in terms of the entropy and stress:

$$\alpha_i = \frac{\partial E_i}{\partial T} = - \frac{\partial}{\partial T} \left(\frac{\partial G}{\partial \sigma_i} \right) \quad \dots (35)$$

∂G is an exact differential, so:

$$- \frac{\partial}{\partial T} \left(\frac{\partial G}{\partial \sigma_i} \right) = \frac{\partial^2 G}{\partial \sigma_i \partial T} = \frac{\partial}{\partial \sigma_i} \left(\frac{\partial G}{\partial T} \right) = \frac{\partial S}{\partial \sigma_i} \quad \dots (36)$$

The six temperature coefficients α_i can be expressed as the components of a 3x3 symmetric matrix α_i .

All six are non-zero for an asymmetric, i.e., triclinic crystalline substance. The symmetry relations of hexagonal, trigonal and tetragonal crystals and for transverse isotropy exclude the shear components and require that all deformations

perpendicular to the axis of symmetry be equal. Hence, the matrix for ice is diagonal and has only two independent components:

$$(\alpha_i) = \begin{pmatrix} \alpha_1 & 0 & 0 \\ 0 & \alpha_1 & 0 \\ 0 & 0 & \alpha_3 \end{pmatrix} \dots (37)$$

Thus the ice crystal expands upon heating at a different rate along the C-axis (coefficient α_3) than in any direction perpendicular to the C-axis (coefficient α_1). Experimental determinations of the linear coefficients of thermal expansion of ice are not very satisfactory. Dorsey (1940) cited data which indicated little difference between the coefficients perpendicular to the C-axis (α_1) and parallel to the C-axis (α_3). However, La Placa and Post (1960) found that the coefficients were approximately proportional to the dimensions of the unit cell of the ice crystal:

$$\begin{aligned} \alpha_1 &= 4.6 \times 10^{-5} \text{ per } ^\circ\text{C.} \\ \alpha_3 &= 6.3 \times 10^{-5} \text{ per } ^\circ\text{C.} \end{aligned} \quad \text{between } -10^\circ \text{ C. and } -20^\circ\text{C.}$$

If this large difference between α_1 and α_3 is assumed, then an aggregate of randomly oriented ice crystals undergoing cooling will be subjected not only to tensile stresses but also to shearing stresses. According to Butkovich (1959) the shearing strength of ice is similar in magnitude to its tensile strength. It is possible, then, that fracture through shear and consequent shear-wave production, can occur in situations of rapid cooling.

Elastic constants.

The elastic constants in equation (32) are determined under isothermal conditions. In general, the adiabatic elastic constants differ from these, and it is with the adiabatic constants that one is chiefly concerned in seismic work. With a rapidly vibrating body little heat is added or subtracted from any elemental volume, and the elastic constants are determined under adiabatic conditions.

Consider again the expressions for the differentials of strain in equations (31). Since there are no residual strains or stresses, let $dE_i \rightarrow E_i$ and $d\sigma_i \rightarrow \sigma_i$. Then by multiplying equation (31g) by T and using the relation of equation (23), the following equations are obtained:

$$\begin{aligned} \text{(a)} \quad E_1 &= S_{11}^T \sigma_1 + \dots + S_{16}^T \sigma_6 + \alpha_1 dT \\ \vdots \\ \text{(f)} \quad E_6 &= S_{16}^T \sigma_1 + \dots + S_{66}^T \sigma_6 + \alpha_6 dT \quad \dots \quad (38) \\ \text{(g)} \quad TdS &= dQ = T (\alpha_1 \sigma_1 + \dots + \alpha_6 \sigma_6) + T \frac{\partial S}{\partial T} dT \end{aligned}$$

The total heat capacity of a unit volume of a body at constant stress is:

$$\rho C_p = T \frac{\partial S}{\partial T} = \frac{\partial Q}{\partial T} \quad \dots \quad (39)$$

where ρ is the density and C_p is the heat capacity at constant stress per gram of the material. The last term on the right-hand side of equation (38g) is then $\rho C_p dT$.

The adiabatic compliances, S_{ij}^S , correspond to the isentropic condition: no heat loss from the volume element:

$$dQ = 0 \quad \dots \quad (40)$$

Then (38g) becomes:

$$T (\alpha_1 \sigma_1 + \dots + \alpha_6 \sigma_6) + \rho C_p dT = 0 \quad \dots (41)$$

Eliminating dT from the set of seven equations (38a...f, 41), we obtain the six equations:

$$\begin{aligned} \text{(a)} \quad E_1 &= S_{11}^T - \frac{\alpha_1^2}{\rho C_p} \sigma_1 + \dots + S_{16}^T - \frac{\alpha_1 \alpha_6}{\rho C_p} \sigma_6 + \frac{\alpha_1}{\rho C_p} dQ \\ \vdots & \\ \text{(f)} \quad E_6 &= S_{16}^T - \frac{\alpha_1 \alpha_6}{\rho C_p} \sigma_1 + \dots + S_{66}^T - \frac{\alpha_6^2}{\rho C_p} \sigma_6 + \frac{\alpha_6}{\rho C_p} dQ \end{aligned} \quad \dots (42)$$

The adiabatic compliances are then defined as the new coefficients of the stresses:

$$S_{ij}^s = S_{ij}^T - \frac{\alpha_i \alpha_j T}{\rho C_p} \quad \dots (43)$$

A direct determination of the adiabatic elastic compliances S_{ij}^s of ice was made by Baas, Rossberg and Ziegler (1957). They measured the natural frequencies of single crystal rods (for S_{11} , S_{33} , S_{13} , and S_{44}) and plates (for S_{12}) under various modes of vibration: longitudinal for S_{11} , S_{13} , and S_{33} ; torsional for S_{44} ; radial and surface for S_{12} . The frequency of oscillation was varied from 5 to 50 kHz, and the temperature from -2 to -30° C. (accurate to 0.25° C.). The test specimens were machined from large single ice crystals. The angular measurements of C-axis inclination, measured under crossed polaroids, were reported to be accurate to 0.1 degree; the angle between rod axis and plate normal to less than 1 degree. The compliances were found to be strongly temperature dependent. The authors give the following values at -16° C.:

$$S_{11} = 10.13 \pm 0.05 \times 10^{-12} \text{ cm.}^2/\text{dyne}$$

$$S_{22} = -4.16 \pm 0.15 \times 10^{-12} \text{ cm.}^2/\text{dyne}$$

$$S_{13} = -1.93 \pm 0.21 \times 10^{-12} \text{ cm.}^2/\text{dyne}$$

$$S_{33} = 8.28 \pm 0.04 \times 10^{-12} \text{ cm.}^2/\text{dyne}$$

$$S_{44} = 32.65 \pm 0.15 \times 10^{-12} \text{ cm.}^2/\text{dyne}$$

Assuming the following values for ice for $T = -16^\circ \text{ C.}$
(257.1° K.) (Dorsey, 1940);

$$C_p = 1.973 \times 10^7 \text{ erg/g.}$$

$$\rho = 0.91 \text{ g./cm.}^3$$

$$\alpha_1 = \alpha_2 = 51.1 \times 10^{-6} \text{ per } ^\circ\text{K.}$$

$$\alpha_3 = 51.8 \times 10^{-6} \text{ per } ^\circ\text{K.}$$

The values of $S_{ij}^T = S_{ij}^S + \frac{\alpha_i \alpha_j T}{\rho C_p}$ are:

$$S_{11} = 10.17 \times 10^{-12} \text{ cm.}^2/\text{dyne}$$

$$S_{12} = -4.12 \times 10^{-12} \text{ cm.}^2/\text{dyne}$$

$$S_{13} = -1.89 \times 10^{-12} \text{ cm.}^2/\text{dyne}$$

$$S_{33} = 8.32 \times 10^{-12} \text{ cm.}^2/\text{dyne}$$

$S_{44} = 32.65 \times 10^{-12} \text{ cm.}^2/\text{dyne}$ (in this case the values are identical because $\alpha_4 = 0$ (equation 37)).

Comparison of the adiabatic with the isothermal compliances indicates that the differences are smaller than the accuracy of the measurements of the constants. Since the difference is so small no distinction will be made here between the adiabatic and isothermal elastic constants. It is assumed that as far as thermal considerations are concerned elastic constants determined dynamically (e.g., by

means of seismic waves) are equivalent to those determined from static tests.

Mechanically there is also a possible discrepancy between static and dynamic constants. Simmons and Brace (1965) found that at atmospheric pressure the compressibility of fused quartz, steel, aluminum and fine-grained limestone calculated from measured velocities of ultrasonic compressional and shear waves did not differ significantly from compressibility measured directly by means of strain gages. However, for some granites the statically and dynamically determined constants differed by large amounts. At high pressure (2-3 kilobars) good agreement was also obtained with the granites. Simmons and Brace attributed the discrepancies in the low-pressure values for the granites to the presence of minute cracks which were closed and ceased to have any effect at high pressure.

It is not known to what extent these considerations are valid for glacier ice. However, in a later section the effect of small pores on the elastic constants of ice will be considered.

Mechanical sources

Non-thermally generated impulses of the type Oelsner associated with glacier flow have been observed under laboratory conditions. Acoustic energy generated by cracking arising from the creep of ice was recorded by Gold (1960) in his investigation of the influence of small fractures in the mechanism of creep.

Depending on the magnitude of the stress and on the time scale of the deformation, three stages or types of creep are observed in general in a specimen subjected to uniaxial stress (Fig. 19):

(1) Transient or primary creep. This corresponds to Griggs' (1939) "elastic flow." It represents the early stages of a long-term creep process or a low stress situation in short-term creep. For most substances the creep rate has a power law relation with time:

$$\dot{\epsilon} = At^{-n} \quad . . . (44)$$

where A and n are constants which depend on the material and the conditions under which the process takes place. n lies between 0 and 1 and for most substances $n = 1$ or $2/3$. In the former case, the process is called alpha creep; in the latter, beta creep. Ice has been found to exhibit beta creep in this stage (Glen, 1955). Setting $n = 2/3$ and integrating (44) one obtains the "Andrade Law" expressing the strain-time relationship for ice and polycrystalline metals:

$$\epsilon = 8t^{1/3} \quad . . . (45)$$

(2) Steady-state, or secondary creep. This corresponds to Griggs' "pseudoviscous flow." It is the second stage in a long-term process and occurs at intermediate stresses in short-term creep. It corresponds to the minimum observed strain rate. The general equation is:

$$\dot{\epsilon} = D \exp \left(\frac{w - q_s}{k_b T} \right) \quad . . . (46)$$

where w is the activation energy for creep to occur, T is

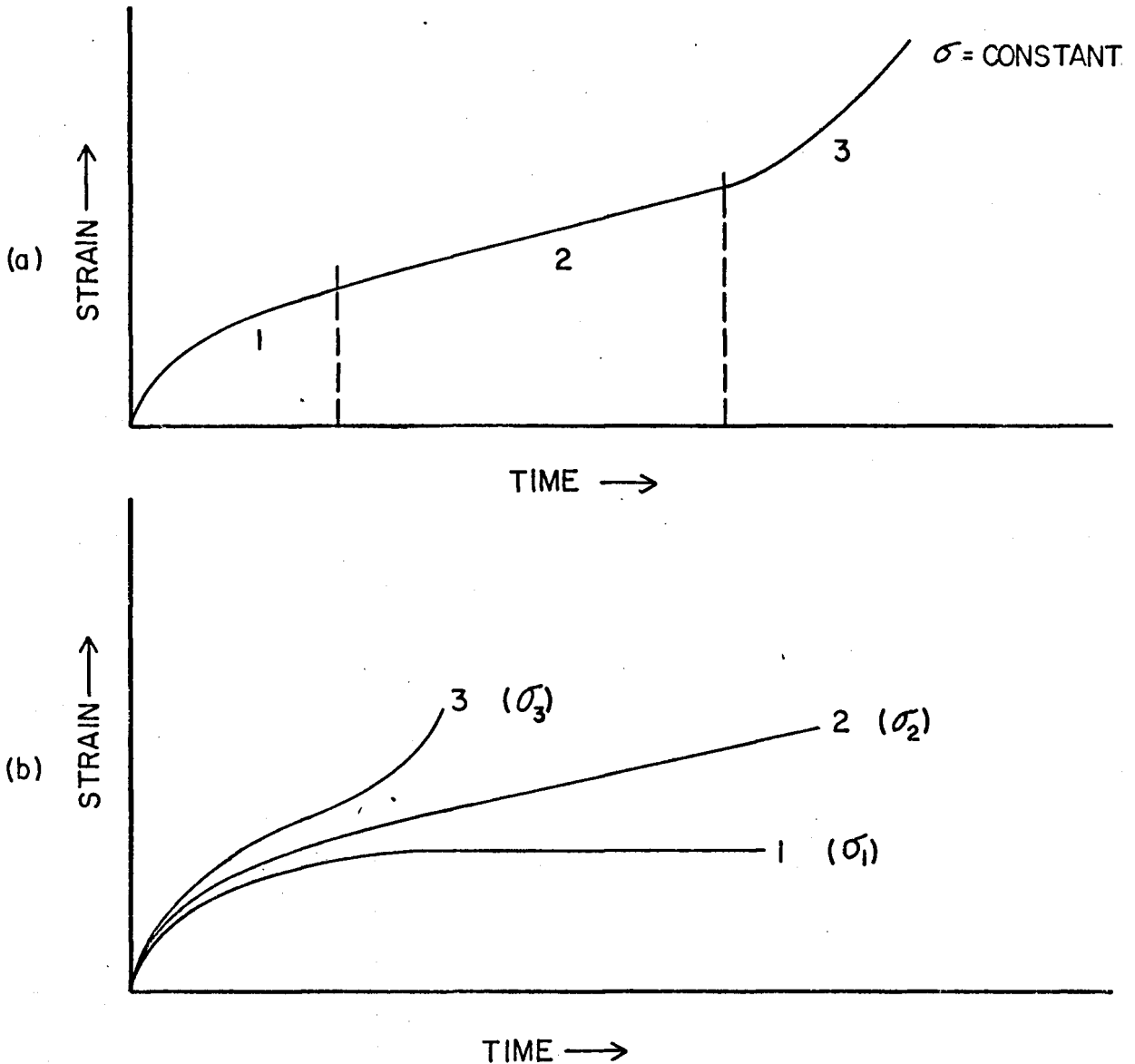


Figure 19. Strain-time curves for: (a) long-term creep; (b) short-term creep. In (a) the stress σ is held constant for a long period of time. In (b) the time scale is much shorter and $\sigma_1 < \sigma_2 < \sigma_3$. In each diagram: 1 = transient (primary) creep; 2 = steady-state (secondary) creep; 3 = accelerating (tertiary) creep.

absolute temperature, k_b is the Boltzmann constant, and D and g_s are parameters which depend on the material. For ice, Glen (1958) has found the relation:

$$E = c \sigma^\beta \quad . . . (47)$$

to be applicable. c is a constant and β increases with σ within the range $1.85 < \beta < 4.16$ for $1 < \sigma < 15 \text{ kg./cm}^2$.

(3) Accelerating creep (Tertiary creep) is observed during the last stage of long-term creep or under high stress for short-term creep. It involves rapid increase in the strain rate and leads to failure of the material through rupture.

Gold (1960) observed two surges of micro-shocks associated with cracking produced during creep. The tests were performed under uniaxial compressive stress at a constant temperature of -10°C . between 9 and 16 kg./cm^2 . The first surge occurred during the transient stage of creep (stage 1, above). The plane of the small cracks tended to be parallel to the grain boundaries and to the direction of the stress, i.e., they were tensile cracks. The rate at which these shocks occurred decreased very markedly as the creep rate approached a constant value (stage 2). During stage 3 creep, the shocks increased again. A logarithmic relation was found between total cracking activity and stress during the transient stage:

$$N = 10^{-4} e^{1.03 \sigma} \quad . . . (48)$$

where N is the number of events and σ is in kg./cm^2 .

It is clear then that eigenimpulses are produced during the creep process in ice and are to be expected from a mass of ice under stress. Following rupture the propagation of cracks produces elastic waves in the compressional and shear modes whose radiation patterns are determined by the velocity of crack propagation (Knopoff and Gilbert, 1960).

There is field evidence (Anderton, 1967) that the Kaskawulsh Glacier seismograph station was located in a region of tensile stress in which cracks were actively propagating. The station was surrounded by a zone of transverse crevasses of small size: less than $\frac{1}{2}$ m. wide and several tens of meters long. Several of these crevasses were observed to enlarge during the summer of 1965. One small crevasse appeared under the moraine near the camp after several days of loud crackling sounds. Presumably the sounds are related to the deformation but it is not known whether or not these audible signals represent the same type of disturbance as the recorded eigenimpulses. Nor is it known whether the initial opening of crevasses and their widening and lengthening take place at such a rate as to produce elastic disturbances in the same frequency range as those recorded. It was not possible to test whether regions with high rates of crevasse formation had higher eigenimpulse rates than more stable regions. However, these mechanisms are put forward as plausible contributors to eigenimpulse production.

The deformation process leading up to the formation of crevasses may also play a part in causing eigenimpulses.

The following factors suggest that they are related:

(1) Crevasses exist and appear to form in the vicinity of the seismograph station.

(2) Crevasses represent ruptures that have occurred within the ice body.

(3) Prior to the rupture that produced the crevasse the ice in the immediate vicinity of the future crevasse must have experienced rapidly accelerating strain, i.e., it must have gone through the process of tertiary creep.

(4) Gold (1960) found that tertiary creep in ice is accompanied by microfracturing and the production of eigenimpulses. Gold's experiments involved compressive stress, whereas the crevasses in question are apparently caused by tensile stress. However, Gold's microfractures were also genetically tensile: they developed perpendicular to the directions of principal tensile stress.

Studies of "eigenimpulses" were originally made by Obert and Duvall (1945, 1957, 1961) in mines threatened by slumping and rockbursts. They found that regions of high stress could be delineated by measurements of the rate and amplitude of small shocks, which they called "microseisms." The rate of shock occurrence was found to be proportional to the rate of change of pressure in the rock. This was true whether the change was positive or negative, though the proportionality function was greater for increases in

pressure. Although the shocks were strongly generated both immediately before and concurrently with the occurrence of visible cracking, the magnitude of the ground movement did not have to result in visible cracking to produce shocks. The rate was found to vary widely with the physical properties of the rock, being highest for coarse-grained rock and lowest for fine-grained metamorphic rock containing lubricating constituents, e.g., mica and talc.

The counterpart to deep mines may exist in glaciers. Crevasses are limited to the upper layers where tensile stresses can exist (Nye, 1951), but moulins go considerably deeper. The greatest depth measured on the Kaskawulsh Glacier was 65 m. This may have been only the first plunge step. In hard rock mines where the rocks have ultimate compressive strengths of the order of 100 kg./cm.^2 rockbursts occur at depths where one-fifth or more of that stress is attained. Relatively pure ice has an unconfined compressive strength of $35\text{-}60 \text{ kg./cm.}^2$ and the value for glacier ice, with its imperfections and inclusions, is probably lower. At 65 m. depth the hydrostatic pressure is about 6 kg./cm.^2 . It is conceivable that stress concentrations in the ice tunnels may exceed the breaking strengths of the ice locally and produce "icebursts."

3.4 Earthquakes

Earthquakes produce both impulsive and continuous noise. The arrival of prominent phases is impulsive but most earthquake energy can be considered continuous in relation to the short spans of time involved in exploration seismic recording. The possibility of high small-earthquake seismicity in the Kaskawulsh area has been discussed above. It should be noted that the high relief of the terrain and the complexity of the geology afford the possibility of a wide variety of reflection and refraction effects on waves arriving from shallow local foci.

Several earthquakes were recorded by the station. Their proportion of the total recording time was very small. The largest was determined by the time lapse between P- and S-waves to have occurred at an epicentral distance of about 350 km. The azimuth was not determined but this is approximately the distance to Prince William Sound and the earthquake may have been one of the long train of aftershocks of the great earthquake of March 28, 1964 (Hansen, et al., 1966; Wood, 1966).

The smallest S-P time noticed was 2.4 seconds. If we assume velocities in rock of 5.57 km./sec. for compressional waves and 3.34 km./sec. for shear waves in the upper layer of the earth's crust (Jeffreys and Bullen, 1948), we obtain a focal distance of 5.3 km. for an all-rock path. Assuming values of $V_p = 3.70$ km./sec. and $V_s = 1.90$ km./sec. for ice,

the focal distance is only 4.8 km. for an all-ice path. Such a shock could have occurred within the part of the glacier under investigation.

3.5 Avalanches

As might be expected from the physiographic description, the steep gulleys on the walls of the Kaskawulsh Glacier are the scene of frequent rock slides. The collisions between boulders can be detected by ear from one side of the glacier to the other. The hanging glaciers above them dislodge masses of ice and snow continually. Sometimes crevasse blocks as large as houses fall hundreds of meters. The times of large observed avalanches were checked against the seismograph record and found to coincide with the type 4 "extended disturbances." Avalanche noise may begin impulsively but as secondary slides are started and the fragments gradually roll to a stop the vibration passes into a prolonged dull rumble of incoherent noise. An average of two large disturbances of this nature, with duration of more than one minute, were recorded per 12 hours of seismograph operation.

3.6 Summary

Seismic noise from several different sources and having differing characteristics was identified on the Kaskawulsh Glacier. The most important from the standpoint of

disturbance on the exploration seismic records was continuous noise. It was found that the time periods during which noise on the exploration seismograph records (frequency 30-200 Hz.) was most troublesome coincided with periods when continuous noise recorded by the station seismograph (frequency 0.5-2 Hz.) was at maximum amplitude. It was concluded that these relatively high and low frequency waves represented parts of the spectrum of the same general type of noise. The major part of this noise appeared to be caused by wind. Other sources of continuous noise that may have been significant were running water and the explosive release of air pressure from bubbles in the ice. Seiches and distant microseismic activity were probably unimportant.

Impulsive noise ("eigenimpulse") was less of a disturbance in the exploration seismological work. It appeared to be associated with thermal contraction during periods of rapid cooling. Other sources of impulsive noise may be the creation and expansion of cracks due to stress conditions within the ice or at the ice-rock interface. Impulse noise may be related to crevasse and moulin formation but no direct evidence exists for this.

Seismic energy from earthquakes and avalanches was recorded, but its frequency of occurrence was insignificant compared with that of eigenimpulses. Avalanche signals were longer in duration than any of the others and were found characteristically to build rapidly to maximum amplitude, then gradually die away.

In general, it may be said that seismic noise on the glacier was predominantly caused by climatic factors -- wind and temperature changes. Noise related to movement of the glacier appeared to be of secondary importance. The extent to which the glacier was a "noisy" place seismically was chiefly the result of the climatic nature of the region. Running water was not an important source of noise but in the course of these investigations it was discovered that the drainage of water from the surface of the glacier involved an extensive system of shafts and tunnels deep within the glacier.

Practically speaking, the quietest part of the day for seismic investigation during the summer was the period from 1500 to 2400 hours, local time.

CHAPTER IV

WIDE-ANGLE REFLECTION SURVEY

4.1 Introduction

The determination of the average velocity of seismic waves through the body of the glacier is essential for the calculation of the depth and configuration of the average elastic properties of glacier ice.

Serious problems arise because of the inhomogeneity of the ice and the variability of the sub-glacial terrain. In the first place, there is no guarantee that the average velocity of waves traveling between the top and bottom of the glacier in a region where such velocity can be easily measured is the same as in other regions where this velocity must be assumed in order to obtain the ice thickness and the orientation of the glacier bed. Secondly, the more valid the velocity value to be obtained, the greater must be the areal extent of sub-glacial topography that must serve as a reflecting or refracting interface.

With these considerations in view, the location of a site for the measurement of average velocity was delayed until some idea of the subsurface had been obtained from

the reflection survey. At this stage an assumed value of average velocity was used in the latter. The survey indicated that the glacier bed was relatively smooth and its slope constant on the Central Arm just below the confluence. This is also a region where the morphology is of considerable interest.

The wide-angle reflection profile was laid out from station 1D to 1B (Fig. 3), a distance of 583.4 m., and beyond, in a straight line, for a total length of 944.9 m. It crosses the direction of flow of the surface ice and the foliation bands at varying angles. The slope from 1D to 1B is about 2%. Beyond 1B the surface is nearly horizontal, so there is a slight concavity in the profile when viewed in a vertical plane, and the direct waves are slightly diffracted.

This is one of the few extensive regions of the glacier in which there are no crevasses. The nearest ones are on the medial moraine, 50-100 m. away. Snow was entirely gone from the surface by the time work began on the profile. A pond which collected meltwater from the surrounding glacier surface had covered part of the profile during the early summer. There is apparently an intricate subsurface drainage system in this part of the glacier (see Section 3.2).

The cable was laid out in overlapping spreads along the profile. Shot points were established at both ends of the line. The forward profile (1D to the down-glacier end)

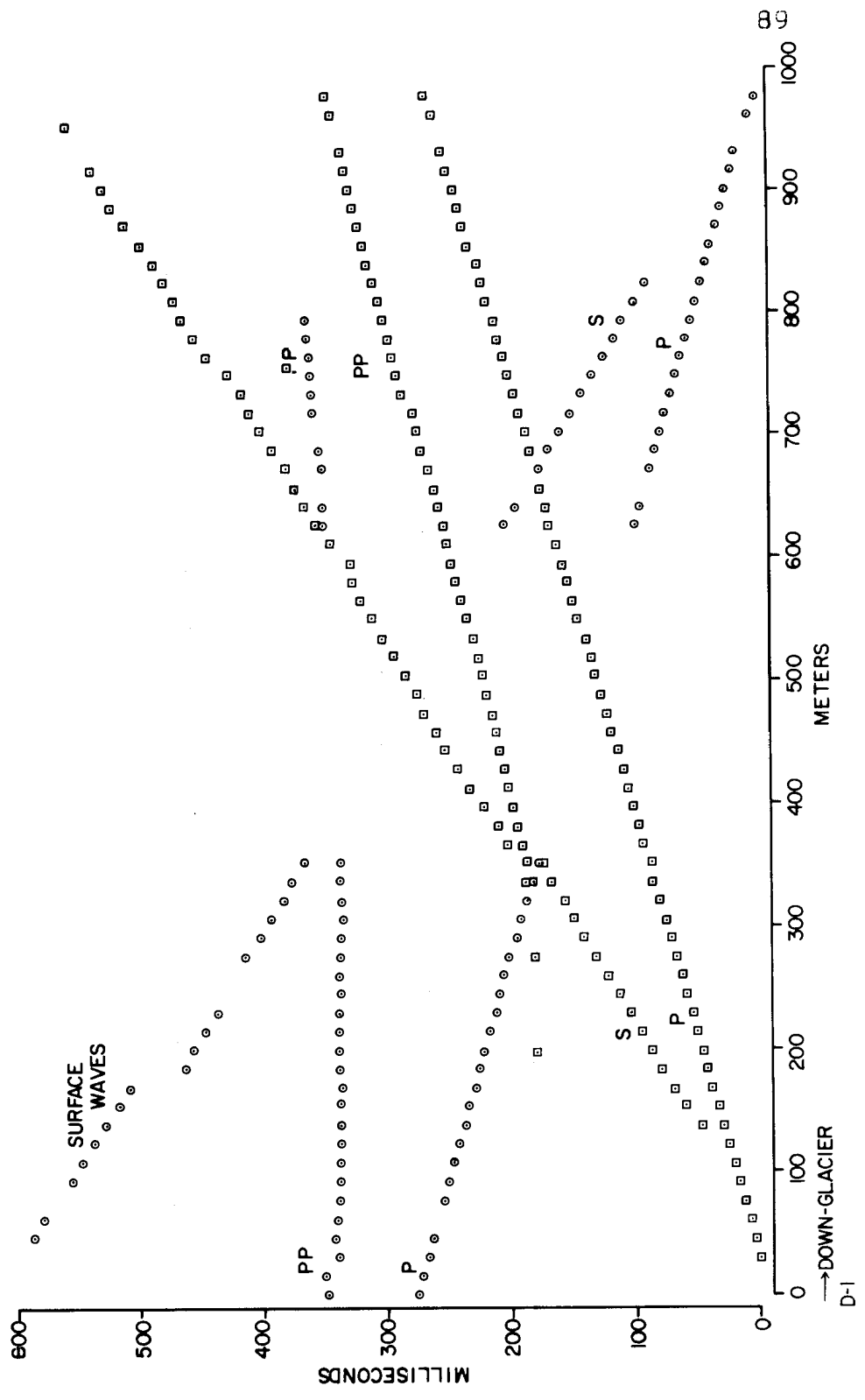
was completely covered. Most of the profile was also shot in the reverse direction. The reverse profile was extended two geophone separations (30.48 m.) beyond 1D so that the total reverse profile length was 975.4 m. Spreads 183 m. long transverse to the profile were shot at 1D, 18 and the end.

The shot holes were bored to 4.5 m. to contain the charges of up to $12\frac{1}{2}$ pounds (5.7 kg.) that were necessary for the most distant spreads. The larger shots (3.4-5.7 kg.) shattered the sides of the holes after three or four shots and at each end of the profile holes had to be re-drilled.

Most of the geophones were oriented in the vertical direction to register the vertical component of reflected compressional wave motion. At least one in each spread was oriented in the transverse horizontal position and one in the longitudinal horizontal position, relative to the profile direction, in order to distinguish direct and reflected shear waves.

The time-distance plot of the definitely-observed phases for the forward and reverse profiles is presented in Figure 20. These phases are the direct compressional, direct shear, surface, and first reflected compressional phases, which will be designated P, S, L and PP, respectively. Vertically and horizontally, polarized shear waves will be called S_v and S_h , respectively.

Figure 20. Time-distance plots of the wide-angle reflection profile.



4.2 Direct P Waves

The P phase was recorded strongly on both the forward and reverse profiles out to about 800 m. Beyond that range its amplitude became small and the first breaks became less distinct. The P phase consisted of a train of 3-4 cycles, strongly represented at low frequencies (20-50 Hz.). The train spread only slightly with increasing distance from the source. The first breaks generally showed up strongly for all three mutually perpendicular orientations of the geophones. By recording at various frequency ranges an approximate spectral analysis was obtained which showed an amplitude peak at 30-35 Hz. Very distinct, almost perfectly sinusoidal waves with amplitude equal to about half of the value at 30-35 Hz. occurred with frequencies between 70 and 100 Hz.

The mean velocity of the P wave along the profile, computed as the least squares slope of the time-distance plot of the first arrivals, is:

$$\bar{V}_p = 3.586 \pm 0.040 \text{ km./sec.}$$

The error is the standard deviation due to scatter about the regression line. The error due to time (read to 0.1 msec.) and distance (read to 0.1 m.) measurement is about 0.002 km./sec.

Aside from the situation very near the surface, which will be described in the next chapter, the plot shows little evidence of increase in velocity with depth. It was divided

into segments which showed the same general slope and least-squares velocities across these segments are shown in Table 3,

The small variations here may indicate lateral inhomogeneity. Only in the last 120 m. of the profile is the velocity significantly different (approximately one standard deviation) from the mean. It may represent refraction from a deep layer of higher velocity.

If it is assumed that the terminal slope of the time-distance plot represents a ray refracted along the top of a high velocity layer with horizontal upper surface, we may use the simple refraction formula to obtain an estimate of the depth of the layer:

$$z = \frac{T_0 V}{2(1 - V_a^2/V_b^2)^{\frac{1}{2}}} \quad . . . (49)$$

where: z = depth to the lower layer

V_a = mean velocity in the upper layer

V_b = mean velocity in the lower layer

T_0 = intercept time of the segment of the time-distance plot with slope $1/V_b$.

Table 3. Mean cross-spread velocities of direct compressional waves (V_p) in glacier ice. The profile segments were distributed along a line 945 meters long. Shots were fired at each end.

Distance from Shot point (meters)	Mean V_p (kilometers per second)
15.2 - 182.9	3.60 \pm 0.02
198.1 - 335.3	3.55 \pm 0.03
350.5 - 533.4	3.58 \pm 0.04
548.6 - 670.6	3.56 \pm 0.03
585.8 - 807.7	3.60 \pm 0.04
823.0 - 944.9	3.63 \pm 0.04

If we take $V_a = 3.575$ km./sec. = the mean of the first five segments of Table 3, and $V_b = 3.53$ km./sec., the layer with velocity 3.53 km./sec. begins at depth of about 64 m. There could be deeper, higher velocity layers whose refracted rays do not show up within the limits of the profile. For example, again using equation (49), one finds that if ice in the upper layer has velocity $\bar{V}_p = 3.59$ km./sec., there could exist a layer in which the velocity is 4.00 km./sec. at depth of 128 m. or more which would remain undetected because the refracted waves would emerge beyond the end of the profile.

The only actual uphole velocity for depths greater than the 3-4 m. of the shot holes is from a shot fired in a moulin about 500 m. south of the profile. The shot was fired at 31.5 m. depth and the uphole velocity was 3.65 ± 0.05 km./sec. This is slightly higher than the velocities found above for the upper layer. It may reflect special conditions in the vicinity of the moulin, such as re-freezing of meltwater.

4.3 Direct S Waves

Direct shear waves are often difficult to distinguish from surface waves. It is sometimes necessary to examine the orbital motion at detector sites where all three components of ground motion were recorded. The vertically polarized shear waves, S_v , are often prominent. They often consist of

three or four waves with frequency 30-50 Hz. and amplitude comparable to that of the direct P waves. They are invariably followed by motion approximating the elliptical retrograde motion of Rayleigh waves. The commencement of the latter is usually indistinct. S_h was not definitely identified. The S-wave arrivals are first separable from the noise following the first breaks at a distance of 106.7 m. They can be followed fairly clearly out to shot point-detector separation of 731.5 m. Over this range the least-squares mean velocity is:

$$\bar{V}_s = 1.722 \pm 0.019 \text{ km./sec.}$$

4.4 Surface Waves

Beyond 731.5 m. the second direct phase that appears has velocity of only 1.63 km./sec. It probably is a Rayleigh wave, the shear wave being too weak to be detected at these distances. The velocity of the few coherent Rayleigh wave crests at shorter distances is 1.625 ± 0.025 km./sec. On the reverse profile weak arrivals with cross-spread velocity of about 1.74 km./sec. are registered between 807.7 m. and 944.9 m.

The low frequency (20-30 Hz.) Rayleigh waves are often protracted for 5-10 cycles. The Rayleigh waves do not exhibit any significant dispersion. This corroborates the evidence from the P wave studies (Section 4.2) that there

is no significant velocity gradient over depths comparable to the wave lengths of the Rayleigh waves, i.e., 10-100 m.

Knopoff (1952) has shown that the ratio of Rayleigh wave velocity, V_r , to shear wave velocity, V_s , can be determined as a function of Poisson's ratio, M . Love's equation relating shear, compressional and Rayleigh wave velocities is written in the form:

$$\left(\frac{V_p}{V_s}\right)^2 = \frac{16 - 24(V_r/V_s)^2 + 8(V_r/V_s)^4 - (V_r/V_s)^6}{16 [1 - (V_r/V_s)^2]} \dots (50)$$

Values of $(V_p/V_s)^2$ are determined for values of $(V_r/V_s)^2$, and the $(V_p/V_s)^2$ values are used to determine values of M :

$$M = \frac{(V_p/V_s)^2 - 1}{2 [(V_p/V_s)^2 - 1]} \dots (51)$$

$(V_r/V_s)^2$ is then plotted against M . For the average, near-surface compressional and shear wave velocities calculated above this yields:

$$M = 0.350 \quad \frac{V_r}{V_s} = 0.935 \quad V_r = 1.610 \text{ km./sec.}$$

It must be emphasized that this solution is for a homogeneous, isotropic, perfectly elastic medium and can only be an approximation to the values for the case of glacier ice. However, the Rayleigh wave velocity calculated on this basis is in fair agreement with the observed values.

4.5 Elastic Constants

The isotropic elastic constants can be determined from the observed velocities by using the standard formulae (Nicholls, 1961):

$$E = \frac{\rho V_s^2 \left[3 \left(\frac{V_p}{V_s} \right)^2 - 4 \right]}{\left(\frac{V_p}{V_s} \right)^2 - 1} = 7.284 \times 10^{10} \text{ dyne/cm.}^2 \quad \dots (52)$$

$$\mu = \rho V_s^2 = 2.698 \times 10^{10} \text{ dyne/cm.}^2 \quad \dots (53)$$

$$\lambda = \rho V_s^2 \left[\left(\frac{V_p}{V_s} \right)^2 - 2 \right] = 6.300 \times 10^{10} \text{ dyne/cm.}^2 \quad \dots (54)$$

$$K = \rho V_s^2 \left[\left(\frac{V_p}{V_s} \right)^2 - \frac{4}{3} \right] = 8.099 \times 10^{10} \text{ dyne/cm.}^2 \quad \dots (55)$$

where: ρ = density - 0.91 g./cm.³

E = Young's Modulus

μ = Rigidity (Shear Modulus)

λ = Lamé's Constant

K = Bulk Modulus (incompressibility)

Poisson's ratio, $M = 0.350$ (see Section 4.4) is somewhat lower than the values obtained by the early workers in the Alps, but higher than those given by Berzon, Bokanenko, and Isaev (1959) for "seismic" frequencies (Table 1). The latter suggest that the high European values might be due to mistaking the Rayleigh waves for shear waves. However, our data indicate that rather high values of M are possible on temperate glaciers.

The reason for the differences in M is not known, but they may be related to variations in elastic properties near the melting point of ice. Near the melting point the rigidity decreases rapidly while the incompressibility remains large. From equation (53) and (55) it can be seen that V_s depends on the rigidity while V_p depends on both rigidity and incompressibility. It follows from equation (51) that near the melting point, M will increase, approaching the value 0.5 as a limit for $\mu = 0$. On the Kaskawulsh Glacier there was a good deal of interstitial water present near the surface, so one would expect the rigidity to be lower, and Poisson's ratio higher than for the case of drier, colder ice.

4.6 Reflected Waves

Strong reflected compressional waves (PP) were obtained on both the direct and reversed profiles, but they did not appear strongly on the direct profile within a distance of 240 m. from D1, or on the reversed profile at all within 183 m. from the shot point. Second P-wave reflections or P-waves converted to S-waves (PS), or vice versa, at the ice-rock interface, were not definitely recorded. The PP reflections usually had sharp first breaks followed by several coherent cycles of ground motion. They were recorded best in the 90-215 Hz. band-pass filter range. The strongest reflections had a frequency of 130-170 Hz. and

their amplitude was only slightly smaller than that of the direct P-waves. A sharp peak occurred in the amplitude of PP at distances 700-750 m. from ID. This will be discussed later in connection with reflection coefficients at the ice-rock interface.

It should be noted here that most of the following discussion involves the apparent dip of the glacier bed, i.e., the component of dip in the plane containing the line of geophones and the shot point and the rays from points on that line to the reflecting interface. The true dip will be designated by θ and the apparent dip by θ_a .

The usual method of obtaining the average vertical seismic velocity from measurements at the earth's surface is to make plots of x^2 vs. t^2 or $x^2 \cos^2 \theta$ vs. t^2 . In these graphs the slope of the curve is the reciprocal of the square of the average velocity. This method proved inapplicable on the wide-angle profile because of the steep dips that were encountered. The following alternative methods were used:

(1) Pflueger (1954) showed that if the zero-distance reflection time is known at two locations and the time for a wave from one of the locations to be reflected to the other location is known, the average velocity can be found from this relation:

$$\bar{V}_p^2 = \frac{x^2}{t_x^2 - t_{01} t_{02}} \quad \dots (56)$$

where: X = separation of the shot points.

t_x = reflection time between shot points.

t_{oi} = zero-distance reflection time at shot point i

(see Fig. 21).

The average apparent dip over the reflection interval is then:

$$\theta_a = \arcsin \frac{Z_1 - Z_2}{X} \quad \dots (57)$$

where: $Z_1 = \frac{1}{2} \bar{V}_p t_{oi}$.

In the present study the value of t_{o2} had to be obtained by the uncertain means of projecting from known reflection times. The results are:

$$\bar{V}_p = 3.78 \text{ km./sec.} \quad \theta_a = 32.2^\circ.$$

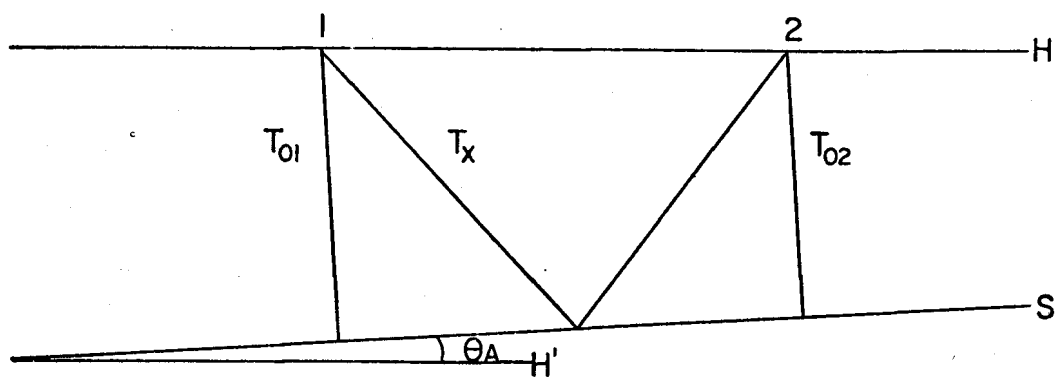
(2) Favre (see Dix, 1955) devised a formula for the case in which shots are made at the center and at one (or both) ends of a line of geophones. If reflection times are known from the center shot directly back to the center of the line (t_o), from the center to each end (t_1 and t_2), and from a shot at end 1 to the geophone at end 2 (t_x), the apparent dip is given by:

$$\theta_a = \arctan \frac{(t_1^2 - t_2^2)}{2 t_o (t_x^2 - t_o^2)^{\frac{1}{2}}} \quad \dots (58)$$

(see Fig. 22).

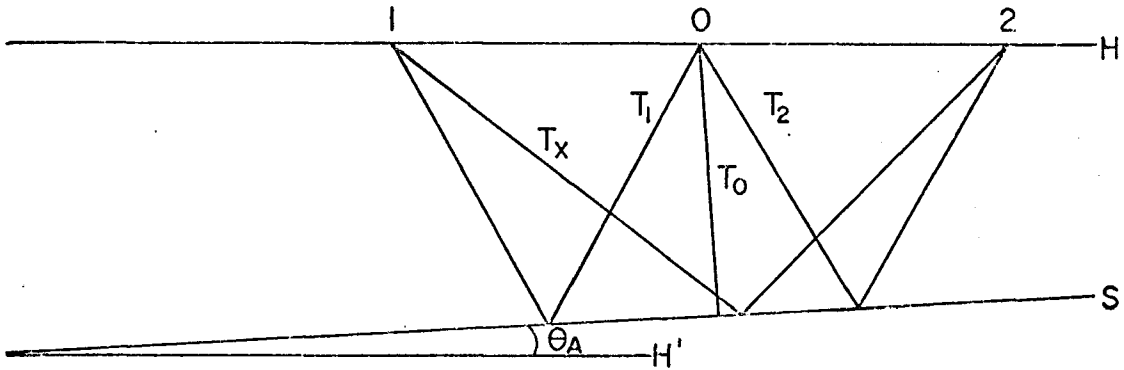
The mean velocity is then:

$$\bar{V}_p = \frac{2 t_o X \sin \theta}{t_2^2 - t_1^2} \quad \dots (59)$$



H = TRACE OF THE PLANE OF THE SPREAD
 H' = TRACE OF A PLANE PARALLEL TO H
 S = TRACE OF THE REFLECTING PLANE
 θ_A = APPARENT DIP PLANE S
 T_{01} = ZERO-DISTANCE REFLECTION TIME FOR SHOT AT 1
 T_{02} = ZERO-DISTANCE REFLECTION TIME FOR SHOT AT 2
 T_x = REFLECTION TIME OF SHOT AT 1, RECORDED AT 2

Figure 21. Geometry of Pflueger's method of obtaining apparent dip of a reflecting interface from reflection times of shots at the ends of a spread.



THE SHOT POINTS ARE AT 0,1,2
 H IS THE TRACE OF THE PLANE OF THE SPREAD
 H' IS THE TRACE OF A PLANE PARALLEL TO H
 S IS THE TRACE OF THE REFLECTING SURFACE
 θ_A IS THE APPARENT DIP OF PLANE S
 T_0 = ZERO-DISTANCE REFLECTION TIME FOR SHOT AT POINT O
 T_1 = REFLECTION TIME OF SHOT AT O, RECORDED AT 1
 T_2 = REFLECTION TIME OF SHOT AT O, RECORDED AT 2
 T_x = REFLECTION TIME OF SHOT AT 1, RECORDED AT 2

Figure 22. Geometry of Favre's method of obtaining apparent dip of a reflecting interface from reflection times of shots at the center and end of a spread.

where: X = total distance from 1 to 2. Using the vertical reflection time at IB to estimate t_0 , the results are:

$$\bar{V}_p = 3.63 \text{ km./sec.} \quad \theta_a = 29.9^\circ.$$

Another method is illustrated in Figure 23. Consider a line of geophones SDEF situated on a surface over a reflecting interface. I is the image point of shot point S. The ray path representing minimum travel time for a ray from the shot point at S to the interface and back to the surface is represented by the path SBE. For this path, SE is perpendicular to BE.

F is another point at which the travel time is known, with ray path SCF. The points IEF form a right triangle. If velocity is constant throughout the region, the sides IE, IF and EF are proportional, respectively, to the minimum reflected travel time, the travel time for the path SCF, and the travel time for the direct path between E and F. The first two of these quantities are known, so the travel time between E and F can be determined. The distance between E and F is known, so the velocity can be found.

In practice the reflection time changed so slowly in the vicinity of the minimum that although the time was known the position corresponding to E in Figure 23 could not be found precisely. However, by taking two points on the time-distance curve far enough from the minimum point so that definite values of reflection time and corresponding distance can be determined, and making use of the Pythagorean

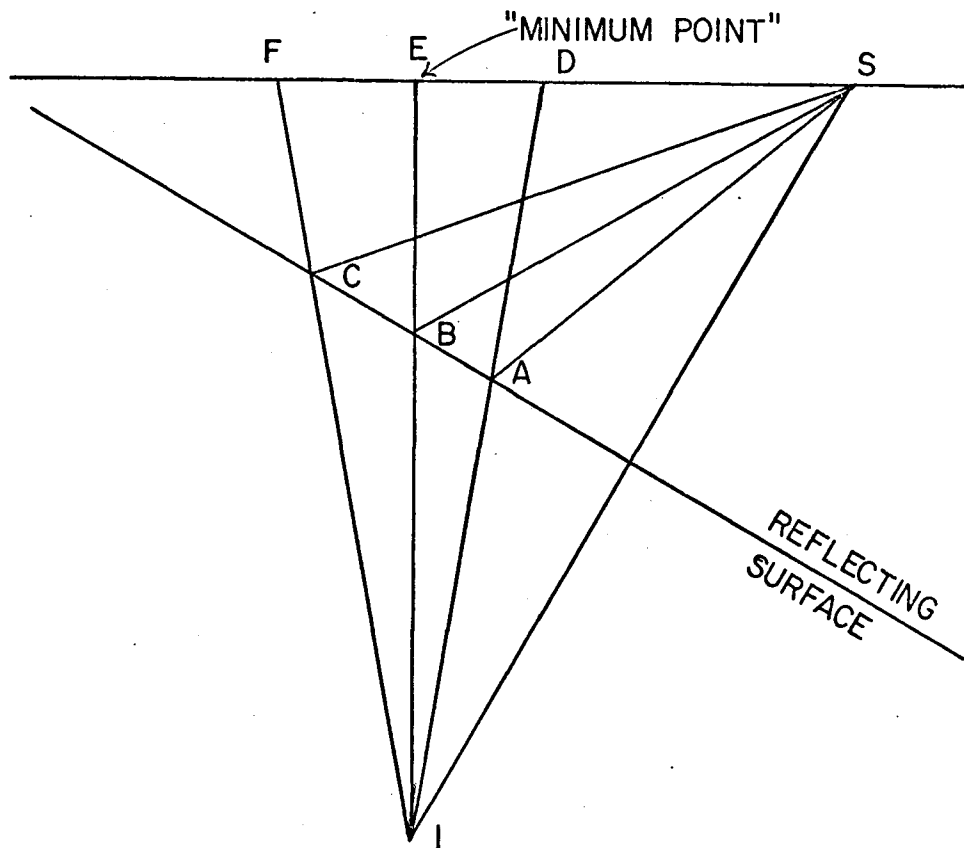


Figure 23. Minimum reflection time when shooting up-dip. Rays from shot point S are reflected at A , B , C and recorded at D , E , F , respectively. Using image point I , the path lengths of the three rays are represented by IAD , IBE , and ICF . As distance from the shot point increases between D and F , a minimum reflection time occurs at E , corresponding to ray IBE .

Theorem, the average velocity can be found from the relation:

$$\bar{V}_p = \frac{X_{12}}{(t_1^2 + t_{\min}^2)^{\frac{1}{2}} + (t_2^2 - t_{\min}^2)^{\frac{1}{2}}} \quad \dots (60)$$

where: X_{12} = distance between detector locations 1 and 2

t_1 = reflection time at point 1.

This method gives the result: $\bar{V}_p = 3.70$ km./sec.

Using this value of velocity, the apparent dip has been constructed by the method of ellipses (Gassaway, 1964). If the velocity, reflection time and shot point-to-detector distances are known, the trace of the reflecting interface must be a tangent to an ellipse which is the locus of points the sum of whose distances from the foci is equal to (the reflection time) X (average velocity). The foci are the shot point and the detector position. If ellipses are drawn in this manner for a number of detectors, the envelope of the ellipses will approximate the intersection of the plane of the rays and the surface of the interface. The slope of the envelope is the apparent dip.

By this method θ_a was found to vary along the profile between 28° and 30° for $\bar{V}_p = 3.70$ km./sec. Changing the value of \bar{V}_p to 3.63 and 3.78 km./sec. did not result in any significant change in dip compared with the possible error indicated by the overlapping of the ellipses in this construction. By comparison, the value of apparent dip in the direction of the profile at point IB was calculated from move-out times along a standard spread length of 182.9 m.

(Chapter VI). For $\bar{V}_p = 3.70$ km./sec. the latter method gave $\theta_a = 31.1^\circ$. True dip from move-out times in two perpendicular directions at 18 was 36.6° , S61° E.

4.7 Amplitude of Reflected Waves

The fractions of incident elastic wave energy that are reflected or refracted from an interface between two different materials are called, respectively, the reflection and refraction coefficients of the waves at the interface. Expressions for these coefficients at the boundary between two solids with greatly different elastic wave velocities were developed by Nafe (1957). From Nafe's relations Røthlisberger (1964) computed graphs of reflection and refraction coefficients at boundaries between ice and 30 different models of solids with physical properties approximating those of common varieties of rocks and frozen ground. Røthlisberger considered shear and compressional plane waves incident at angles from 0° to 90° upon a plane interface. In seismic reflection studies the portion of the real, more or less spherical, wave surface that is considered is usually small enough so that it approximates a plane. All the materials were defined as isotropic and homogeneous. Ice was assumed to have compressional wave velocity 3.60 km./sec., shear wave velocity 1.80 km./sec., Poisson's ratio 0.333 and density 0.9 g./cm.³. These values are not very different from the values obtained from refraction data in this chapter:

$V_p = 3.63$ km./sec., $V_s = 1.72$ km./sec., $M = 0.35$. Actually, the mean vertical compressional wave velocity, $\bar{V}_p = 3.70$ km./sec., would be more applicable in this discussion. For $M = 0.35$, V_s would then be 1.78 km./sec. In either case, the difference from R thlisberger's model is slight.

The properties of the rock underlying the glacier in the region of the wide-angle profile were not known. However, samples were collected from bedrock outcrops near the point of confluence, 200-300 m. from the west end of the profile. The densities and compressional wave velocities of these samples were determined (see Section 6.4). Typical of the samples was a greenstone with $V_p = 5.77$ km./sec. and $\rho = 2.95$ g./cm.³. Poisson's ratio is usually about 0.25 for igneous and metamorphic rocks (Jakosky, 1961). These properties are closely approximated by R thlisberger's rock model number 29: $V_p = 6.00$ km./sec., $\rho = 3.00$ g./cm.³, $M = 0.25$. The PP reflection from this model has a sharp peak in wave amplitude, reaching 90% of incident wave amplitude, at angles of incidence between 30^o and 40^o.

According to the reflection survey (Chapter VI), the reflecting surface under the wide-angle profile has a down-glacier dip of approximately 36^o and depth of 485 m. below the glacier surface at point IB. A ray from shot point ID with angle of incidence of 30^o-40^o on this reflecting surface, corresponding to the theoretical reflection amplitude

peak, will have a PP reflection that emerges at the glacier surface between 700 and 750 m. from 1D. This is in agreement with the observation given in the preceding section. The width of the observed peak, about 100 m. on the glacier surface, corresponds to the angular width of the theoretical curve, about 3° - 5° in angle of incidence. Furthermore, comparison of the observed PP amplitude with the amplitude of direct P-waves on the glacier surface that have traversed an equivalent length of path from an equivalent size of explosion reveals that the peak of PP amplitude is approximately 80-90% of the unreflected P-wave amplitude. This is also in fair agreement with R^uthlisberger's theoretical value. Hence, there is at least a rough check between the reflection survey results and seismic reflection coefficient theory.

Theoretically, there should also be a peak in the amplitude of the PS reflection at a distance of about 800 m. from 1D. This would not be as strong or sharp as the PP peak. Unfortunately, the travel time for the PS arrival at this distance, about 540 milliseconds, is such that the PS phase falls among high amplitude surface waves. There does appear to be a reflection on the record at this time and distance, but it cannot be considered definite.

R^uthlisberger's curves also show total reflection of incident S-waves for angles of incidence corresponding to the distant half of the profile from 1D. SS reflections,

however, were not observed. This may be attributed to deficient production of shear waves at the shot point and to the much higher attenuation that is commonly observed for shear waves, in comparison with compressional waves. The positioning of the shot in a shallow borehole in a relatively homogeneous medium like ice was not conducive to large shear wave production (White and Sengbush, 1963).

4.8 Conclusions

Because the value 3.70 km./sec. is obtained entirely from observed data, it appears to be the best value for the average velocity. The error in distance measurement over the whole profile was probably less than ± 10 cm., or 1 part in 10,000. The seismogram reading error is estimated at about 1% of travel time, which gives a velocity error of about ± 0.04 km./sec. However, in view of the variation in dip and surface slope that enter into the geometry upon which the calculations are based, twice this amount seems to be a more realistic estimate of the probable error. The true mean vertical velocity seems unlikely to be lower than 3.63 km./sec., since this is the velocity apparently reached at depth of 60-70 m., while ice thickness along the profile is much greater: 200-650 m., and velocity generally increases with increasing pressure. Near the bottom there may be a decrease in P-wave velocity due to pressure-melting.

There are no reliable data on reflected shear waves, so that Poisson's ratio at depth is unknown. It is probably lower than the value $M = 0.350$ found above for the near-surface zone if that zone contains much ice at the melting point. As mentioned above, near the melting point rigidity and shear-wave velocity decrease greatly while compressibility and compressional wave velocity do not decrease as much proportionally, so Poisson's ratio becomes smaller.

The closing of fractures at depth in a glacier has been demonstrated by Meier, et al. (1957) and Holdsworth (1965), among others. Fracture closing under pressure apparently increases compressional wave velocity in rocks (Simmons and Brace, 1965), but the effects on shear wave velocity and on Poisson's ratio have not been determined. Birch (1961) found that at very high pressures (4 to 10 kilobars) Poisson's ratio in rocks increased gradually with increasing pressure, but near atmospheric pressure the results were erratic.

The values of the isotropic elastic constants of ice, other than M , obtained on the Kaskawulsh Glacier, agree reasonably well with results for Eurasian glaciers obtained recently by Russian investigators (see Table 1 and Section 4.5).

The glacier bed along the wide angle reflection profile was found to have an apparent dip down-glacier of approximately 30° .

CHAPTER V

ANISOTROPY OF SEISMIC WAVE PROPAGATION

5.1 Introduction

A glacier consists predominantly of ice crystals but it also includes air bubbles, meltwater, dissolved salts, and particles of water-insoluble rocks and minerals. This chapter will be concerned chiefly with the effects of ice crystal orientation and air bubble distribution on the velocities of seismic waves. The other factors mentioned may be important locally, as in the case of meltwater at the surface (Chapter IV) and rock fragments near the base of the glacier (Robinson, 1964). However, crystal orientation and the heterogeneous distribution of air bubbles are of particular interest because of their pervasive character and their apparent connection with glacier mechanics (Shumskii, 1964; Anderton, 1967). For the purposes of the present discussion, the glacier will be considered to consist of an aggregate of ice crystals containing air bubbles. The crystals are assumed to have hexagonal symmetry and their axes of six-fold symmetry, i.e., optic axes, may have almost any degree of preferred orientation.

5.2 Crystal Orientation

In Section 1.9 it was shown that the elastic behavior of the individual ice crystal is determined by five independent elastic moduli: C_{11} , C_{12} , C_{13} , C_{33} , C_{44} (another modulus, C_{66} , is not independent, since it is equal to $\frac{1}{2}(C_{11}-C_{12})$). In an aggregate of a great many randomly oriented crystals the number of independent elastic constants reduces to the two of an isotropic substance, λ and μ . These two represent an average of the crystal moduli (Musgrave, 1959). If the C-axes are all parallel, the elastic properties of the aggregate will approximate those of a single crystal. In the case of thin lake ice, the latter condition is closely approached (Brockamp and Querfurth, 1964). In a temperate glacier, the degree of preferred orientation lies between these extremes (Kamb, 1959a, 1959b; Rigsby, 1951, 1960; Anderton, 1967). It is a function of position in the glacier and is related to the rate of strain of the ice, among other things.

On the Kaskawulsh Glacier, three major types of ice petrofabric, consistent over extensive areas of the glacier surface, have been found. They are largely confined to the margins of the glacier and the region near the medial moraine (Fig. 24). In the central zones of both arms, there is no consistency of pattern, though small areas show definite and often strong fabrics (Anderton, 1967).

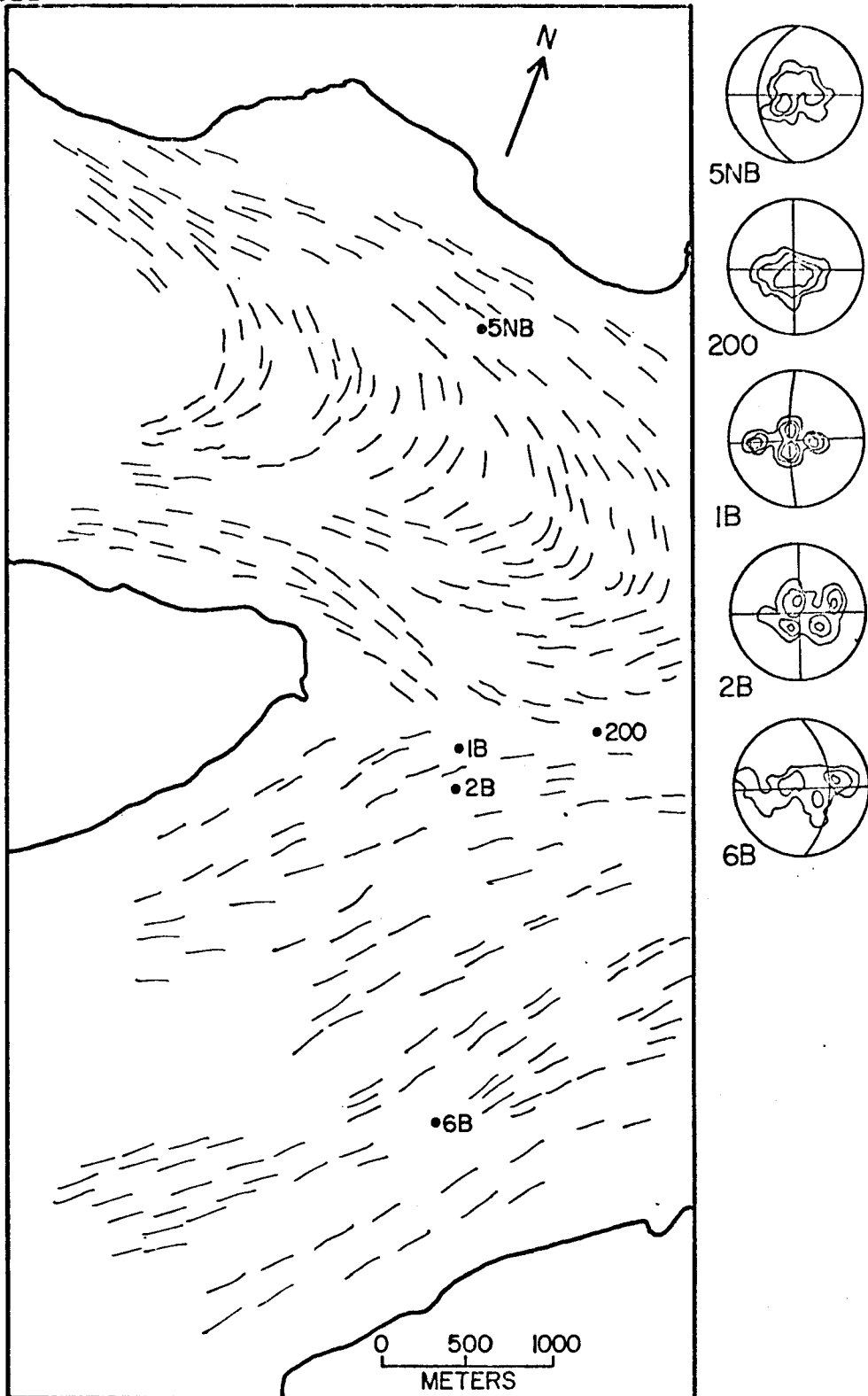


Figure 24. Map of confluence area showing fabric diagrams and trends of foliation. The fabric contour intervals are 1, 3, and 5 percent (see Fig. 25).

The fabrics of highly preferred orientation on the Kaskawulsh Glacier can be described in terms of the distribution of C-axes on an equal-area stereographic projection by the following three types:

(1) The "girdle" fabric has a circular band of high concentration tilted up-glacier at about 10° to the surface of the glacier. The band is about 90° in width. The highest concentration within the band falls approximately perpendicular to the direction of maximum shearing strain rate. This fabric is found near the sides of the glacier where the velocity of the ice movement increases smoothly from the margin of the glacier inward.

(2) The multiple-maxima fabric has a variable number of directions of C-axes concentrations. Frequently there are four maxima distributed more or less symmetrically by pairs about a center. Near point 18, this fabric occurs in such a way that one pair of maxima lies in a horizontal plane and the maxima are about 85° apart; the other pair is nearly vertical and the maxima are about 50° apart. Ten to 15% of the poles are concentrated in cones of $7\frac{1}{2}^{\circ}$ radius about the center of each maximum, so that more than 50% of the C-axes are within 50° of the axis of symmetry of the fabric (Fig. 25). This axis is often nearly perpendicular to the direction of maximum shearing strain rate.

(3) The single-maximum fabric has approximately the same degree of C-axis concentration as (2). This type of fabric is found under the medial moraine. The axis of

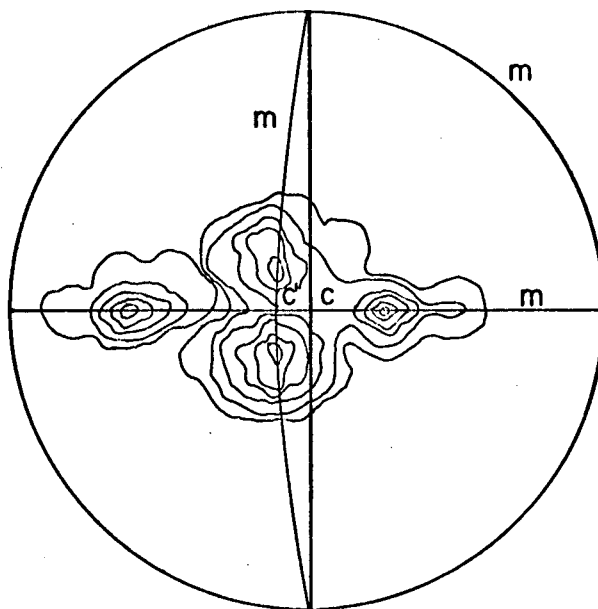


Figure 25. Equal-area contour diagram of 4-maxima optic-axis fabric. The contours represent the percent of points lying within 1% of the total area and have the values 1, 3, 6, 9, 12, 15, and 18 percent. C' is the axis of symmetry of the fabric and C is the axis of symmetry of the foliation. The m 's are symmetry planes of the optic-axis fabric. This fabric is typical of the region near point 1B (see Fig. 24).

symmetry is nearly perpendicular to the direction of maximum tensile strain rate.

The figures given above for percentage concentrations of C-axes are based upon counts of crystals in sections cut from vertical cores. They do not necessarily imply a one-to-one correspondence to the volumes of the crystals involved. If preferred orientation comes about through preferential growth of advantageously oriented crystals, one would expect the crystals that have approximately this orientation to be larger than the others. The volume orientation of the aggregate would then be greater than the count indicates.

In Section 1.7, it was pointed out that seismic wave velocities in crystalline materials are functions of the density, ρ , and the elastic constants of the crystal, C_{ij} . If symmetry is less than isotropic, three modes of vibration occur which are not distinct except along certain directions determined by the symmetry of the medium. One mode usually predominates, either the quasi-compressional wave (velocity V_1) or one of the two quasi-shear waves (velocities V_2 and V_3).

If the elastic constants are known, the velocity of a wave whose normal has a given angular relationship to the symmetry axes of a crystal can be determined precisely from the Christoffel equations (Christoffel, 1877; Hearmon, 1956; Bechmann and Ayers, 1957). For media of transversely isotropic (i.e., hexagonal) symmetry, Postma (1955) gives a

graphic method for determining V_1 and V_2 . V_3 , the velocity of the wave whose particle motion is perpendicular to a plane through the axis of ∞ -fold symmetry (meridional plane), can be determined from a simple relationship between the two shear constants of a transversely isotropic medium, C_{44} and C_{66} :

$$\rho V_3^2 = C_{66} \cos^2 \theta + C_{44} \sin^2 \theta \quad . . . (61)$$

According to the experimental results of Bass, Rossberg and Ziegler (1957), the elastic moduli of the single ice crystal are:

$$\begin{aligned} C_{11} &= 13.3 \times 10^{10} \text{ dynes/cm.}^2 \\ C_{12} &= 6.3 \times 10^{10} \text{ dynes/cm.}^2 \\ C_{13} &= 4.6 \times 10^{10} \text{ dynes/cm.}^2 \\ C_{33} &= 14.2 \times 10^{10} \text{ dynes/cm.}^2 \\ C_{44} &= 3.06 \times 10^{10} \text{ dynes/cm.}^2 \\ (C_{66} &= 3.50 \times 10^{10} \text{ dynes/cm.}^2) \end{aligned}$$

Using these values and $\rho = 0.91 \text{ g./cm.}^2$, the maximum variation in V_1 , which occurs between $\theta = 0$ (maximum value) and $\theta = \pi/2$ (minimum value) is found to be 4%. The maximum variation for V_2 , between $\theta = 0$ or $\pi/2$ (minimum) and $\theta = \pi/4$ (maximum) is 3%, and the maximum variation for V_3 , between $\theta = 0$ (minimum) and $\theta = \pi/2$ (maximum) is 5%.

Now consider the case of the C-axis fabric pattern in Figure 25. The simplifying assumption is made that each of the four concentrations of C-axis poles is reduced to a

single point located at the center of the concentration. Then, with respect to the axis C' , perpendicular to the pattern and passing through its center, 30% of the crystals are inclined at 25° and 30% are inclined at 42.5° . The other 40% of crystals can be considered randomly oriented, i.e., they act in the aggregate like an isotropic medium. If the crystals are assumed to be equidimensional, a wave whose normal N is parallel to the axis C' covers 30% of its path at the velocity dictated by the angle of 25° to the C -axis, 30% at the 42.5° velocity and 40% at the isotropic velocity. The velocities at the given angular relationship can be calculated by Postma's method using the data of Bass, Rossberg and Ziegler and the mean velocity over the total path can be found.

The procedure outlined above was repeated for various angles between N and C' and the pattern of velocity variations for V_1 , V_2 , and V_3 was sampled. The maximal and minimal values occurred at the axis C' and at approximately 90° to the axis, respectively. (Since the pattern is not axially symmetric, there are small variations with longitude - cf. Fig. 25.) This result was similar to the case of the single crystal given above, with C' representing the C -axis. However, the magnitude of the maximum variations of V_1 , V_2 , and V_3 were considerably less than for the case of the single crystal. For the simplified fabric:

$$\Delta V_1 = 2\%; \Delta V_2 = 2\%; \Delta V_3 = 3\%.$$

The usual scatter on velocity measurements from readings of first breaks across the spread ("cross-spread velocity") was about $\pm 1\%$. Hence, it was clear that great care would have to be taken to detect velocity variations by field measurements.

5.3 Field Experiment

A field test of seismic wave velocity versus ice crystal C-axis orientation was made at point 18. This point lies in a region of strong preferred orientation of type (2) (Section 5.2). This region is also relatively free of fractures. Geophone spreads were laid out at angles of 0, $\pi/4$, and $\pi/2$ to the symmetry direction defined by the axis C' in Figure 25.

The geophones were closely spaced in order to detect any vertical refraction: every 2 m. out to 24 m. from the shot point; every 4 m. out to 48 m.; every 6 m. out to 72 m.; every 8 m. out to 96 m.; and the normal spread out to 182.9 m. The geometry is shown in Figure 26.

Detonators alone were sufficient for the shorter spreads. Detonators and small quantities of explosive (30-50 g.) were used for the 96 m. and 182.9 m. spreads. The shots were fired at the surface in holes cut to the dimensions of the charges.

Geophones implanted with their axes parallel to the spreads recorded the compressional (longitudinal) wave

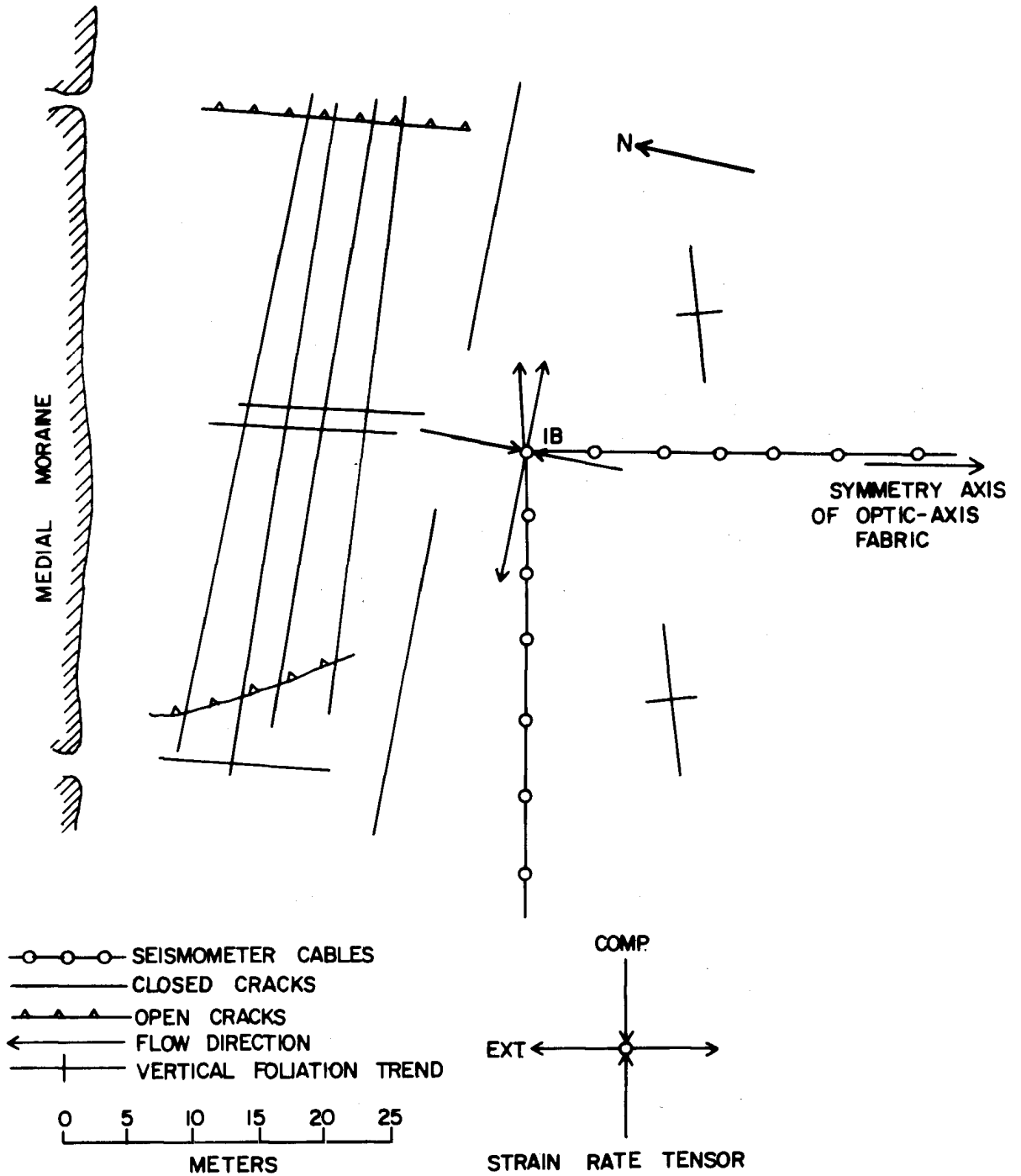


Figure 26. Spread geometry at point 1B, showing crystallographic fabric, foliation, flow, and strain rate in the vicinity.

displacement best, although vertical geophones also record this well. Since the plane of the spreads is also a meridional plane of the medium, vertical geophones, which are perpendicular to this plane, are best oriented to pick up the ground motion of the wave with velocity V_3 . Geophones which are horizontal and perpendicular to the spreads respond principally to the V_2 movement and thereby differentiate it from the V_3 movement. However, since V_2 (minimum) = V_3 (minimum) on the "axial" spread ($\theta = \pi/2$) while V_3 = maximum and V_2 = minimum on the "basal" spread ($\theta = 0$), the vertical geophones alone will serve for recording the maximum and minimum values of V_2 and V_3 . However, on each spread at least one geophone was oriented in each of the mutually perpendicular directions for a check.

The time-distance plots of the first breaks indicated an increase of velocity with depth, so numerical Herglotz-Wiechert integrations were made of the time-distance curves to obtain the velocity-depth relationship (Slichter, 1932):

$$h_d = \frac{1}{\pi} \int_0^{X_d} \cosh^{-1} \frac{V_d}{V_x} dx \approx \frac{\Delta X}{\pi} \sum_{x=0}^{X_d} \cosh^{-1} \frac{V_d}{V_x} \dots (62)$$

where: h_d = depth at which velocity V_d is reached = depth of greatest penetration of the ray from the origin to X_d .

X_d = distance at which ray of maximum velocity V_d is recorded at the surface.

V_x = reciprocal of the slope of the t^{vsx} curve at distance x . (This is determined by obtaining the least-squares slope of a segment of length Δx .)

V_d = reciprocal of the slope of the t^{vsx} curve at distance x_d .

This relationship assumes that the velocity increases continuously with depth and that the velocity gradient is perpendicular to the surface and does not vary horizontally.

The velocity-depth curves for V_1 for $\phi = 0$ and $\phi = 90^\circ$ are shown in Figure 27. The low-velocity zone near the surface is apparent. Upon close inspection of direct P-wave velocities at other shotpoints it was found to exist at all of them. It is also clear that, down to the depth of 8 m., $V_1(\phi = \pi/2) > V_1(\phi = 0)$. This is the reverse of what would be expected on the basis of the known ice crystal anisotropy. The observed anisotropy was not only different in kind, but also considerably larger in magnitude than the small percentages estimated from crystal orientation data (Section 5.2).

The V_2 and V_3 data were insufficient for the construction of complete velocity-depth curves, but the velocity gradients were found to be similar in general form to those for V_1 . At a shotpoint-detector distance of 30 m., the velocities are:

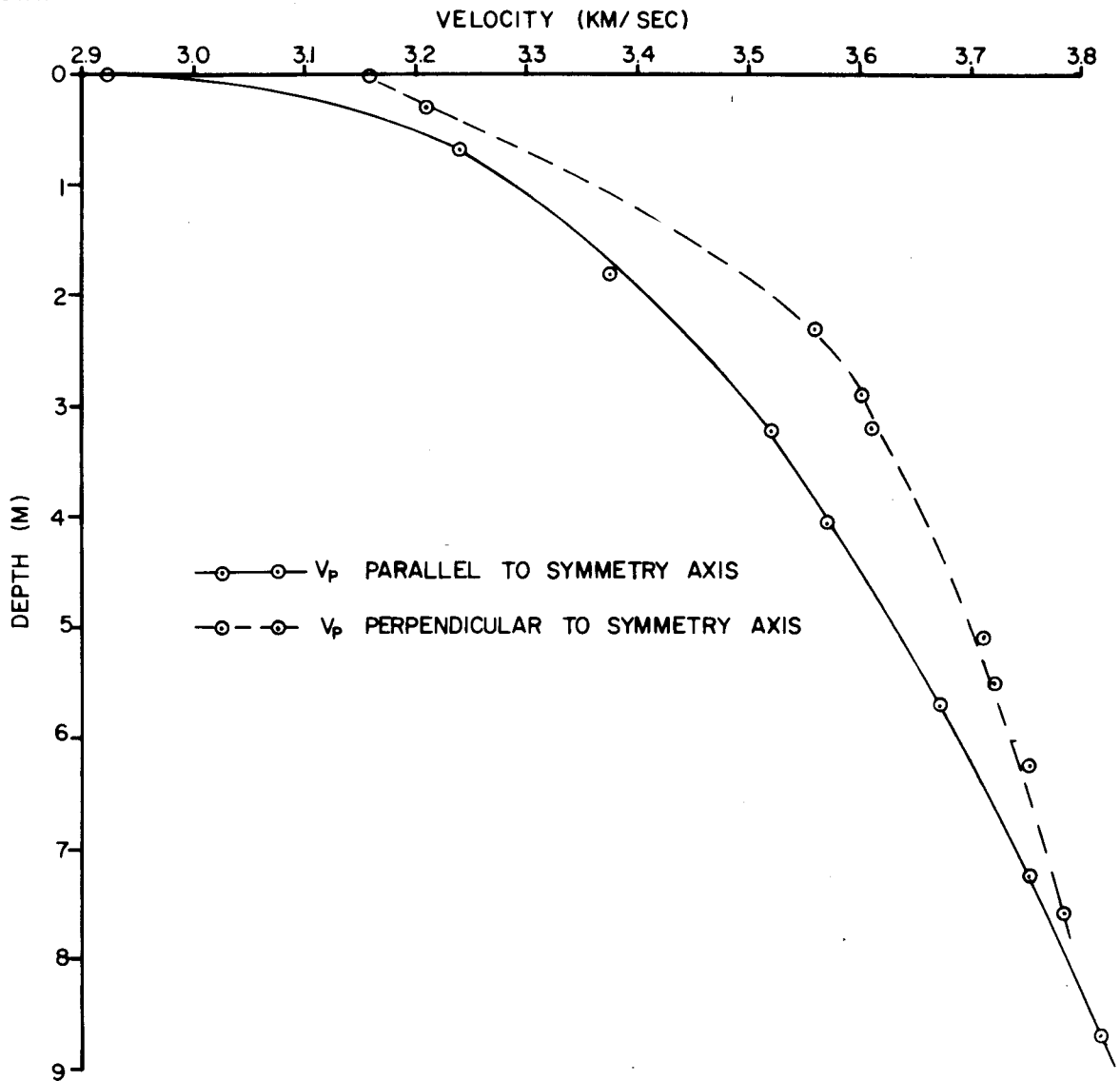


Figure 27. Velocity-depth curves at point 1B for P-waves traveling parallel and perpendicular to the crystallographic axis of symmetry.

$$V_3 \text{ (maximum)} = 1.71 \text{ km./sec. } (\phi = 0)$$

$$V_3 \text{ (minimum)} = 1.67 \text{ km./sec. } (\phi = \pi/2)$$

$$V_2 \text{ (maximum)} = 1.70 \text{ km./sec. } (\phi = \pi/4)$$

$$V_2 \text{ (minimum)} = 1.67 \text{ km./sec. } (\phi = 0)$$

In this case, the inequalities are in the directions predicted: $V_3 (\phi = 0) > V_3 (\phi = \pi/2)$; $V_2 (\phi = \pi/4) > V_2 (\phi = 0)$. The anisotropy factor, the ratio of $V_3 (\phi = 0)$ to $V_3 (\phi = \pi/2)$ is: $A_3 = 1.024$.

If the assumption is made that the ice aggregate in the vicinity of B1 approximates a transversely isotropic medium whose axis of ∞ -fold symmetry is parallel to the axis of symmetry of the crystallographic fabric, elastic moduli for this medium can be determined from the velocity data. For the directions $\phi = 0$, $\phi = \pi/4$, and $\phi = \pi/2$ in a transversely isotropic medium, the Christoffel equations are as follows:

$$\begin{aligned} C_{11} &= (V_1 [0])^2 \rho & C_{33} &= (V_1 [\pi/2])^2 \rho \\ C_{44} &= (V_2 [0])^2 \rho & C_{66} &= \frac{1}{2}(C_{11} - C_{12}) = (V_3 [\pi/2])^2 \rho \\ C_{13} &= \left\{ [2\rho(V_1 [\pi/4])^2 - \frac{1}{2}(C_{11} + C_{33} + 2C_{44})^2 - \right. \\ &\quad \left. \frac{1}{2}(C_{11} - C_{33})^2 \right\}^{\frac{1}{2}} - C_{44} \end{aligned} \quad \dots (63)$$

Since the velocities and elastic constants change with depth, velocity values for the same depth for the different modes must be used if consistent values for the moduli are to be obtained. The best V_2 and V_3 values obtained are those given above, so values of V_1 corresponding to the same depth (3 m.) were used. These velocities are:

$$V_1[0] = 3.52 \text{ km./sec.}$$

$$V_1[\pi/2] = 3.60 \text{ km./sec.}$$

$$V_1[\pi/4] = 3.54 \text{ km./sec.}$$

and the anisotropy factor is: $A_1 = 0.977$. The moduli computed from these data are:

$$C_{11} = 11.09 \times 10^{10} \text{ dynes/cm.}^2$$

$$C_{12} = 6.10 \times 10^{10} \text{ dynes/cm.}^2$$

$$C_{13} = 5.72 \times 10^{10} \text{ dynes/cm.}^2$$

$$C_{33} = 10.61 \times 10^{10} \text{ dynes/cm.}^2$$

$$C_{44} = 2.39 \times 10^{10} \text{ dynes/cm.}^2$$

$$(C_{66} = 2.50 \times 10^{10} \text{ dynes/cm.}^2)$$

Note that, in contrast to the results of Bass, Rossberg and Ziegler, $C_{11} > C_{33}$. However, in both instances $C_{55} > C_{44}$.

5.4 Foliation

A reason for the anomalous result obtained above has been sought in terms of the effects of foliation on elastic wave velocity. A medium consisting of periodically layered isotropic materials of different density and elastic moduli approximate a homogeneous transversely isotropic medium for the propagation of elastic waves if the wave-lengths are large compared with the thickness of the layers. A "large" wave-length is one for which the difference in ground displacement from one layer to the adjacent one is an insignificant fraction of the total displacement in the vicinity of those layers. A wave-length 100 or more times the thickness

of the thickest layer may be considered to fulfill this condition (Riznichenko, 1949; Thomson, 1950; Anderson, 1961). Such a homogeneous transversely isotropic medium is called the "long-wave equivalent" of the periodically layered isotropic medium (Backus, 1962). The axis of ∞ -fold symmetry in the long-wave equivalent medium is perpendicular to the faces of the layers in the periodically layered isotropic medium.

The simplest type of periodic structure which can approximate a homogeneous transversely isotropic medium for elastic waves with long wave-lengths is one which consists of two alternating isotropic layers with thicknesses d_1 and d_2 , Lamé constants λ_1, μ_1 and λ_2, μ_2 , and densities ρ_1 and ρ_2 . Consider now the homogeneous transversely isotropic medium which is the long-wave equivalent of such a periodic, isotropic, two-layered medium. A homogeneous, transversely isotropic medium, like a medium of hexagonal symmetry, is characterized by five independent elastic moduli, $C_{11}, C_{12}, C_{13}, C_{33}, C_{44}$. These moduli can be calculated explicitly as algebraic combinations of the Lamé constants λ_1, μ_1 and μ_2, λ_2 of the isotropic layered medium. The effective density ρ' of the long-wave equivalent medium is simply the average density of the layered medium. Just as there are three elastic wave velocities, V_1, V_2, V_3 , associated with a homogeneous transversely isotropic medium, there are also three elastic wave velocities, V_1', V_2', V_3' , associated with a long-wave equivalent

transversely isotropic medium. Likewise, the three elastic wave velocities in the long-wave equivalent medium are related to the five elastic moduli in that medium through the Christoffel equations (Postma, 1955).

Various layered structures occur in the Kaskawulsh Glacier. The most prominent is foliation consisting of alternating layers of relatively bubbly and bubble-free ice (Anderton, 1967). This type of structure appeared to approximate the periodic two-layered medium discussed above because a bubbly layer would have different elastic constants and density from a bubble-free layer. Consequently, an investigation was made into the effects of this type of layering on elastic wave velocities.

Any planar metamorphic structure is generally referred to as "foliation." In the context of this chapter, only foliation consisting of clear and bubbly layers of ice will be considered.

On the Kaskawulsh Glacier strong preferred orientation of ice crystal C-axes generally coincides with pronounced foliation (Anderton, 1967). The only exception appears to be that in a zone under the medial moraine there is strong single-maximum preferred orientation, but very weak foliation. However, even here there are bubbles present (1-3 mm. diameter) which are somewhat flattened with the short axis perpendicular to the foliation surfaces in adjacent foliated parts of the glacier.

The alternating clear and bubbly bands comprising this type of glacial foliation usually have vertical or near-vertical dip. Untersteiner (1955), in his study of the similar "feinbänder" on the Pasterze Glacier in the Alps, observed that they appeared to die out at depth. The evidence from shallow cores and from observations in moulins suggests that this may also be the case on the Kaskawulsh Glacier, at least in the region near the point of confluence.

The clear bands, which appeared transparent or blue, had a few bubbles scattered through them, but the porosity was insignificant. They often contained many fine planar cracks, which were generally oriented parallel to the foliation surfaces.

The pores in the bubbly bands, which appeared opaque or white, varied greatly in shape, size and distribution. Near the center of either arm of the glacier, they were generally spherical. Near the margins, where foliation was more strongly developed, they often assumed a triaxial ellipsoidal form, with the major axis horizontal and parallel to the foliation surfaces, the minor axis horizontal and perpendicular to the foliation surfaces, and the intermediate axis vertical.

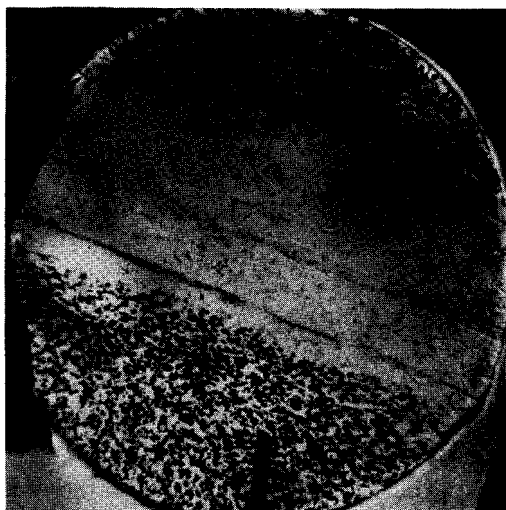
There was a preponderance of bubbles with maximum dimensions in the range 2-5 mm. However, in some layers the bubbles were smaller (0.5-2 mm. diameter) and closer together and showed little preferred orientation. In this

finely-bubbled ice the porosity was considerably greater than in the more common coarsely-bubbled ice. Foliation in which the bubbly bands contained predominantly very fine bubbles was well developed in a band adjacent to the lateral moraine on the south side of the glacier (e.g., near point 190). Estimates were made of porosity by measurements on photographs of core cross-sections (Fig. 28). Porosities ranged from 0.7% in the bubbly bands of weak foliation to 6.2% for the finely-bubbled layers.

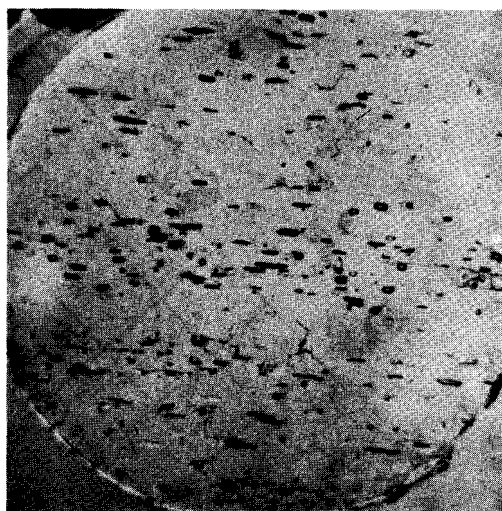
The layers ranged in width from 5 to 30 cm. The smallest wave-lengths with which this investigation was concerned was about 10 m., corresponding to a frequency of about 300 Hz. Hence, the smallest wave-length is more than 100 times the thickness of the layers, and the layer thickness condition for the long-wave equivalent medium is met.

In the vicinity of point 18, the dip of the foliation was nearly vertical and the strike was about N 70° E. The foliation made a solid angle of about 20° to the "basal" plane of the crystallographic fabric (Fig. 26). The clear and bubbly layers were of approximately the same width: 5-20 cm., averaging about 10 cm. The porosity was about 2.8%.

The elastic behavior of a solid is altered by the presence of pores. If the pore concentration is small enough so that each pore can be considered as an isolated cavity in an infinite medium, and if the pores are assumed



(a)



(b)



(c)

Figure 28. Illustration of types of bubbly ice. (a) Fine bubbles, cut by clean band. Porosity 6 percent. (b) Coarse bubbles. Porosity 2 percent. (c) Irregular boundary between clear band and ice with coarse bubbles.

to be spherical, the relationships between the elastic constants are as follows (Walsh and Brace, 1966):

$$\frac{1}{K_p} - \frac{1}{K} = \frac{1}{K} \frac{1-M}{1-2M} \frac{2\pi a^3}{\bar{V}} \quad \dots (64)$$

$$\frac{1}{Y_p} - \frac{1}{Y} = \frac{1}{Y} \frac{(1-M)(9+5M)}{(7-5M)} \frac{2\pi a^3}{\bar{V}} \quad \dots (65)$$

$$m_p - m = m \frac{(1-M)^2(5M-1)}{(7-5M)} \frac{2\pi a^3}{\bar{V}} \quad \dots (66)$$

Here the subscript p refers to the constant for the porous medium; K = compressibility; Y = Young's modulus; M = Poisson's ratio; a = average pore diameter; \bar{V} = the volume of the body divided by the number of pores.

The isotropic elastic moduli for the porous medium can be found from the standard formulae:

$$\mu = \frac{Y}{2(1+M)} \quad \dots (67)$$

$$\lambda = K - \frac{2}{3}\mu \quad \dots (68)$$

If it is assumed that a layered structure of alternating porous and non-porous isotropic sheets exists, a long-wave equivalent transversely isotropic model can be constructed whose elastic moduli are determined by the elastic constants of the non-porous medium and the elastic constants of the porous medium. The latter are determined by equations (64) through (68).

For a layered structure comprising two media of thicknesses and moduli d_1 , μ_1 , λ_1 , and d_2 , μ_2 , λ_2 , respectively.

The long-wave equivalent transversely isotropic elastic moduli are given by the following formulae (Postma, 1955):

$$C_{11}' = \frac{\{(d_1+d_2)^2 (\lambda_1+2\mu_1)(\lambda_2+2\mu_2) + 4 d_1 d_2(\mu_1-\mu_2) [(\lambda_1+\mu_1) - (\lambda_2+\mu_2)] \}}{(d_1+d_2) d_1(\lambda_2+2\mu_2) + d_2(\lambda_1+2\mu_1)} \quad (a)$$

$$C_{12}' = \frac{(d_1+d_2)^2 \lambda_1 \lambda_2 + 2(\lambda_1 d_1 + \lambda_2 d_2)(\mu_2 d_1 + \mu_1 d_2)}{(d_1+d_2) d_1(\lambda_2+2\mu_2) + d_2(\lambda_1+2\mu_1)} \quad (b)$$

$$C_{13}' = \frac{(d_1+d_2)[\lambda_1 d_1(\lambda_2+2\mu_2) + \lambda_2 d_2(\lambda_1+2\mu_1)]}{(d_1+d_2) [d_1(\lambda_2+2\mu_2) + d_2(\lambda_1+2\mu_1)]} \quad (b)$$

$$C_{33}' = \frac{(d_1+d_2)^2 (\lambda_1+2\mu_1)(\lambda_2+2\mu_2)}{(d_1+d_2)[d_1(\lambda_2+2\mu_2) + d_2(\lambda_1+2\mu_1)]} \quad (d)$$

$$C_{44}' = \frac{(d_1 + d_2) \mu_1 \mu_2}{d_1 \mu_2 + d_2 \mu_1} \quad (e)$$

$$C_{66}' = \frac{\mu_1 d_1 + \mu_2 d_2}{d_1 + d_2} \quad (f)$$

. . . (69)

The assumption is made that the isotropic elastic constants determined in Chapter IV are applicable to the non-porous layers in the foliation. These constants are called λ_1 and μ_1 . This assumption would be strictly true only if the bubbly layers died out rapidly with depth and the velocities obtained in Chapter IV applied to ray paths in the unfoliated ice below. The isotropic elastic constants for the bubbly layers are obtained from the constants of the

non-porous layers by using equations (67) and (68) for measured values of porosity. These constants are called λ_2 and μ_2 . The elastic constants for the clear and bubbly layers are combined according to equations (69) and the five transversely isotropic elastic moduli for the long-wave equivalent medium representing the foliation are computed. These moduli are given for three different values of porosity of the bubbly layers in Table 4.

Note that in Table 4 $C_{11}' > C_{33}'$, while $C_{66}' > C_{44}'$. These results are in agreement with the inequalities obtained experimentally (Section 5.3). They are the reverse of the inequalities cited in Section 5.2 for un-foliated ice in which the ice crystals have strong preferred orientation.

The values of the velocities V_1' and V_3' corresponding to the elastic moduli of Table 4 are given in Table 5. The velocity for each mode is given for ray paths perpendicular and parallel to the plane of the foliation, and the corresponding anisotropy factor is given.

It can be seen that weak foliation has a negligible effect in producing velocity anisotropy. Strong foliation has an effect that is of the same order of magnitude, and in the same sense, as that observed at point IB. The effect is strongest for foliation involving finely-bubbled layers of ice.

Table 4. Transvers isotropio elastic constants C_{ij} corresponding to "weak" foliation (porosity of bubbly layers = 0.7%), "strong" foliation (porosity = 2.6%), and foliation containing fine, densely distributed bubbles (porosity = 6.2%). ρ = average denaity of bubbly and clear layers, μ_2 = Lamé's constant of bubbly layers, λ_2 = rigidity of bubbly layers. In all oases, layer thickness $d = 10$ cm., $\lambda_1 = 6.30 \times 10^{10}$ dyne/cm.², $\mu_1 = 2.698 \times 10^{10}$ dynes/cm.² (see Chapter IV). All elaatio constants are in units of 10^{10} dynes/cm.²

Porosity (%)	ρ (g./cm. ³)	λ_2	μ_2	C_{11}	C_{12}	C_{13}	C_{33}	C_{44}	C_{66}
0.7	0.91	5.19	2.43	10.85	5.72	5.70	10.81	2.56	2.57
2.8	0.90	3.40	1.84	9.17	4.63	4.49	8.82	2.19	2.27
6.2	0.88	2.17	1.36	7.78	3.72	3.88	6.90	1.81	2.03

Table 5. Computed velocities V_1' and V_3' for propagation directions parallel and perpendicular to the foliation planes. The velocities and the corresponding anisotropy factors, A_1 and A_3 , are given for different porosities of the bubbly layers of the foliation. ϕ is the angle, in radians, between the foliation planes and the direction of wave propagation.

Porosity (%)	ϕ (radians)	V_1' (km./sec.)	A_1	V_3' (km./sec.)	A_3
0.7	0	3.453	1.002	1.679	1.002
	$\pi/2$	3.447		1.676	
2.8	0	3.228	1.019	1.606	1.043
	$\pi/2$	3.165		1.540	
6.2	0	3.015	1.062	1.540	1.060
	$\pi/2$	2.839		1.453	

Because $A_1 > 1$ for foliation, while $A_1 < 1$ for crystal preferred orientation, a decrease in intensity of foliation with depth should be accompanied by a decrease in the anisotropy factor for V_1 . In a region of strong crystallographic fabric in which the normal to the foliation layering is nearly parallel to the maximum C-axis concentration, as at site IB, A_1 should change with depth, decreasing from a value equal to or greater than unity to a value less than unity. $A_3 > 1$ for both types of anisotropy, so while it will decrease in magnitude, it will remain greater than unity. These are the observed effects.

The assumption that the air bubbles are spherical tends to understate the effects of porosity on the physical properties. For a given porosity, "cracks," with two dimensions sub-equal and the other significantly smaller, have a greater effect in altering the elastic constants than spherical cavities (Walsh and Brace, 1966). In some strongly foliated ice the bubbles tend to take this form. Furthermore, the flattened bubbles are not randomly oriented, but tend to be aligned parallel to the foliation layering. Consequently, the bubbly layers are themselves anisotropic, and in a sense such that the foliation anisotropy is reinforced. A similar effect may be brought about by the small cracks in the clear layers.

The assumption of "small" porosity appears to be justified. Even when pores are separated by distances equal to their own dimensions, interactions are small and the

equations of Walsh and Brace (equations 64, 65, 66) are valid. In most of the foliation examined on the Kaskawulsh Glacier the bubbles were separated by at least several times their own dimensions.

The presence of meltwater in the bubbles will affect the elastic properties of the bubbly layers. Shumskii (1964) has stated that during the melting out of ice containing air bubbles (see Section 3.2), the bubbles become surrounded by a "waterbag." No quantitative estimate is available for the amount of water present in the ice of the Kaskawulsh Glacier. During the seismic investigations, water was generally observed to be present on the surface of the glacier. If the assumption of complete saturation is made, some qualitative estimates can be given as to the effect of the water on elastic wave propagation.

Biot (1956) made a theoretical study of elastic wave propagation in a porous solid saturated with liquid. He found a difference in behavior between low frequency waves, for which Poiseuille flow applies, and high frequency waves, for which there is appreciable slippage of the liquid in contact with the pore walls. For high frequencies both compressional and shear waves are dispersive: their velocities increase (asymptotically) with increasing frequency. The compressional wave velocity is higher for the liquid-saturated porous solid than for the dry porous solid, but the shear wave velocity is slightly lower for the saturated solid than for the dry solid.

King (1966) tested Biot's theory for sandstones at ultrasonic frequency (500 kHz.) and at various confining pressures up to 15,000 psi. He obtained general agreement with theory in the high-frequency range, except that at low confining pressures shear wave velocity was found to increase slightly when the rock was saturated with liquid, rather than decrease, as theory requires. King attributed this effect to interactions between the liquid and the solid that increased the rigidity of the latter.

The critical frequency that marks the beginning of non-laminar flow is given by Biot as:

$$f_t = \frac{\pi \nu}{4d^2} \quad . . . (70)$$

where: ν = viscosity of the saturating liquid in poises
 d = pore diameter in centimeters.

For water at 0° C., Dorsey (1940) gives $\nu = 17.94 \times 10^{-3}$ poise. Then for bubbles 1 mm. in diameter, a common value for the Kaskawulsh Glacier, $f_t = 1.4$ Hz. The seismic frequencies concerned in this study are generally greater than 30 Hz., so Biot's high-frequency theory can be considered applicable.

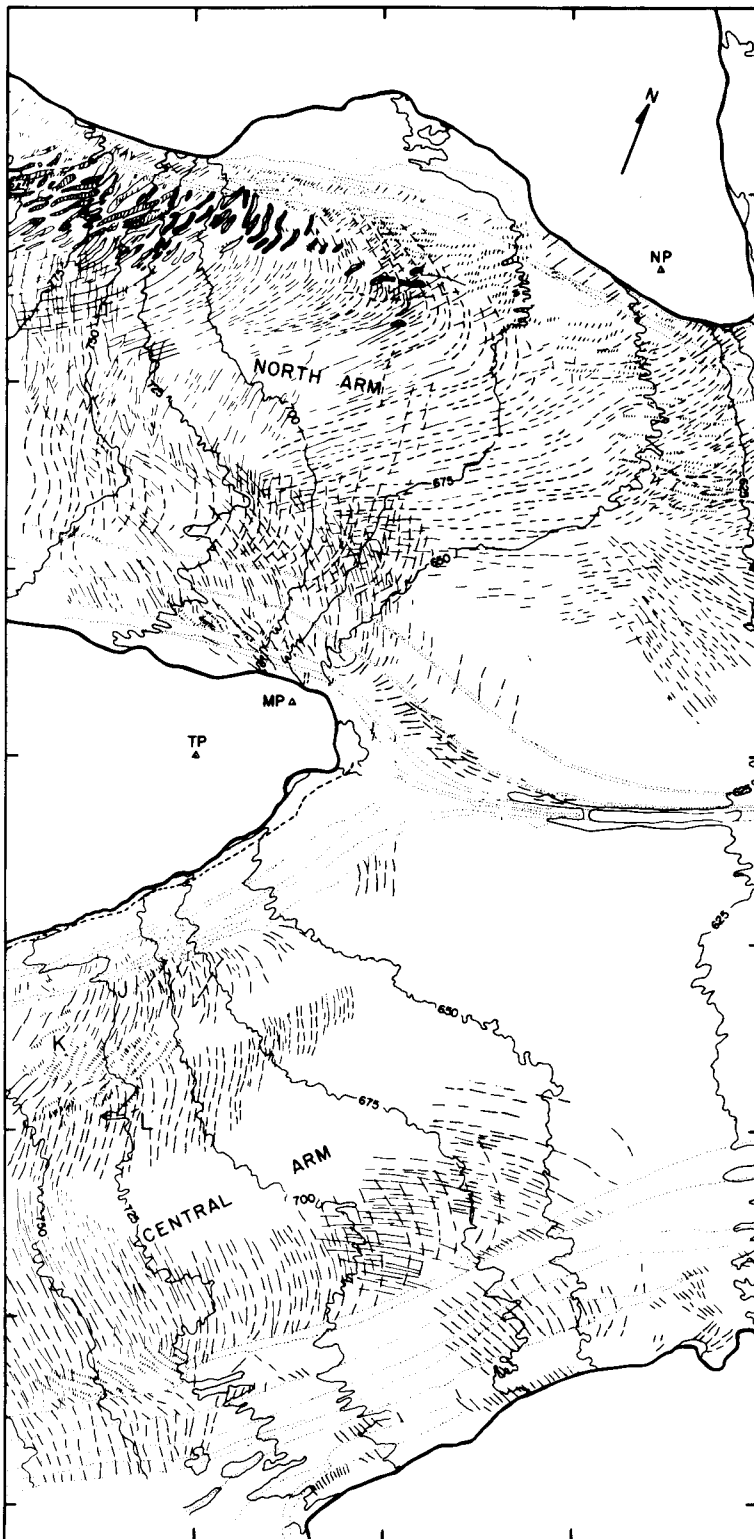
If, as the results cited indicate, water saturation tends to increase compressional wave velocity in the porous layers of foliated ice, then saturated ice will have a smaller velocity difference between layers and hence less velocity anisotropy than water-free ice. Velocities in all directions will be greater, but the differences between their magnitudes

will be smaller. For shear waves the effects are less clear. Theoretically, anisotropy should increase slightly, and average velocity decrease slightly, with water saturation. However, at the low confining pressures near the surface of the glacier, the effect will apparently depend on water-ice interactions.

5.5 Fractures

Jones (1952) found significant anisotropy in the velocity of ultrasonic waves in concrete in which parallel cracks were pre-formed by casting or created by the application of stress. Because fractures and crevasses are characteristic of much of the glacier surface, it appeared likely that they might cause significant anisotropy if suitably oriented. The effects of density of spacing and orientation of fractures were investigated on the Kaskawulsh Glacier by comparing the highest direct P-wave cross-spread velocities in two perpendicular directions in parts of the glacier in which the fracture patterns were distinct and relatively simple. A map of surface fractures, taken from aerial photographs, is shown in Figure 29. The results of the velocity measurements are given in Table 6.

It can be seen that where fractures cut across a spread at a large angle, the velocity along that spread is reduced relative to the velocity along the perpendicular spread. If the region is intensely fractured, velocities along both



CREVASSES AT CONFLUENCE OF NORTH AND CENTRAL ARMS, KASKAWULSH GLACIER, YUKON TERRITORY

CREVASSE

TRIANGULATION STATION 1964, 1965

MORAINE

CONTOUR INTERVALS 25 METERS

REFERENCE AXES

0 500 1000 1500 METERS
SCALE

ELEVATIONS REFERRED TO ARBITRARY DATUM. TP = 1000 METERS.

SP

Figure 29. Crevasse patterns at the confluence of the North and Central Arms of the Kaskawulsh Glacier.

Table 6. Velocity of compressional waves at locations on the surface of the Kaskawulsh Glacier compared with orientation and estimated intensity of local fractures. A_F = anisotropy factor for P-waves: the velocity is a direction approximately parallel to the primary fracture trend divided by the velocity in a direction approximately perpendicular to it. ψ = angle between the trend of the primary fracture set and the normal to the reflection survey profile on which the station lies (Fig. 3). The foliation generally strikes more or less perpendicular to the profiles.

Station	Maximum P-wave velocity (km./sec.)	A_F	Intensity Fracture Foliation		ψ (degrees)
190	3.73	1.02	weak	strong	25
195	3.70	1.02	weak	weak	20
199	3.69	1.05	weak	weak	0
201	3.70	0.98	weak	strong	90
204	3.40	1.07	strong	weak	25
205	3.59	1.12	strong	weak	30
58	3.74	1.02	weak	weak	5
68	3.72	1.05	weak	strong	90
2NB	3.64	0.99	strong	strong	90
4NB	3.47	0.97	strong	strong	90
8	3.65	1.03	none	strong	0
10	3.68	1.00	weak	strong	45
107	3.43	1.05	strong	none	10
105	3.54	1.04	weak	none	25
103	3.71	0.98	weak	none	80

spreads are lower than they are in relatively unfractured regions. Intense fracturing can have an effect on seismic wave velocity comparable in magnitude to the effect of strong foliation.

5.6 Conclusions

To sum up, seismic wave velocities in the ice of the Kaskawulsh Glacier were found to be affected by crystallographic fabric, foliation and fracture. Ice near the surface of the glacier was heterogeneous with respect to porosity and elastic properties. Anisotropy due to foliation and anisotropy due to crystal orientation were superposed near the margins of the glacier and below the confluence in zones flanking the medial moraine. A low-velocity zone several meters thick was found at the upper surface of the glacier; P-wave velocity measured at the surface was as much as 25% less than it was 10 m. below. Low velocity in this zone may be due to melting, fracturing, and high porosity of the ice. The zone appeared to contain a considerable amount of meltwater.

Even when the effects of foliation and fracture are disregarded, the low symmetry of most of the ice petrofabrics observed near the surface of the Kaskawulsh Glacier results in complex relationships between seismic wave velocity and the direction of wave propagation. The velocity anisotropy of the aggregates of ice crystals with the

strongest preferred orientation in the glacier is much smaller than the anisotropy observed for a single crystal. Anisotropy due to the preferred orientation of ice crystals does not appear to be substantial enough to affect seismic reflection measurements in the glacier significantly.

Because fracture and foliation affect seismic velocities so strongly, the use of the seismic method to study ice crystal fabrics appears to be severely limited. However, there are regions in the Kaskawulsh Glacier in which foliation and fracture are virtually absent, for example, under the medial moraine, and similar situations can undoubtedly be found in other glaciers. The use of more precise apparatus for measuring seismic wave velocity than was available in this study might permit the investigation of small unfractured and unfoliated domains. Where the study of foliation itself is sought, the relatively strong anisotropic effect of some types of layering involving clear and bubbly ice suggests that the seismic method might be applicable.

CHAPTER VI

REFLECTION SURVEY

6.1 Introduction

A seismic reflection survey was carried out to determine the ice thickness and the shape of the glacier bed in the region of the confluence of the North and Central Arms of the Kaskawulsh Glacier. The distance to the bed of the glacier, converted to vertical depth, and the strike and dip of the bed was determined at 40 points, most of them on the three trans-glacier profiles described in Chapter I (Fig. 3).

In accordance with the results of the investigations reported in Chapters III and IV, the ice has been assumed to be isotropic and homogeneous with respect to seismic wave propagation. It has also been assumed that the glacier surface in the vicinity of each shot point, and the sub-glacial interface from which the seismic waves from that shot point are reflected, are planes. Hence, the seismic rays are straight lines and their lengths are directly proportional to their travel times.

The reflection data have been corrected for the displacement and rotation of stations resulting from variations

in strain rate along the profiles, because appreciable surface movement took place while the investigation was in progress. Corrections also have been applied for the slope of the glacier surface, and the change in ice thickness due to ablation of the surface during the field season.

6.2 Procedure for Determining Depth and Strike and Dip of Glacier Bed

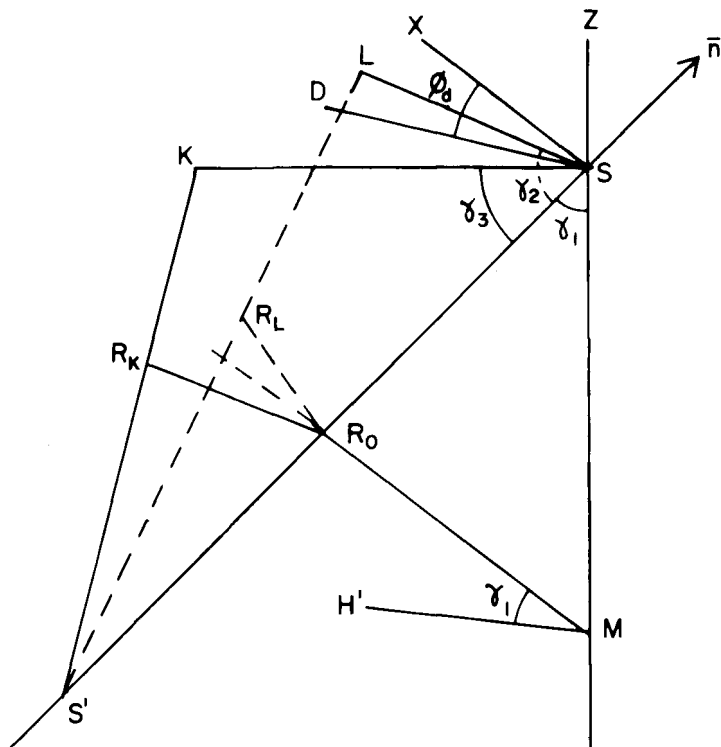
The survey data were determined by reading the times T_0 , T_k , and T_1 from the records (Fig. 30). In the figure the shot point is at S; the spreads are represented by the line segments SK and SL. The reflecting plane is represented by the points R_0 , R_k , and R_1 , which are the points of reflection of rays reflected back to the shot point (the zero-distance reflection), and to the ends of SK and SL. S' is the image of the shot point. $SS' = VT_0$, $KS = VT_k$, and $LS' = VT_1$. In the triangle $SS'K$, from the law of cosines:

$$\cos \beta = \frac{SK^2 + V^2(T_0^2 - T_k^2)}{2 SKVT_0} \quad \dots (71)$$

and in triangle $SS'L$:

$$\cos \alpha = \frac{SL^2 + V^2(T_0^2 - T_1^2)}{2 SLVT_0} \quad \dots (72)$$

If n is a vector normal to the reflection plane $R_0R_kR_1$ and parallel to SS' , and γ is the angle between n and the Z axis,



- X = COORDINATE DIRECTION ON SURFACE
 Z = VERTICAL DIRECTION
 S = SHOT POINT
 S' = IMAGE OF SHOT POINT
 \bar{n} = VECTOR NORMAL TO REFLECTING INTERFACE
 $\delta_1, \delta_2, \delta_3$ = DIRECTION COSINES OF \bar{n} ; γ_1 = DIP
 K, L = ENDS OF SPREADS
 R_0 = POINT ON REFLECTING INTERFACE AT MIDPOINT OF SS'
 R_K, R_L = POINTS ON REFLECTING INTERFACE CUTTING KS' AND LS' RESPECTIVELY
 D = POINT ON SURFACE VERTICALLY ABOVE R_0
 M = INTERSECTION OF REFLECTING INTERFACE AND VERTICAL AXIS Z
 $H'M$ = INTERSECTION OF VERTICAL PLANE THROUGH R_0M AND PLANE PARALLEL TO SURFACE THROUGH M
 THE ZERO DISTANCE REFLECTION TIME T_0 IS THE TIME FROM S TO R_0 TO S
 THE REFLECTION TIMES AT POINTS K, L ARE T_K, T_L RESPECTIVELY
 ϕ_d = AZIMUTH OF DIP

Figure 30. Geometrical relationship between a dipping reflecting interface and spreads on the glacier surface.

$$\cos^2 \alpha + \cos^2 \beta + \cos^2 \gamma = 1 \quad . . . (73)$$

and

$$\gamma = \cos^{-1}(1 - \cos^2 \alpha - \cos^2 \beta)^{\frac{1}{2}} = \text{dip of the reflecting interface.} \quad . . . (74)$$

The dip azimuth, perpendicular to the strike of the interface = $\theta = \tan^{-1} \frac{\cos \beta}{\cos \alpha}$. . . (75)

The point D is the projection of R_0 on the plane of the spreads and the offset of this point from the shot point is:

$$SD = \frac{1}{2} VT_0 \sin \quad . . . (76)$$

The distance from D to R_0 is the ice thickness at R_0 :

$$d = R_0D = \frac{1}{2} VT_0 \cos \gamma \quad . . . (77)$$

At some stations only the slant depth could be determined:

$$\frac{1}{2} SS' = \frac{1}{2} VT_0 \quad . . . (78)$$

6.3 Corrections to Seismic Reflection Data

The stations were surveyed on July 19, 1964 and again on May 24, 28, and 30, 1965, and their movement was computed (Anderton, 1967). The position of each station at the time it was used as a shot point on the reflection survey was obtained by time interpolation or extrapolation. Since the movement was more rapid during the summer months when the seismic survey was taking place, and this acceleration was greater on the Central Arm than on the North Arm, the interpolation had to be corrected for these factors. Based upon

measurements taken during July and August, 1964, Anderton (personal communication) estimated that on the North Arm movement was 7% faster in the summer than the average for the year and on the Central Arm 23% faster in the summer than the average for the year.

The spreads were oriented by sighting from one station to the next, so the spread azimuths had to be corrected for the effects of relative motion. The principle is illustrated in Figure 31. At the time of the first survey, the positions of two adjacent stations are A and B and the true azimuth from A to B is the angle δ . At the time of the second survey, the positions are A' and B' and the azimuth is δ' . At an intermediate time that A is used as a shot point, its position, by interpolation, is A'' and the point used for the aligning of spreads K and L is at B''. The true azimuth is then δ'' . The dip azimuth with respect to the spread coordinate system is θ_d and the true dip azimuth is ϕ_d ; the true strike is $\phi_d + 90^\circ$. The position of the sighting station B'' can be expressed as:

$$X_{i''} = X_{i'} - \frac{T_{j''} - T_{i'}}{T_{i'} - T_l} \frac{V(S)}{V(A)} (X_{i'} - X_i) \quad \dots (79)$$

where:

$X_{i''}$ = X-coordinate of point i when point j is being shot

$T_{j''}$ = time when j is shot

$T_{i'}$ = time of second survey of i

T_i = time of first survey of i

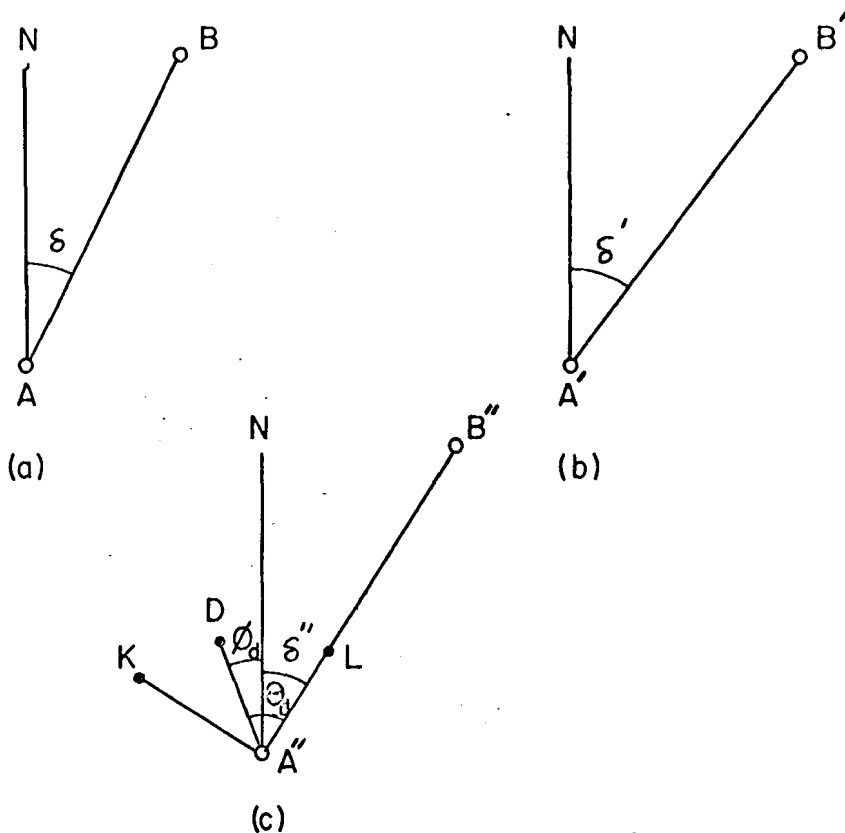


Figure 31. Azimuth correction for relative movement of survey markers. At time (a) the azimuth of the line from A to B is δ . By time (b) the azimuth has increased to δ' . At some intermediate time (c) the azimuth is an interpolated value, δ'' . The dip azimuth $\phi_D = \theta_D - \delta''$, where θ_D is the angle between the surface trace of the dip azimuth, AD, and the line AB.

$V(S)/V(A)$ = ratio of summer velocity to average velocity

X_i' = X-coordinate of point i at second survey

X_i = X-coordinate of point i at first survey

The equation for the Y-coordinate is analogous.

Surface slope varies from 0° to about 5° along the profiles. The resulting angular errors are small but the horizontal displacements they cause in the position of the reflecting interface are significant. The correction is illustrated in Figure 32. In Figure 32(a) the shot point is at S, with altitude Z_1 . The surface projection of the zero reflection point D is at altitude Z_2 . The slope is indicated by the gradient vector. The projection of SD on grad Z is PD and the angle between SD and grad Z is η_s . The projection of the zero reflection point on the horizontal plane is D' and the distance DD' in the surface plane is Δ .

The relation of Δ and the angular correction for the reflecting interface ξ_s to the known quantities PD, d and Z is shown in Figure 32(b). Here:

$$\xi_s = \frac{Z_2 - Z_1}{PD} \quad . . . (80)$$

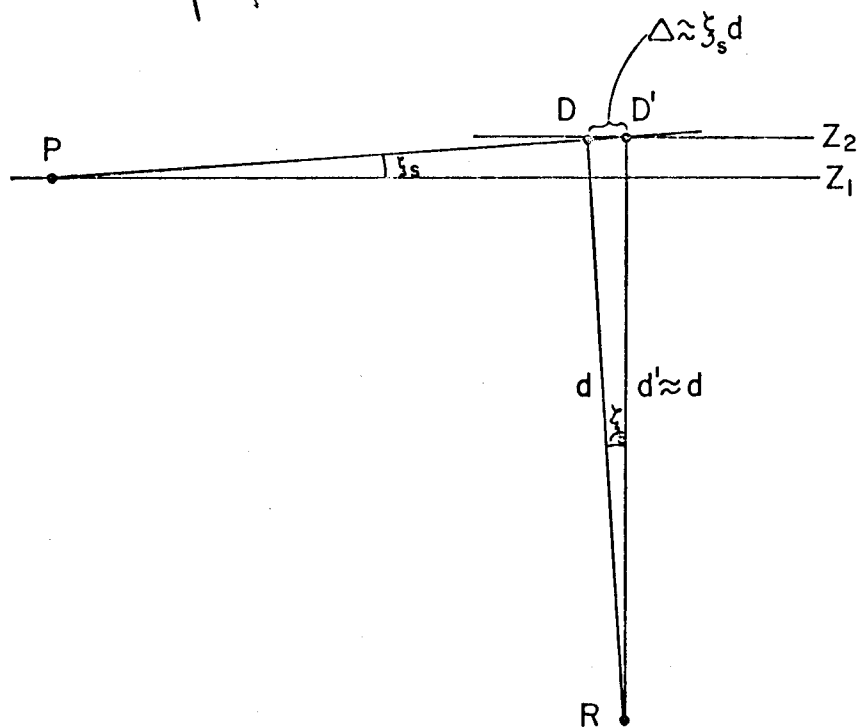
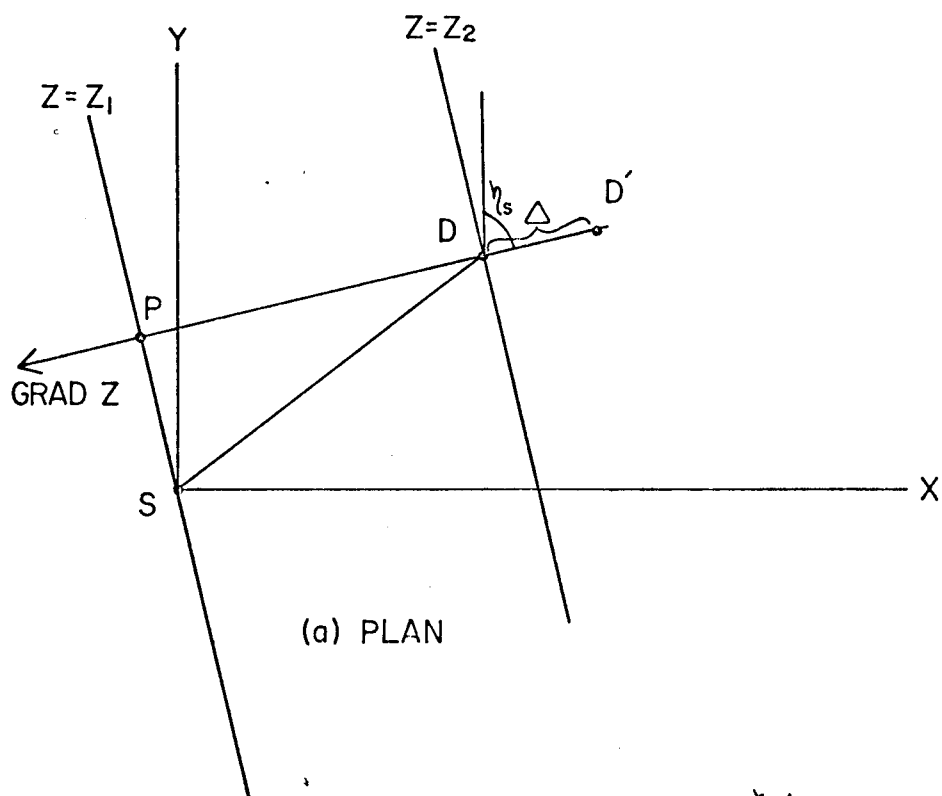
and

$$\Delta = \xi_s d \quad . . . (81)$$

If the slope changes appreciably in the vicinity of D', the plane of the spread must be extended to D' and a

Figure 32. Position correction for the slope of the glacier surface. R_0 , S and D are as defined in Figure 30. S is at elevation Z_1 and D is at elevation Z_2 . The slope of the surface is $\xi_s \cong Z_2 - Z_1 / \overline{PD}$, in the direction grad Z. The perpendicular distance from D to R_0 is d. The vertical distance from R_0 to the surface at D' is $d' \cong d$. If ξ_s is a small angle the offset between D and D' is $\Delta \cong \xi_s d$. The direction of the offset is the azimuth of the slope gradient, η_s .

Figure 32.



correction made to d' for the difference between this plane and the actual surface at D' . This correction is usually very small, and never more than a few meters.

The cumulative ablation from the beginning of the melt season until the shot time of a given station is added to the depth d' for that station to bring all the depths to a common time datum. Ablation rates varied from 3 cm. of ice per day at station 68 to 4.6 cm. of ice per day at NB5. This correction was never more than three meters.

The total position correction was greatest for the shot points in the central zone of each glacier arm, where the velocity of ice movement was greatest. On the other hand, the azimuth correction was greatest near the margins of the glacier, where the shearing strain rate, $\dot{\epsilon}$, was maximal. The corrections for the slope and unevenness of the glacier surface were small except on the upper line of the North Arm, especially at its south end, which is just below an ice fall. Because the ice depth was found to be relatively small here, the percentage correction was considerably greater than anywhere else.

The results of the reflection survey are presented in Table 7. Figure 33 is a contour map of the sub-glacial surface, constructed from the data of this table. Cross-sections of the glacier along the survey profiles are plotted in Figure 34.

Table 7. Vertical ice depth and strike and dip of the ice-rock interface at points on the Kaskawish Glacier. These data were determined by the seismic reflection method. Locations are tabulated according to the profile and of the glacier on which they lie (see map, Fig. 3). The shot point does not, in general, coincide with the point at which depth is measured. The latter is designated "surface point." One shot point may have more than one surface point, corresponding to different reflecting horizons. For some shot points only apparent dip, and slant depth to the interface could be determined, and for these the surface point is indeterminate. All data have been corrected for the effects of ice movement and terrain, hence the location of a point is for the day on which the shot was made there.

Profile	Glacier Arm	Shot Point	Shot Point X	Shot Point Y	Location X	Location Y	Surface X	Surface Y	Point Location X	Point Location Y	Depth	Dip of Interface	Azimuth of dip	Strike of Interface (degrees)		
Upper Line	Central	5	10,766	7,986							(1) 790					
		6	10,744	8,230							(1) 11,010					
		8	10,629	8,831								532	24.0	151.0	61.0	
		9	10,864	9,023				12,649	9,039			368	34.8	135.2	55.2	
		10	10,966	9,276				10,966	9,224			250	36.6	145.9	45.9	
		11	10,629	9,363				10,493	9,489			207	41.0	135.2	45.2	
	North	102	10,966	10,966				10,898	10,898			457	12.5	49.0	139.0	
		108	10,783	11,031				10,742	11,102			618	12.0	180.8	90.8	
		102	10,629	11,201				10,686	10,826			815	33.2	20.9	110.9	
		106	10,881	11,591				10,854	11,205			778	21.8	68.9	158.9	
		108	10,917	11,874				11,084	11,289			714	28.0	36.2	125.2	
		108	10,966	12,574				11,087	12,037			778	13.5	209.6	119.6	
	Strain Network Line	Central	98	10,960	12,378			11,087	12,275			651	20.9	227.2	137.2	
			98	10,968	12,608				11,087	12,076			728	21.7	185.5	95.5
			98	11,584	7,476				11,714	7,307			457	25.2	322.2	52.2
			98	11,618	7,642				11,562	7,654			737	14.9	16.9	106.9
			98	12,649	8,413				11,588	8,348			964	6.7	304.3	34.3
			98	11,689	8,889				11,588	9,114			473	42.4	138.9	48.9
Lower Line	Central	28	11,720	9,373				11,588	8,596			1,040	6.7	12.5	102.5	
		18	11,781	9,628				11,588	9,607			576	23.8	158.4	68.4	
		28	11,781	10,025				11,588	9,778			427	36.3	119.0	29.0	
		28	11,781	10,025				11,588	9,893			488	29.8	61.5	151.5	
		348	11,889	10,560				11,801	10,436			843	36.2	51.0	141.0	
		48	11,910	11,418				11,689	10,924			843	14.6	57.4	138.2	
	North	58	12,051	12,107				12,587	11,593			843	25.1	234.7	144.7	
		198	12,479	7,691				12,480	7,415			892	28.8	69.5	159.5	
		191	12,523	7,825								488	28.8	191.9	101.9	
		198	12,523	8,642								(1) 488	46.7	0.5	90.5	
		198	12,523	8,478								(1) 832	9.3	(2) 93.0	3.0	
		198	12,539	8,642				12,652	9,385			(1) 925	(2) 25.7	344.0	74.0	
X	Central	202	12,574	9,139							(1) 11,006	(2) 8.5	(2) 3.0	93.0		
		202	12,574	9,385							(1) 11,005	(2) 4.0	(2) 92.0	2.0		
		204	12,649	9,752				12,523	9,482			925	6.2	165.0	75.0	
		206	12,574	9,385				12,467	9,758			905	12.8	145.7	55.7	
		206	12,574	9,385				12,523	9,752			915	10.6	196.7	6.7	
		206	12,649	9,953				12,756	10,784			916	4.9	131.0	41.0	
X	Central	X1	11,607	9,285			11,375	9,350			480	4.2	148.0	58.0		
		X1	11,607	9,285			11,375	9,350			480	18.9	193.7	103.7		

Units: Locations: meters measured geographically east (X) and north (Y) of an arbitrary origin of a rectangular coordinate system.

Depth: meters measured vertically (with exceptions noted).

Dip: degrees

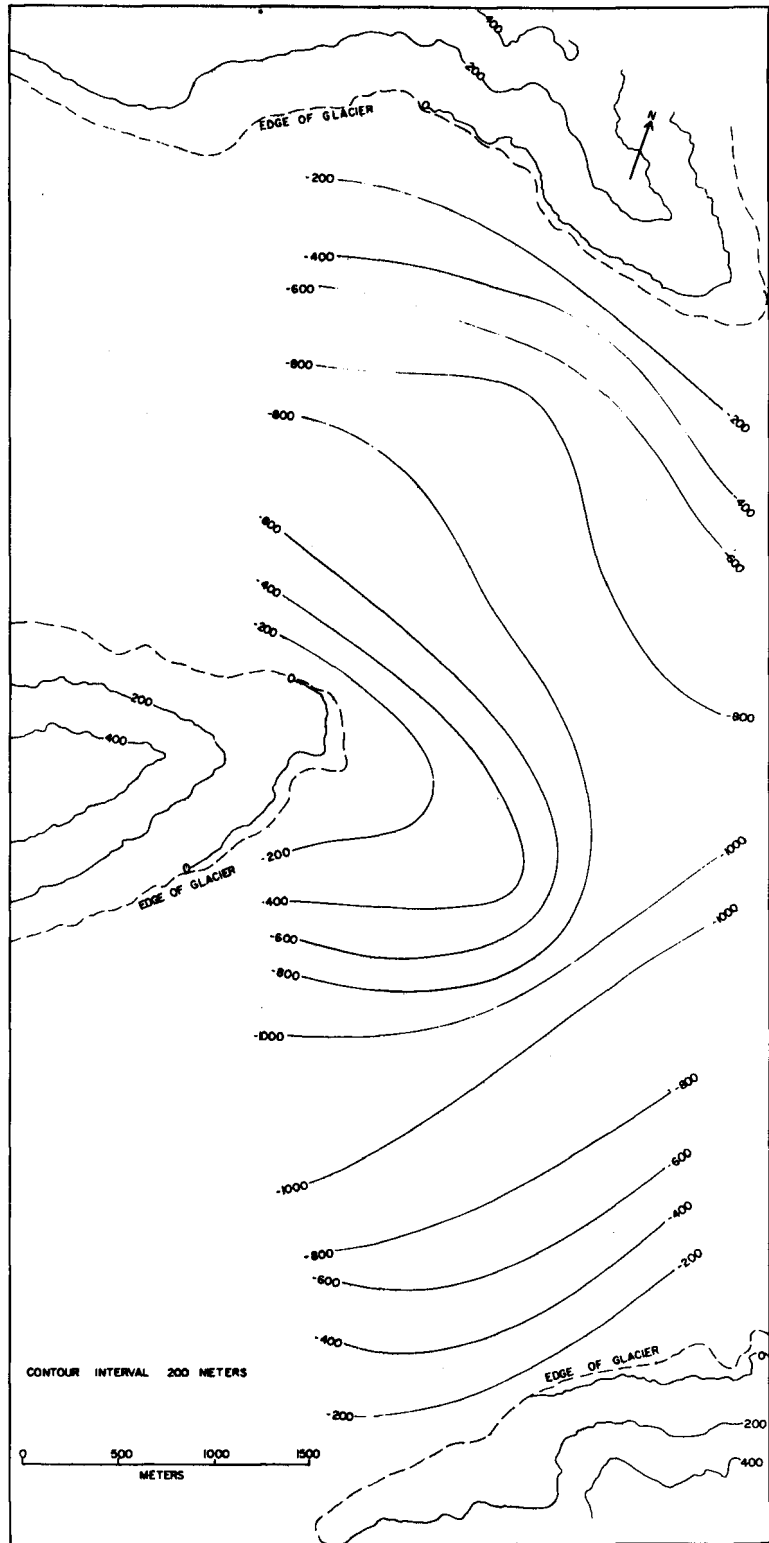
Dip azimuth: degrees measured clockwise from geographical north (0-360°).

Strike: degrees measured clockwise from geographical north (0-180°).

NOTES: (1) Slant depth.

(2) Apparent dip.

Figure 33. Contour map of the sub-glacial topography et the confluence of the North and Central Arms of the Kaskawulah Glacier. The contour interval is 200 m. The zero contour is taken as a contour on the valley wall that approximately coincides with the edge of the glacier. Its elevation is 675 m. referred to the datum of Figure 3, and approximately 1800 m. above sea level.



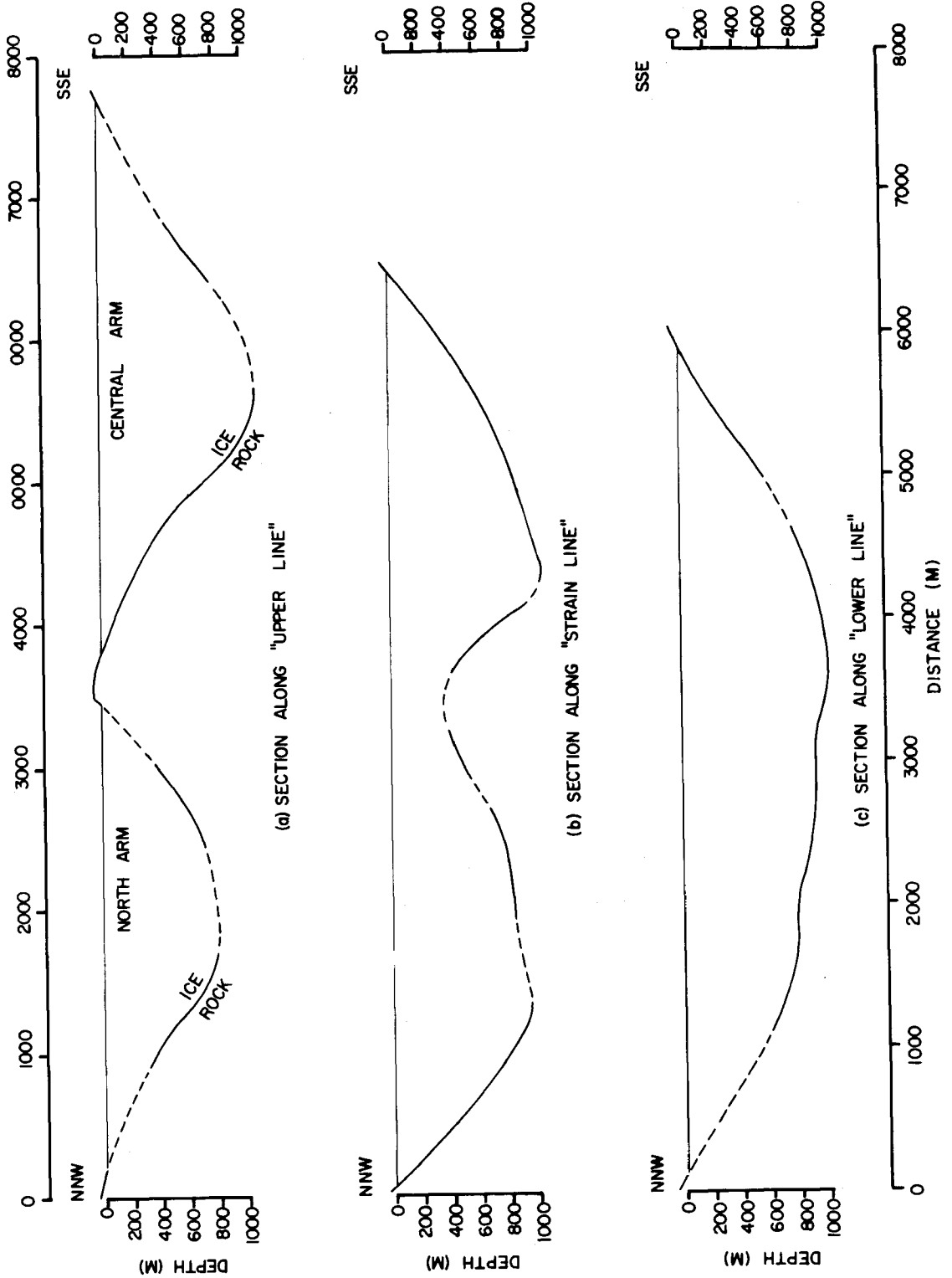


Figure 34. Transverse sections across the Kaskawulsh Glacier on the lines of survey markers (see Fig. 3). The directions are approximate. The vertical and horizontal scales are equal.

6.4 Interpretation of Seismic Reflection Data

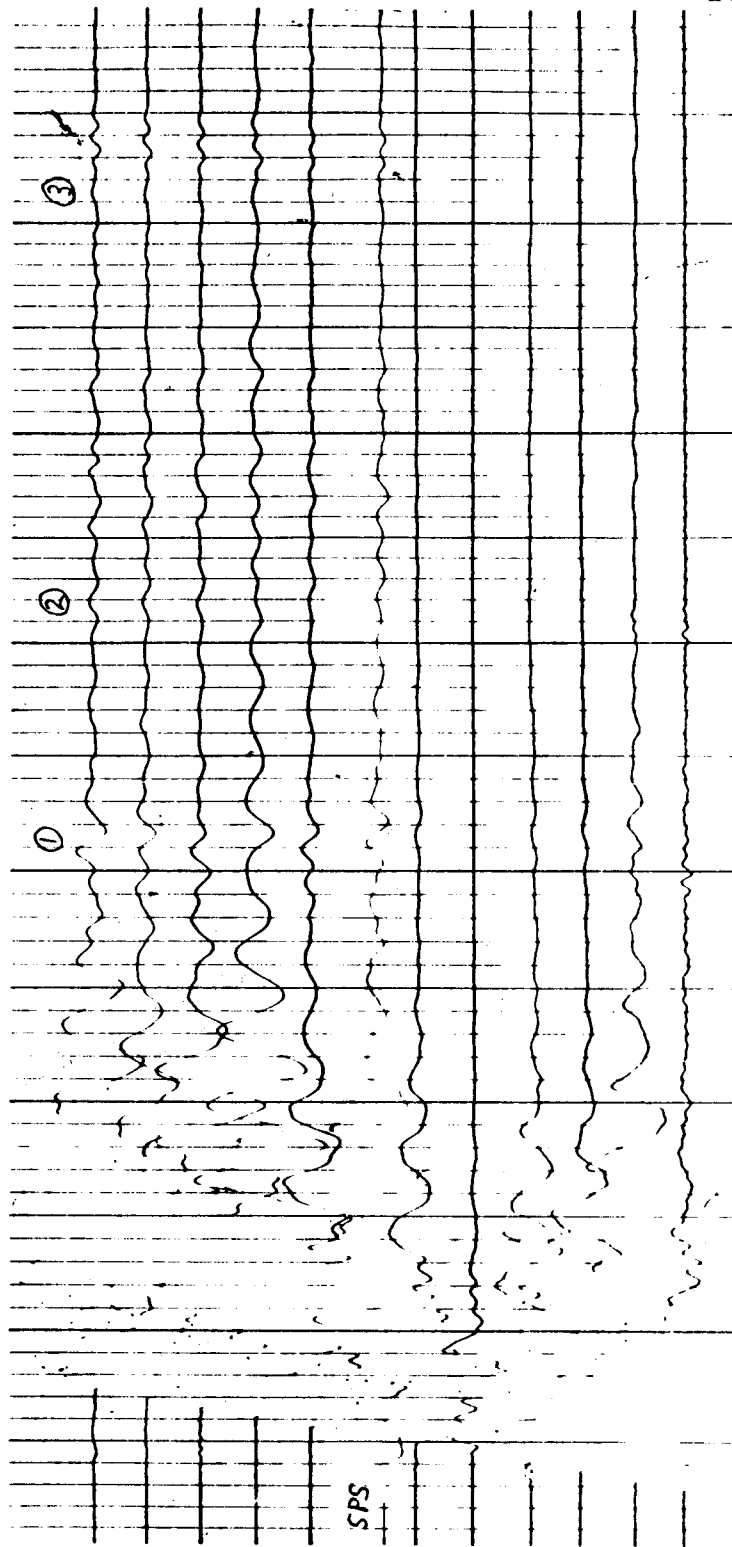
The results of the reflection survey are based entirely upon reflected P-waves. The frequency of most of the good reflections was about 100 Hz. The records are notable for the lack of SS or PS reflections or multiple P reflections. The large dips of the glacier floor probably prevented multiple reflections from being recorded on the relatively short spreads that were used.

As was noted in Section 4.7, the normal method of reflection shooting in shallow holes and the high attenuation of shear waves militate against the production and propagation of shear waves. These factors may account for the lack of SS reflections. For the high angles of incidence involved in the reflection survey, the reflection coefficients for PS are small (Röthlisberger, 1964).

Sometimes more than one reflection appears on a record. When the stepouts of separate reflections on the same record are correlated, the reflections usually turn out to be from different parts of the glacier bed suitably oriented for return of waves to the spreads. Thus, the reflections indicated on the record shown in Figure 35 are interpreted as due to reflecting horizons disposed as in Figure 36.

However, at stations 195, N83, 104 and 106 low amplitude phases follow the first reflected phases after a few milliseconds (Fig. 37). They appear to be "sub-bottom"

Figure 35. Seismogram taken at point 38. Reflections occur at 1, 2, and 3. This was a $\frac{1}{2}$ pound (227 g.) shot at $2\frac{1}{2}$ m. depth, with filter passband 30-160 Hz. The heavy vertical lines represent one-tenth of a second.



SPS

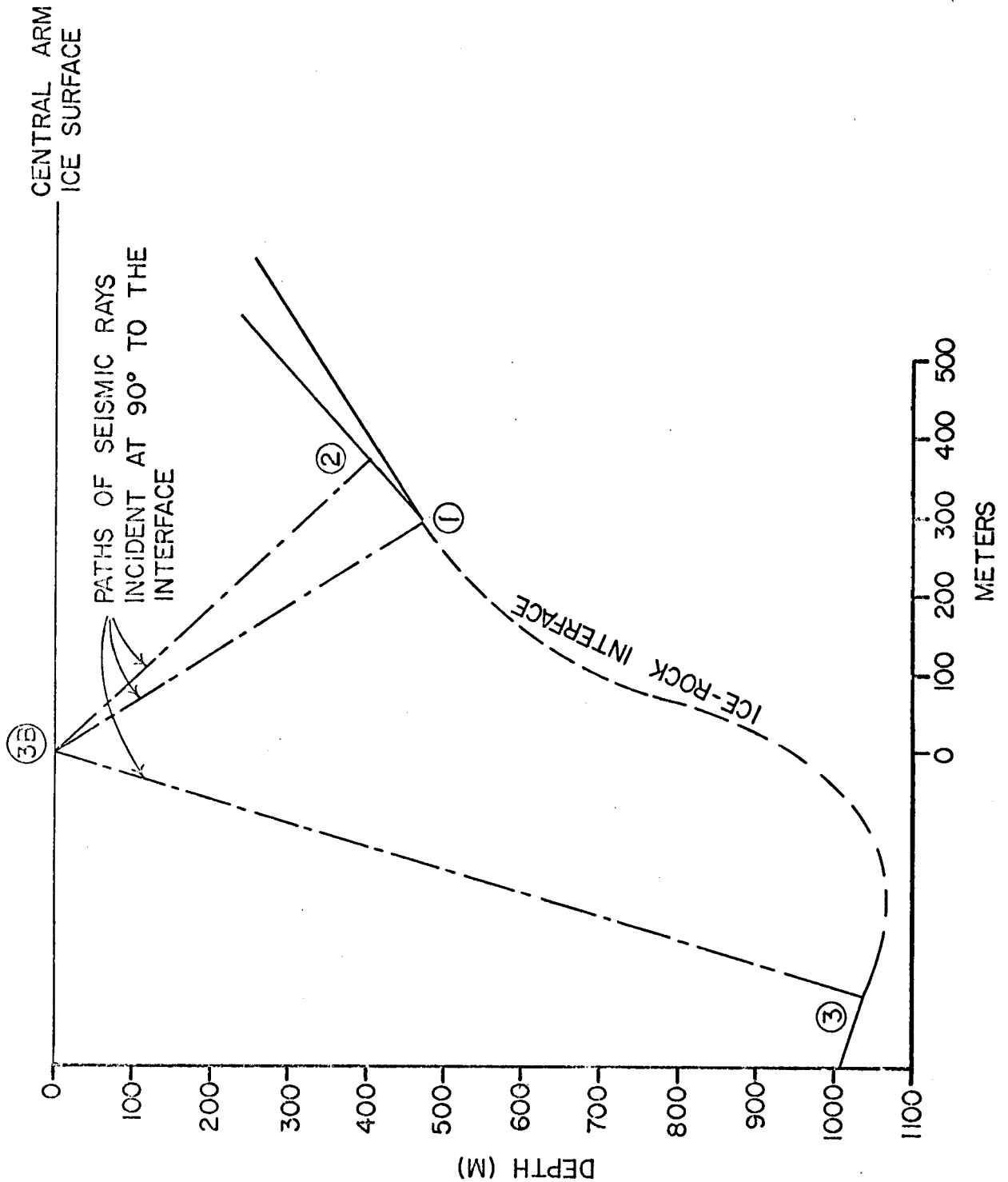
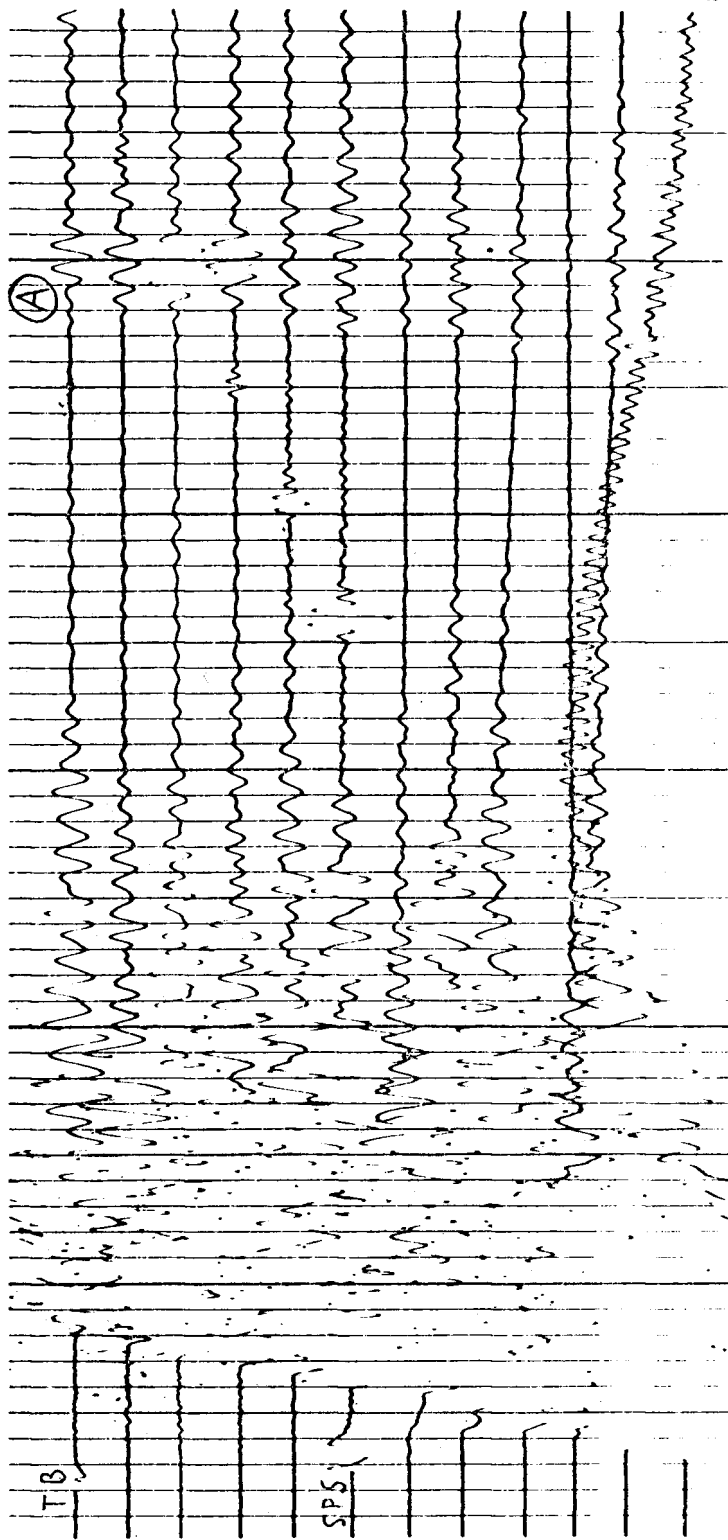


Figure 36. Interpretation of seismogram at point 3B (Fig. 35).

Figure 37. Seismogram taken at point 106. A reflection occurs at A.
This was a 1 1/4 pound (567 g.) shot at 3 m. depth, with filter pass-
band 90-160 Hz.



reflections. The two phases may represent reflection from the top and bottom of a layer of moraine or sediment at the bottom of the glacier. These cases all occur near the centers of the valleys. The thickness of the layer can only be guessed at in the absence of velocity data. If the velocity is between 4 and 6 km./sec. the layer is 40-120 m. thick.

Stations at which no reflections at all were recorded were rare, but at some stations there were no readable reflections in one of the perpendicular spread directions so only slant depth and apparent dip are known. However, reasonable interpolations can be made when more complete data are available at adjacent stations.

Poor recording of reflections may be due to roughness or convexity of the interface or the presence of debris in the ice that could scatter the seismic waves. If there is water at the base of the glacier only weak reflections will be returned from the ice-water interface, but there may be strong reflections from the underlying water-rock interface. At each boundary that is encountered by the seismic waves, energy is lost by refraction or reflection downward, and the signal that ultimately returns to the glacier surface is correspondingly weakened.

6.5 Laboratory Studies

The reflection coefficient of a plane elastic wave, i.e., the fraction of incident energy that is reflected from a plane interface, depends upon the angle of incidence of the wave and the acoustic impedances of the media. In Section 4.7 there was a discussion of the results of R thlisberger (1964) for the reflection and transmission coefficients at an ice-solid interface for solids of various densities and P- and S-wave velocities and for various angles of incidence. For small angles of incidence, such as were involved in this survey, the signal amplitude ratio is, approximately:

$$R = \frac{A_r}{A_i} = \frac{\frac{Z_2}{Z_1} - 1}{\frac{Z_2}{Z_1} + 1} \quad \dots (82)$$

where: A_r = amplitude of reflected P-wave

A_i = amplitude of incident P-wave

$Z_1 = \rho_1 V_{p1}$ = acoustic impedance of upper medium

$Z_2 = \rho_2 V_{p2}$ = acoustic impedance of lower medium

It proved impracticable to measure the seismic velocities of the valley wall rock in situ, so samples were brought back for laboratory study.

The densities of specimens of rock were determined to about 1 part in 300 with a Jolly balance. Compressional wave velocities were calculated from the travel times of ultrasonic waves through cut specimens with measured dimensions.

In this experiment, pulses of radio frequency alternating voltage were applied to a piezoelectric transducer to generate ultrasonic compressional wave pulses. The latter were transmitted through specimens immersed in water and were received by another transducer which converted the acoustic pulses back into electrical pulses. The applied and received electrical pulses were displayed on a calibrated cathode ray oscilloscope so that the time difference between them could be read directly. With corrections for circuit delays, the transit time of the ultrasonic pulse between the transducers could then be obtained. Water immersion eliminated the problems of machining the specimen surfaces and applying the optimum pressure between specimen and transducer. The geometry of the experiment is shown in Figure 38.

Medium I has velocity V_I ; medium II has velocity V_{II} . The transit time for a pulse to go from the transmitter to the receiver through medium I only is: $t = \frac{l}{V_I}$ (83)

When the block of medium II is inserted the transit time is:

$$t_2 = \frac{l-d}{V_I} + \frac{d}{V_{II}} \quad . . . (84)$$

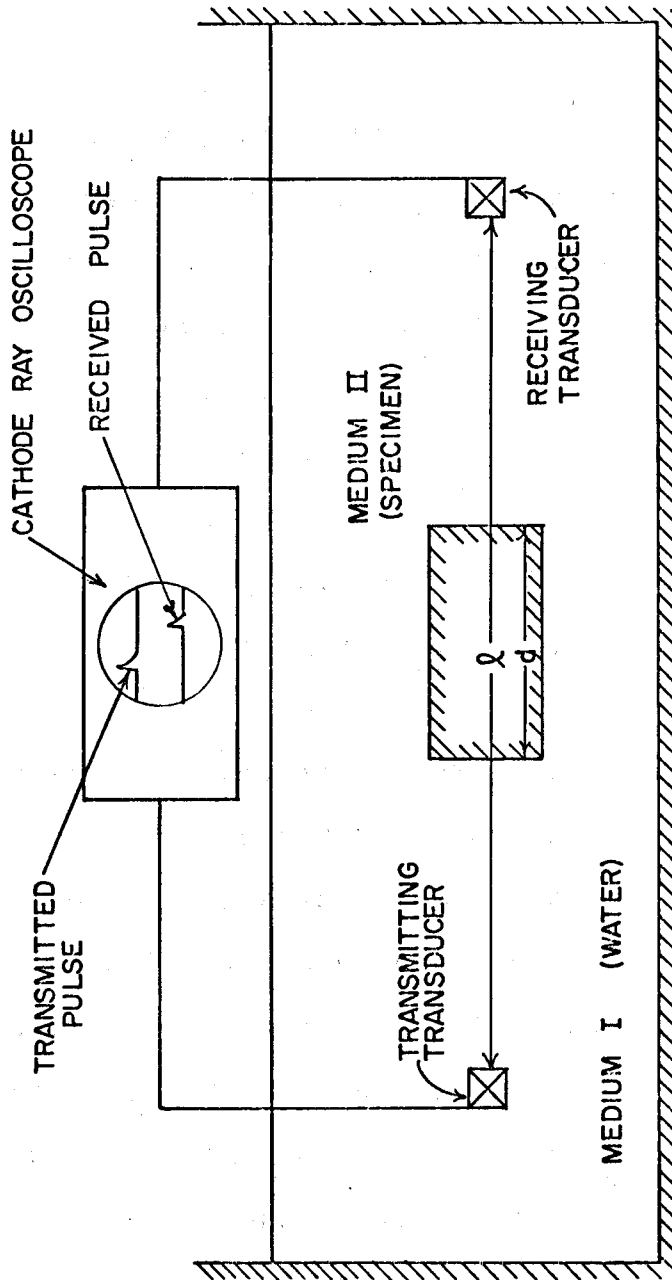


Figure 38. Geometry of the ultrasonic experiment for determining the velocity of elastic waves in rock specimens.

$$\text{Then: } \Delta t = t_1 - t_2 = \frac{l}{V_I} - \frac{l-d}{V_I} - \frac{d}{V_{II}} \quad \dots (85)$$

$$\text{and: } V_{II} = \frac{d}{(d/V_I) - \Delta t} \quad \dots (86)$$

d was measured with calipers to an accuracy of ± 0.1 mm., or better than 1 part in 500. t_1 and t_2 were read on the calibrated cathode ray oscilloscope and Δt could usually be obtained to about 1 part in 100. V_I was determined from repeated measurements of transit time through the water at known transducer separations. It was found to be 1490 m./sec., with accuracy of about 1 part in 100. (Dorsey, 1940, gives a value of 1483.1 m./sec. for the velocity of acoustic waves in distilled water at 20°C.) V_{II} was probably accurate to $\pm 2\%$.

The specimens were cut into orthorhombic blocks with dimensions between 5 and 10 cm. The frequency of the waves was 1 MHz. At this frequency the wave-length (about 5 mm.) was small enough so that disturbing boundary effects that arise when wave-length is similar to specimen diameter did not occur. The grain diameter in most of the specimens was small enough (< 0.1 mm.) so that loss of energy through Rayleigh scattering, which takes place when grain diameter is similar to wave-length, did not occur. The blocky grains of the granodiorite had dimensions up to 1-2 mm., but moderately strong signals were still obtained with these specimens.

For each specimen, measurements were made with all three pairs of sides perpendicular to the ultrasonic beam. With the exception of one of the limestones, all samples were isotropic with respect to velocity within the limits of error of the experiment. The exceptional limestone specimen, which possessed marked foliation, was not included in the results.

The results obtained at a frequency of 1 MHz. were to be applied in field operations in which frequencies of approximately 100 Hz. were used. Hampton (1964), in a study of water-saturated, laboratory-prepared sediments, found that compressional wave velocity through this material was 6% higher at 600 kHz. than at 4 kHz. It may be that for seismic frequencies the velocities and acoustic impedance given here are too high and that consequently the amplitude ratios should be somewhat lower.

The impedance and reflection data for the specimens are given in Table 8. The ratios of the amplitudes of reflected signal to incident signal calculated here are high compared with those encountered in most seismic reflection work, where the reflecting horizon is an interface between different kinds of rock of low velocity contrast. If the rock-ice boundary in the present case is a distinct interface, these data lead one to expect strong seismic reflections. However, the amplitude ratios for the different rock types are so similar that there appears to be little chance of

Table 8. Acoustic impedance and reflected signal amplitude ratios for ice and rocks found in the Kaakawulah Glacier confluence area. A plane compressional wave from the ice is considered to be incident upon a plane interface between the ice and rock. The wave normal is perpendicular to the interface. The rock names are descriptive, not necessarily definitive, and are taken from Wheeler (1963).

Rock type	Collection site	ρ	V_p	Z	Z_r/Z_i	R_0
Ice		0.91	3.70	3.36		
Quartzite	North side of North Arm	2.76	4.78	13.19	3.91	0.59
Granodiorite	South side of South Arm	2.78	5.20	14.46	4.29	0.52
Limestone	Medial moraine	2.70	5.83	15.74	4.67	0.65
Greywacke	Dividing ridge at point of confluence	2.95	5.50	16.23	4.82	0.56
Greenstone	Dividing ridge at point of confluence	2.95	5.77	17.02	5.05	0.57

Units: ρ = density : g./cm.³

V_p = compressional wave velocity : km./sec.

Z = acoustic impedance : g km./cm.³ sec.

Z_r = acoustic impedance of rock

Z_i = acoustic impedance of ice

R_0 = ratio of amplitude of P-waves incident on the ice-rock interface to amplitude of P-waves reflected back into the ice, for 0° angle of incidence.

locating contacts between the different types of rock in the valley floor by comparing amplitudes of reflected waves.

The calculated amplitude ratios can be compared with field data. Consider a uniform medium with spherical waves of initial energy ψ_0 per steradian emanating from a point source. There will be some attenuation constant a , and after the waves have moved distance X from the source, their energy per unit area will be:

$$\psi_x = \frac{\psi_0}{X^2} e^{-ax} \quad \dots (87)$$

Now assume that between distance 0 and X the waves are reflected at an interface with reflection coefficient C . Their energy per unit area at X is then:

$$\psi_x' = \frac{\psi_0 C}{X^2} e^{-ax} \quad \dots (88)$$

The ratio of the energy of the reflected wave to an unreflected wave that has traveled the same distance is:

$$\frac{\psi_x'}{\psi_x} = C \quad \dots (89)$$

and the amplitude ratio of the two waves is:

$$R = \sqrt{C} \quad \dots (90)$$

The amplitude of unreflected P-waves at a given distance from a shot of known size, recorded at known instrument gain (most recordings were made at linear

amplification), is available from the direct P-wave records of the wide-angle profile (Chapter IV). Reflected waves of known path length can be compared directly with unreflected waves at equal path length along the profile.

The amplitude must be corrected for charge size, instrument gain and seismometer response. Assume that the energy of P-wave generation by an explosion is proportional to the amount of the explosive (Robin, 1958). Then to compare the amplitude A' of a wave from a shot of size W_0' to the amplitude for a shot of size W_0 , A' must be multiplied by $\frac{W_0'}{W_0}$. If A' was recorded at e' db. amplification, and it is to be compared with amplitude obtained at e db., A' must be multiplied by $\frac{1}{\sqrt{e' - e}}$ if $e' > e$, or by $\sqrt{e - e'}$ if $e' < e$. The PP reflection is received by the seismometer with its base parallel to the wave front, while in most cases the direct P-wave is received with the base of the seismometer perpendicular to the wave front. A correction must be made for the difference in response of the seismometer in these cases.

Strong PP reflections were obtained at shot point 10 and 11, which had ray paths of approximately 500 and 400 m., respectively. These shot points were near the point of confluence, where the bedrock is apparently composed chiefly of greenstone and greywacke, which have amplitude ratios of approximately 2/3 (Table 8). The observed amplitude ratios were about $\frac{1}{2}$. The disagreement is small but apparently

significant. It is probably caused by a less than perfect ice-rock interface, but velocity dispersion and a greater attenuation constant, a , at depth may also be factors.

6.6 Conclusions

Consideration of the results of the reflection survey leads to the following conclusions:

(1) The great thickness of the glacier--a maximum of approximately 1000 m.-- requires that the bed of the glacier at the confluence (about 750 m.) be somewhat lower than the elevation of the terminus, 40 km. down-glacier (800-850 m.), where the ice is resting on outwash.

(2) In the immediate vicinity of the confluence, the mean longitudinal slope of the valley floor is approximately equal to the slope of the glacier surface.

The trend of stepout times along the seismic spreads often indicates a slight concavity in the reflecting surface rather than the planarity assumed. This results in focusing of the reflected waves and should enhance the signals. The effect does not appear to be strong enough to cause spurious reflections from buried foci. The concavity, of course, is not unexpected in a glacial valley.

The assumption that the bottom is locally nearly planar does not seem to lead to any large errors. There is a large increase in dip from station 7 to station 11,

but in the vicinity of each station the change is not large. At station 10 the dip, azimuth and depth computed on the basis of the westward and northward spreads and again for the westward and southward spreads are nearly identical.

(3) The valleys of the two arms and the valley of the combined glacier have fairly symmetrical transverse sections. The valleys of the arms are roughly parabolic in section. The combined glacier is twice as wide as either of the arms but all have approximately the same depth: the floor of the combined glacier is merely wider and flatter than the floor of either of the arms.

(4) The rate of change of slope of the valley walls above and below the surface of the glacier is essentially constant. There is no evidence that glacial erosion has caused a break in slope.

(5) The floors of the two valleys merge only two kilometers below the point of confluence. This is approximately where the ice flow of the two arms becomes merged into a uniform pattern of flow.

(6) In the introduction attention was drawn to the depression in the valley floor at the confluence of the glaciers that combine to form the Grosser Aletsch Glacier in the Alps. No similar depression was found at the Kaskawulsh confluence. However, there may be a bedrock sill down-glacier from the surveyed area. At the lowest

profile on the Kaakawulsh Glacier, Anderton (1967) found that flow was unified--the glacier was behaving as a single stream of ice. If there is a sill down-glacier from the lowest profile, it can be concluded that the bedrock depression thus formed extends beyond the region of converging ice flow.

(7) The North Arm, which has greater surface slope and surface velocity than the Central Arm (Anderton, 1967), also has a steeper valley floor and smaller ice thickness.

(8) Features of significant relief on the valley floor, such as the irregularity illustrated in Figure 36, may not be reflected in any obvious way at the surface of the glacier. Presumably the feature illustrated presents no transverse obstruction to glacier flow. A transverse obstruction of similar magnitude would probably have greater surface expression (Nye, 1959).

CHAPTER VII

DISCUSSION

7.1 General Remarks

Brace (1965) has found significant correlations between measured variations of linear compressibility in quartzite, mica schist, marble, phyllite, slate and gneiss, and the preferred orientation of mica, calcite and quartz grains in these rocks. Similar agreement was found between thermal expansion and thermal conductivity and the preferred orientation fabric of calcite in Yule marble. The use of directional physical properties to determine the nature of a rock fabric is suggested by Brace's results. In the present work, one aspect of directional physical properties --the anisotropic propagation of elastic waves--has been used to explore the crystallographic and non-crystallographic fabrics of one metamorphic rock--glacier ice.

Glacier ice has certain characteristics that are advantageous for the study of rock fabric. In most situations encountered in nature such studies are obscured by the compositional complexity of the rock material, the indefiniteness of the boundaries of the geologic body

concerned, and the slow response of rock fabric to stress changes. The glacier is a monomineralic body with sharply defined boundaries and relative rapidity of fabric response to changes in the stress field. On the other hand, the glacier presents some serious difficulties for the study of its fabric. Problems arising from fractures, variations in porosity, and closeness to the melting point of the medium have been encountered in the course of this investigation. It has also been found that crystallographic fabrics in a glacier can be far from simple.

Rudzki (1898, 1911) was apparently the first investigator to draw attention to the possibility of anisotropic elastic wave propagation within the earth. The apparent double refraction of transverse seismic waves in the earth was noted by Byerly in 1938. Stoneley (1949) investigated the possible effects, including double refraction, of anisotropic wave propagation in the earth's crust on seismological observations. Analogies between tectonophysics and glacier physics were pointed out by Kamb (1964), and he suggested that studies of glacier flow and the structures associated with it could have great theoretical significance in the understanding of deformation within the earth. Anderson (1963) proposed the application of seismological techniques involving anisotropic wave propagation for the determination of crystal orientation in glaciers as an aid to the study of stresses and flow processes in the

ice. If the glacier can be considered as a model for the material of the earth's interior in some respects, anisotropic wave propagation, a phenomenon common to both the glacier and the earth's interior, may serve both as a diagnostic tool and as a link between them. The present work leads one to suggest that this would be a promising direction for further study.

7.2 Factors Affecting the Elastic Constants

This work has relied primarily on measurements of elastic wave velocities, which are functions of the elastic moduli and densities of the media through which they are propagated. The moduli are influenced by several factors which require some comment.

Temperature

The temperature dependence of the elastic constants of single crystals of ice was discussed above in connection with the experiments of Bass, Rossberg and Ziegler (1957). The elastic moduli of polycrystalline lake ice in which the crystals showed strong preferred orientation with their C-axes vertical were determined by Brockamp and Querfurth (1964) over the temperature range 0° to -20.5°C . The moduli were derived by means of the Christoffel equations from ultrasonic wave velocities. All five moduli C_{ij} increase with decreasing temperature, but the rate of change

decreases. Thermodynamic considerations and some experimental results indicate that for all substances $\partial C_{ij} / \partial T$ becomes zero at 0°K . (Hearmon, 1956). The temperature dependence of elastic wave velocities in polycrystalline ice that is assumed to be isotropic has been treated by Robin (1958), Brockamp and Kohnen (1965), and Thyssen (1967).

Information on temperature distribution in the interior of a temperate glacier is limited. No temperature-depth data are available for the Kaskawulsh ice. Sharp (1951), working on the firn of the upper Seward Glacier, on the Pacific side of the St. Elias Mountains, found that the annual chilled layer disappeared within the first 10 days of July at an elevation of 1791 m. Grew and Mellor (1966) obtained temperature profiles at Seward Camp (1900 m.), near the site of Sharp's studies, and at Divide Camp (2600 m.), on the ice divide between the Hubbard and Kaskawulsh Glaciers (see Fig. 2--map of icefield area). Seward Camp is comparable in elevation to Kaskawulsh Camp but winter temperatures are probably higher at Seward because of its more maritime location. On August 3, 1964, no definite chilled zone was apparent in the upper 4 m. of snow and the maximum temperature range over this depth was less than 2°C . At Divide Camp, which is somewhat colder than the Kaskawulsh confluence (Marcus, 1965b; Marcus, Rens and Taylor, 1966), the winter chilled zone was still

in evidence on August 16, 1964: 1 m. and 15 m. temperatures were near 0°C . while a minimum of about -2.3°C . was reached at 7.5 m. depth. According to the data of Brockamp and Querfurth, a temperature variation of 2.3°C . at temperatures just below 0°C . corresponds to velocity variations of about 10 m./sec. and 15 m./sec. for P-waves and S-waves, respectively. This is barely above the margin of error for seismic velocity measurements in the present study.

The data above pertain to the snow-firn layer. More applicable to the case of ice are the measurements taken by McCall (1952) in an ice tunnel about 50 m. below the firn line of the Skauthøe cirque glacier in Jotunheim, Norway. This location is comparable in latitude (Skauthøe is at $61^{\circ}37.5'\text{N}$.) and elevation (approximately 2000 m.) to the Kaskawulsh confluence area. Like the Kaskawulsh Glacier, Skauthøe is situated on the continental side of an extensively glacierized coastal mountain range. McCall found that a cold zone outlined by hoar frost deposition on the tunnel wall extended from the surface to a depth of 30 m. in both August and December, and he inferred that it persisted throughout the year. The profile for August showed that the temperature was 0°C . at the surface, $-0.6 \pm 0.1^{\circ}\text{C}$. at a depth of 12 m. (minimum temperature), and nearly 0°C . again at 30 m. depth. This temperature range corresponds to only about 2 or 3 m./sec. in seismic wave

velocity according to the data of Brockamp and Querfurth (1964). Consequently, a temperature difference of this magnitude would have no measurable effect on seismic wave velocity.

For ice at the melting point, Brockamp and Querfurth found anomalous behavior, with some velocity values falling far below the intercept of the velocity-temperature curve. Robin (1958) also noted this effect. The low value of seismic wave velocity in the near-surface zone of the glacier, discovered through the short refraction experiments in the present investigation, may be due in part to this lowered velocity in ice at the melting point. It is not known if ice below the surface is actually brought to the melting point during the summer. Of course, if an actual phase change to the liquid state takes place, the velocity is sharply reduced because P-wave velocity in water is only about 38% of its value in ice (Dorsey, 1940). Shumskii (1964) asserts that after the surface layer of a glacier begins to melt, the radiational melting does not go deeper than 1-2 m. in the ice.

Stress

Compressional wave velocity in a solid body is known to increase as the body is subjected to increasing pressure (Birch, 1960, 1961). This occurs partly as the result of reduction of pore volume and closing of cracks and partly,

as pressure is increased, by changes in the elastic constants. In the latter case, Hooke's law becomes effectively non-linear and the "third order" elastic constants are introduced (Hearmon, 1956). In a glacier the first effect is considerable and is undoubtedly connected with the disappearance of the "low velocity" effect several meters below the surface. The fractures evident at the surface, from minute cracks to crevasses, become closed at depth (Holdsworth, 1965). Air bubbles also decrease in size. As noted above in Chapter V, this effect tends to decrease porosity in the more porous laminae and hence the difference in the density and elastic properties between foliation laminae. This results in greater isotropy at depth.

The second effect is probably not great. Pressure at the base of the Kaskawulsh is less than 100 bars. For most crystalline materials the change in elastic modulus with pressure is of the order of 10^{-5} (modulus and pressure both expressed in cm^2/kg). Robin (1958) measured P-wave velocity in samples of compacted snow compressed to a pressure of 200 bars at temperatures between -5° and -60°C . Extrapolation to -3°C . gave a value within experimental error of the velocity of P-waves in clear ice from the Jungfrauoch icefield, Switzerland, at -3°C .

The effect of deviatoric stresses on polycrystalline aggregates is not well known. Tocher (1957) measured P-wave velocities in several types of rock under unidirectional

stress and found that the velocity parallel to the stress direction increases as much as it does in the same substance under hydrostatic pressure of the same magnitude. Perpendicular to this direction, velocity increases at a much lower rate with increasing stress. Since glacier ice does not sustain deviatoric stresses of much more than 1 kg./cm.^2 (Shumskii, 1964), the effect on elastic constants and wave velocities would appear to be slight. The evidence from strain release in Chapter III that locally large stresses may build up temporarily probably does not alter this picture appreciably.

Other effects

The elastic properties of crystals are affected by anelasticity and deformation of the medium, electromagnetic and nuclear radiation, and, in crystals exhibiting piezoelectricity, electrical conditions. Pounder (1965) has demonstrated that for periods less than one second, which correspond to all but the longest surface waves encountered in this study, anelastic effects on wave propagation in ice are small. Plastic deformation and concomitant dislocations are known to decrease elastic moduli by small amounts (Huntington, 1958). Because these processes are present to varying degrees throughout the glacier, some inhomogeneity and anisotropy in elastic behavior are undoubtedly introduced by them, but the magnitude of these effects is unknown. Elastic properties of quartz, silicon and sodium

chloride crystals have been altered by X-ray, γ -ray, electron, neutron, deuteron and α -particle bombardment by as much as 1% (Hearmon, 1956; Huntington, 1958) but the effect of natural radiation on the elastic properties of ice has not been investigated. Although ice crystals exhibit external hemimorphism and the C-axis appears to be polar, the piezoelectric effect, which occurs with polar symmetry, has not been demonstrated in ice (Shumskii, 1964). Brill and Camp (1961) suggest that this is due to random orientation of polar domains within the crystal.

It should be noted that in the shock zone in the immediate vicinity of a shot the temperature, stress and rate of deformation will be greatly different from the magnitudes considered here.

7.3 Seismology and Structural Analysis

This discussion will use the concepts and terminology of Turner and Weiss (1963) and their interpretation of the structural ideas of Sander (1930). In discussing symmetry the convenient Schoenflies notation will be used, e.g., $D_{\infty h}$ to represent the symmetry of an axis of infinite-fold symmetry perpendicular to a plane of reflection (Phillips, 1949).

Structural analysis seeks to describe the internal order of deformed rocks, reconstruct the movements that

brought them to their present positions and derive the external and internal stresses that produced the deformation. The internal order, or fabric, of the rock is deformed or replaced by another fabric and this deformed or new fabric provides a record of the deformation. The study of the effects of fabrics on the propagation of seismic waves in rocks is also a study of the efficacy of seismology as a technique of structural analysis. This can be on the scale of geologic bodies, such as glaciers, and on the scale of tectonophysics mentioned at the beginning of this chapter. In other words, the question may be asked: What can seismic methods tell us about the fabric of a deformed rock?

Structural analysis involves the study of two types of fabric: crystallographic and non-crystallographic. In the present work, fabrics of both types have been found superposed: the crystallographic fabric consisting of preferred orientation of ice crystal C-axes, and the non-crystallographic foliation fabric consisting of alternating layers of relatively bubbly and bubble-free ice. These fabrics differ in their relationship to the principal strain-rate axes and hence to the stress system of the glacier. Anderton's analysis (1967) of surface strain-rates and petrographic data on crystal orientation led him to the conclusion that in regions of high strain rate ($> 10^{-4}$ /day), where there is a direct relationship between fabric and

current deformation, the stress field is symmetrically related to the crystallographic fabric.

The multiple-maxima fabric patterns are centered on a direction of maximum shearing strain rate or, near the medial moraine, the single maximum is centered on the direction of principal compressive strain rate (see also Brace, 1960). However, foliation in this region does not show any symmetrical relationship to the stress field: the foliation S-planes are not parallel to planes of maximum shearing stress but rather to the median plane of the combined glacier below the confluence. At the edge of the glacier, where the ice is apparently deforming by simple shear, the foliation does tend to form parallel to planes of maximum shearing stress, and to the ice-rock interface.

It has been shown above that both basic types of fabric can be treated as transversely isotropic media, or superpositions of such media, with respect to the propagation of seismic waves. Furthermore, since the anisotropy figure of the crystallographic fabric is "prolate," while that of the non-crystallographic (foliation) fabric is "oblate," with respect to seismic wave propagation, the two types of fabric are clearly distinguishable. If one fabric type is absent, or if the anisotropy factor of one strongly predominates, then the type and strength of that fabric can, in principle, be gauged by seismic means.

Seismology then appears to be a potential tool in structural analysis. However, the present study indicates that the absolute magnitudes of the anisotropy factors of the two fabric types can be very similar, in which case cancellation of the effect occurs and the usefulness of the technique is limited. In regions of high strain rate ($>10^{-4}$ /day) on a glacier, flow appears to take place mainly along the basal planes of ice crystals, while flow is also related to the differentiation process that results in foliation (Shumskii, 1964; Anderton, 1967). Hence, foliations and crystallographic fabric are clearly related to flow, although, as noted above, they are not generally coincident with one another. The S-planes of both fabrics, however, are often sub-parallel, and near-cancellation can be achieved.

7.4 Symmetry Considerations

In the investigation of seismic wave velocities in structures defined by crystallographic and non-crystallographic fabrics, we are concerned with the symmetry of the fabrics. In crystallographic fabrics, the symmetry is derived from the symmetry of the constituent crystals and the symmetry of the fabric pattern. A fabric may have the same or lower symmetry than its component elements; it cannot have higher symmetry. In the case of the fabric defined by the preferred orientation of ice crystal C-axes,

each individual crystal has $D_{\infty h}$ symmetry. If the fabric likewise had $D_{\infty h}$ symmetry, the symmetry exhibited in the angular distribution of seismic wave velocities will be $D_{\infty h}$. This is the case in the vicinity of the medial moraine, where the crystallographic fabric has a single circular maximum, and in the case of concentric girdle fabrics. Crystallographic fabrics in regions of high shearing strain rate tend to assume D_{2h} (orthorhombic) or D_{4h} (tetragonal) symmetry. In these cases, the pattern of seismic wave velocities will have the lower symmetries, D_{2h} or D_{4h} , rather than the $D_{\infty h}$ symmetry of the individual crystal. Strictly speaking, they will also have more independent elastic constants.

It may be remarked that foliation has $D_{\infty h}$ symmetry and superposition of this symmetry with the lower symmetry of a crystallographic fabric, such as D_{2h} , will result in a total fabric with D_{2h} symmetry. If the crystallographic anisotropy is great enough, the lower symmetry fabric may be detected even when the two fabrics are superposed and the anisotropy factors are similar.

The processes of deformation and the internal mechanical and crystallographic responses to it tend to alter the internal symmetry of a geologic body. The development of preferential crystal growth, zones of cataclasis or bubble-layering, fracturing, etc., in homogeneous, isotropic ice result in a change from spherical symmetry to

transverse isotropic symmetry, as in the case of single-pole crystal orientation, foliation, and parallel fracture: $K_{\infty h} \rightarrow D_{\infty h}$. Still lower symmetry, such as D_{2h} , D_{3h} , and D_{4h} , may develop, but not necessarily progressively. Anderton (1967) found no evidence that D_{2h} fabrics had passed through a $D_{\infty h}$ stage.

Seismic wave velocities are functions of the elastic constants, which are symmetry-determined. In a sense, the seismic applications presented here are symmetry-detecting techniques using symmetry-dependent tools. Changes in symmetry, which go on continuously in a glacier, are accompanied by changes in the anisotropy of seismic wave propagation.

7.5 Additional Non-crystallographic Fabrics

Heretofore, foliation consisting of a simple model of alternating layers of porous and non-porous ice of equal thickness has been treated. Variations were introduced by changing the porosity of the "bubbly" layers. There can, of course, be cyclic stratification of any number of layers of different thicknesses and porosities. Any model consisting of infinitely extending layers with parallel planar boundaries and homogeneous, isotropic composition can be only an approximation of the real foliation which typically consists of irregular, discontinuous, lenticular,

en echelon, and sometimes folded layers. Internally the layers are often inhomogeneous, though they do not seem to be so in any regular fashion, such as by having graded porosity.

In deducing particular foliation parameters from field data on seismic wave velocities, one encounters the familiar geophysical problem that there is no unique configuration that produces the measured effect. The velocities of the three wave modes propagated in a transversely isotropic medium consisting of alternating or cyclically repeated isotropic layers depend not only on the elastic constants of the layers, but also on their densities (i.e., porosities) and the relative thicknesses of the layers. All these parameters may vary. Measurements on the Kaskawulsh Glacier indicate that while porosities vary widely, they tend to be fairly constant among corresponding layers of a particular foliation domain. Similarly, layer spacing in foliation for a given domain can usually be described as "fine" (blue layers, 0.5 - 10 cm. wide and spaced 5 - 50 cm. apart) or "coarse" (blue layers, 10 - 30 cm. thick and spaced 50 - 200 cm. apart) (Anderton, 1967). It is the relative, not absolute, spacing that is pertinent to velocity anisotropy (assuming that all spacing is small compared to wave-length) and, hence, very fine layering must be taken into consideration. With these known limitations on the parameters, the problem of interpretation can be considerably simplified.

The problem of uniqueness in replacing a stratified inhomogeneous medium by a transversely isotropic homogeneous medium when the wave lengths are long compared with strata thicknesses has been studied by Backus (1962). He found that if a homogeneous transversely isotropic medium can be replaced by any medium consisting of cyclically arranged isotropic layers, it is also equal to a layered medium consisting of only three homogeneous isotropic materials, and under certain inequality relations among the elastic moduli C_{ij} , it is equivalent to such a medium consisting of only two homogeneous isotropic materials. The latter case applies in the examples used in the present work. Backus also found that, in general, there exist transversely isotropic media that cannot be replaced by layers of isotropic material.

This study has been confined to the consideration of three types of fabric: foliation defined by bubble layering, crystallographic fabric defined by preferred orientation of ice crystal C-axes, and fracture fabrics defined by parallel alignment of planar discontinuities. Other types of structures defined by layering or preferred orientation of elements can exist in glacier ice. To the extent that layered structures consist of alternating or otherwise cyclically arranged laminae of differing elastic properties and densities, they may be approximated by long-wave equivalent media in the manner described above. Such structures

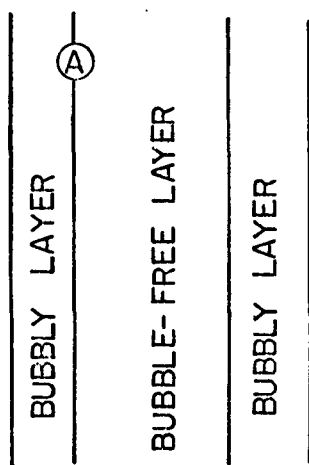
include layering of different mean grain size and alternate layers relatively full of and free from impurities.

Non-crystallographic elements may display preferred orientation, e.g., tabular ice crystals or debris fragments and flattened bubbles. The latter form a fabric similar to fracture fabric. More commonly, bubbles assume tri-axial ellipsoidal forms with D_{2h} instead of $D_{\infty h}$ symmetry.

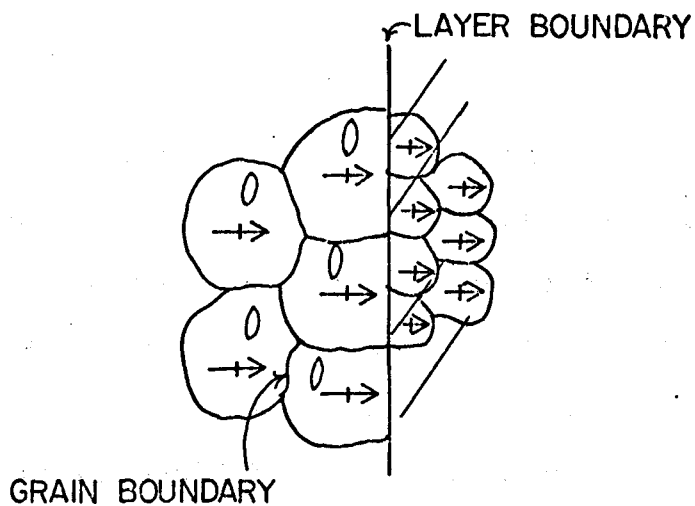
Linear structures can also exist. They include preferred orientation of elongate bubbles or debris fragments and linear distributions of bubbles or fragments of any shape or orientation. These structures also have $D_{\infty h}$ symmetry, with the axis of ∞ -fold symmetry parallel to the long axis of the structural elements.

The effects of these oriented inclusions of various shapes and of linear structures on the elastic constants of materials are not well known. Only randomly oriented planar discontinuities have been treated in any detail (Walsh and Brace, 1966).

Actual situations in a glacier will often find several of these fabric types superposed. A common example from near the flank of the Kaskawulsh Glacier is presented diagrammatically in figure 39.



a. GENERAL SCHEME

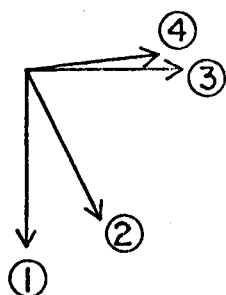


b. DETAIL AT (A)

-i→ DIRECTION OF OPTIC AXIS

0 ELONGATE BUBBLE

/// FRACTURES



① BUBBLE ORIENTATION

② FRACTURE

③ GRAIN TEXTURE AND BUBBLE FOLIATION

④ OPTIC AXIS OF CRYSTALS

c. ORIENTATION OF SYMMETRY AXES OF THE FABRICS

Figure 39. Examples of superposed fabrics.

7.6 Conclusions

Continuous seismograph recording on the Kaskawulsh Glacier established that it is a source of seismic energy. Some of the energy is released in discrete events resembling minute earthquakes. These may be related to discontinuous movement of the ice mass.

Despite the large difference in acoustic impedance between ice and the surrounding rock demonstrated by laboratory studies of rock samples, the reflection of seismic energy from the bottom of the glacier was often poor. These non-reflecting areas may be characterized by the presence of morainal material in the lower layers of ice, melting in these layers, or unsuitable configuration of the ice-rock interface for the reflection of coherent energy.

No significant inhomogeneities were found within the glacier. Velocities of compressional and shear waves do not vary appreciably except near the surface. There, a layer several meters thick possesses a positive velocity gradient apparently related to decreasing amount of porosity, melting, and open fracturing with depth.

The porosity of foliated ice was measured and porosity in bubbly layers was found to range up to 6%. The effect of foliation on seismic wave velocity anisotropy was calculated. Both foliation and preferred orientation of ice crystal symmetry axes were found to produce small but measurable anisotropy in seismic wave propagation.

With respect to the symmetry axis of the fabric, the anisotropy factor is greater than unity for foliation and less than unity for crystallographic fabric. In regions of high strain rate, the S-planes of both fabrics tend to be sub-parallel and the two anisotropy effects are opposed. Where porosity differences between foliation layers diminish with depth, the resultant anisotropy factor becomes less than unity at depth.

The gross structure of the confluence of the North and Central Arms of the Kaskawulsh Glacier was revealed by seismic reflection investigations. The valleys were found to be roughly parabolic and symmetrical in profile. Maximum ice thickness measured was slightly over 1000 m. in the center of the Central Arm. The slope of the valley walls is continuous from above to below the surface of the glacier. The ridge separating the two arms ends at the same distance downstream from the point of confluence at which the two arms achieve unity of flow. The Central Arm ice is thicker than the faster flowing North Arm ice. There is no basin and sill structure in the immediate confluence area.

7.7 Suggestions for Further Work

Several lines of investigation in theory, in the field and in the laboratory, are suggested by the results of the present study and the problems encountered while carrying

it out. It is clear that a great deal remains to be learned about the effect of inclusions and pores in media on the transmission of seismic waves. The effects of various shapes and orientations of pores, cracks, and included fragments are of special interest. The consequences of superposing different types of fabric at various orientations on the propagation of different modes of seismic wave propagation should be explored. Wave propagation in anisotropic polycrystalline aggregates deserves some theoretical consideration.

The differentiation of pure and mixed modes of wave propagation might be fruitful in the exploration of anisotropic structures. Pure modes are transmitted only along the axes of symmetry and the detection of such modes might be useful in the determination of the fabric symmetry of a geologic body.

In the field, in situ studies of rock properties call for more effective means of producing and detecting shear waves, and possibly other modes of wave propagation. Field studies that might yield valuable information on seismic wave propagation in deformed material include investigations of strong and relatively simple fabrics in glaciers. For example, the snouts of some cold glaciers show very strong preferred orientation of ice crystal optic axes.

Laboratory work on wave propagation in models and in ice samples under various conditions of temperature, stress,

strain rate, etc., are recommended. The use of ultrasonic waves is clearly applicable here and in some field investigations. More knowledge of the variation of physical properties of rocks and ice with elastic wave frequency would be valuable in comparing the results of laboratory and field investigations.



Figure 40. Seismic shooting on the Kaskawulsh Glacier.

APPENDIX I

MAPPING

The base map of the confluence area of the Kaskawulsh Glacier (Fig. 3) was prepared by the Department of Geodetic Science, of The Ohio State University, from aerial photographs taken by the Royal Canadian Air Force. A detailed discussion of the preparation and adequacy of the map is presented by Anderton (1967). The aerial photographs were taken in 1951. Ground observation indicated that the major features of the glacier surface had not changed significantly between that time and 1964-1965.

Location of the points used as shot points in the seismic survey was carried out as part of the glacier movement survey of the Icefield Ranges Research Project during the summers of 1964 and 1965. This operation is also discussed by Anderton (1967).

REFERENCES

- Adams, W. P., 1966, Ablation and run-off on the White Glacier, Axel Heiberg Island, Canadian Arctic Archipelago: Axel Heiberg Island Res. Rept., Glaciology, No. 1, McGill Univ., Montreal, 77 p.
- Allen, C. R., and Smith, G. I., 1953, Seismic and gravity investigations on the Malaspina Glacier, Alaska: Trans., Amer. Geophys. Union, v. 34, n. 5, p. 755-760.
- Allen, C. R., Kamb, W. B., Meier, M. F., and Sharp, R. P., 1960, Structure of the lower Blue Glacier, Washington: J. Geol., v. 68, n. 6, p. 601-625.
- Anderson, D. L., 1961, Elastic wave propagation in layered anisotropic media: J. Geophys. Res., v. 66, n. 9, p. 2953-2963.
- , 1963, Use of long-period surface waves for determination of elastic and petrological properties of ice masses: in Ice and Snow (W. D. Kingery, ed.), M.I.T. Press, Cambridge, Mass., p. 63-68.
- Anderton, P. W., 1967, Structural glaciology of a glacier confluence, Kaskawulsh Glacier, Yukon Territory, Canada: Ph.D. Dissertation, The Ohio State University.
- Backus, G. E., 1962, Long-wave elastic anisotropy produced by horizontal layering: J. Geophys. Res., v. 67, n. 11, p. 4427-4440.
- Bader, Henri, 1950, The significance of air bubbles in glacier ice: J. Glaciol., v. 1, n. 8, p. 443-451.
- Bass, R., Rossberg, D., and Ziegler, G., 1957, Die elastischen Konstanten des Eises: Zeitschrift für Physik, v. 149, p. 199-203.
- Bechmann, R., and Ayers, S., 1957, Thickness modes of plates excited piezoelectrically: in "Piezoelectricity," British G. P. O. Res. Sta. Engineering Rept., p. 33-41.
- Berzon, I. S., Bokanenko, L. I., and Isaev, V. S., 1959, Seismicheskie issledovaniya na lednike Tuyuksu: Glyatz. i Seismol. Razd. Prog. M. G. G., n. 3, 68 p.

- Berzon, I. S., Pak, V. A., and Yakovlev, V. N., 1960, Seismicheskoe zondirovanie lednika Fedchenko: Glyatziologicheskaya ekspeditsiya na lednik Fedchenko, V. L. Shul'tz, Red., Izdat. Akad. Nauk Uzbekakoi SSR, Tashkent, p. 84-109.
- Blot, M. A., 1956, Theory of propagation of elastic waves in a fluid-saturated porous solid: J. Acoust. Soc. America, v. 28, n. 2, p. 168-191.
- Birch, Francis, 1960, The velocity of compressional waves in rocks to 10 kilobars, Part I: J. Geophys. Res., v. 65, n. 4, p. 1083-1102.
- , 1961, The velocity of compressional waves in rocks to 10 kilobars, Part 2: J. Geophys. Res., v. 66, n. 7, p. 2199-2224.
- Bokanenko, L. I., and Isaev, V. S., 1960, Predvaritel'nie resul'tati opredeleniya moshchnosti l'dov El'brusa seismicheskim metodom: El'brusskaya ekspeditsiya Moskovskogo Gosudarstvennogo Universiteta i Instituta Prikladnoi Geofizika Akademii Nauk SSSR, G. K. Tushinskii, Red., Informatzionii Sbornik o Rabotakh po M. G. G., n. 5, p. 10-58.
- Borns, H. W., Jr., and Goldthwait, R. P., 1966, Late-Pleistocene fluctuations of Kaskawulsh glacier, southwestern Yukon Territory, Canada: Amer. J. Sci., v. 264, n. 8, p. 600-619.
- Borovinskii, B. A., 1963, Izuchenie lednikov Zailiiskogo Alatau geofizicheskimi metodami: Glyatziologiya i seismologiya, IX i XII Razdeli Programmi MGG, n. 10 i n. 5, Izdat. Akad. Nauk SSSR, Moskva, 112 p.
- Bostock, H. S., 1948, Physiography of the Canadian cordillera with special reference to the area north of the fifty-fifth parallel: Geol. Surv. Canada, Memoir 247, 106 p.
- Brace, W. F., 1960, Orientation of anisotropic minerals in a stress field: discussion: Geol. Soc. America, Memoir 79, p. 9-20.
- , 1965, Relation of elastic properties of rocks to fabric: J. Geophys. Res., v. 70, n. 22, p. 5657-5667.
- Brill, R., and Camp, P. R., 1961, Properties of ice: CRREL Res. Rept. 68, 75 p.
- Brockamp, B., and Mothes, H., 1930, Seismische Untersuchungen auf dem Pasterzegletscher. I: Zeitschrift für Geophysik, Bd. 6, p. 482-500.

- Brockamp, B., and Mothes, H., 1931, Seismische Untersuchungen auf dem Pasterzegletscher. II: Zeitschrift für Geophysik, Bd. 7, p. 232-240.
- Kohnen, H., 1965 (pub. 1967), Ein Beitrag zu den seismischen Untersuchungen auf dem grönländischen Inlandeis: Polarforschung, Bd. 6, J. 35, Ht. 1/2, p. 2-12.
- Querfurth, H., 1964 (pub. 1965), Untersuchungen über die Elastizitätskonstanten von See- und Kunsteis: Polarforschung, Bd. 5, J. 34, Ht. 1/2, p. 253-262.
- Butkovich, T. R., 1959, Mechanical properties of ice: Quart. Colo. Sch. Mines, v. 54, n. 3, p. 349-360.
- Byerly, Perry, 1938, The earthquake of July 6, 1934: amplitudes and first motion: Bull. Seismol. Soc. America, v. 28, n. 1, p. 1-13.
- Cady, W. G., 1964, Piezoelectricity, an Introduction to the Theory and Applications of Electromechanical Phenomena in Crystals: Dover Publications, New York (revised edition), 822 p.
- Carabelli, Edmondo, 1961, Esplorazione geofisica: Boll. Com. Glac. Italiano, n. 9, II Serie, Parte Prima, p. 87-94.
- Carder, D. S., 1956, The seismograph and the seismograph station: U. S. Dept. of Commerce, Coast and Geodetic Survey, 24 p.
- Cassinis, R., and Carabelli, E., 1953, Misure sismiche di spessore del ghiaccio al ghiacciaio del Forni (Lombardia): Riv. Geofis. Appl., An. XIV, n. 2, p. 87-99.
- Christoffel, E. B., 1877, Ueber die Fortpflanzung von Stößen durch elastische feste Körper: Annali di Matematica pura ed applicata, Serie II, Tomo VIII, p. 193-243.
- Clarke, G. K. C., 1964, Geophysical measurements on the Kaskawulsh and Hubbard glaciers, Yukon Territory, Canada: Dept. of Physics, Univ. of Toronto, Canada (M. A. Thesis), 81 p.
- Denton, G. H., 1965, Late Pleistocene glacial chronology, northeastern St. Elias Mountains, Canada: Ph.D. Dissertation, Yale University.

- Denton, G. H., and Stuiver, M., 1966, Neoglacial chronology, northeastern St. Elias Mountains, Canada: Amer. J. Sci., v. 264, n. 8, p. 577-599.
- De Visintini, Guido, 1963, Rilievo sismico a riflessione sul ghiacciaio del Belvedere (Monte Rosa): Boll. Com. Glac. Italiano, n. 10, II Serie, Parte Prima, p. 65-70.
- Dewart, G., 1965, Preliminary report on the Kaskawulsh Glacier geophysical program, May-August, 1965: Icefield Ranges Research Program, Arctic Institute of North America, unpublished, 6 p.
- , 1966, Moulins on Kaskawulsh Glacier, Yukon Territory: J. Glaciol., v. 6, n. 44, p. 320-321.
- Dix, C. H., 1955, Seismic velocities from surface measurements: Geophysics, v. 20, n. 1, p. 68-86.
- Doell, R. R., 1963, Seismic depth study of the Salmon Glacier, British Columbia: J. Glaciol., v. 4, n. 34, p. 425-437.
- Dorsey, N. E., 1940, Properties of ordinary water-substance in all its phases: water-vapor, water, and all the ices: Amer. Chem. Soc. Monograph Series, Reinhold Pub. Corp., New York, 673 p.
- Förtsch, O., Schneider, H. J., and Vidal, H., 1955, Seismische Messungen auf dem Gepatsch- und Kesselwandferner in den Ötztaler Alpen: Gerlands Beiträge zur Geophysik, Bd. 64, Ht. 4, p. 233-261.
- and Vidal, H., 1956, Die Ergebnisse der seismischen Messungen auf dem Hintereisferner in den Ötztaler Alpen, 1954: Gerlands Beiträge zur Geophysik, Bd. 65, Ht. 2, p. 131-156.
- , 1958, Die seismische Vermessung des Grossen Gurgler Ferners in den Ötztaler Alpen im Spätsommer, 1956: Gerlands Beiträge zur Geophysik, Bd. 67, Ht. 1, p. 1-30.
- Gassaway, G. S., 1964, Method using ellipses to interpret seismic reflection data: Geophysics, v. 29, n. 6, p. 926-934.
- Glen, J. W., 1955, The creep of polycrystalline ice: Proc. Roy. Soc., Ser. A, v. 228, n. 1175, p. 519-538.
- , 1958, The mechanical properties of ice, I: The plastic properties of ice: Advances in Physics, v. 7, n. 26, p. 254-265.

- Gold, L. W., 1960, The cracking activity in ice during creep: Canadian J. Physics, v. 38, n. 9, p. 1137-1148.
- , 1963, Crack formation in ice plates by thermal shock: Canadian J. Physics, v. 41, n. 10, p. 1712-1728.
- Goldthwait, R. P., 1936, Seismic soundings on South Crillon and Kloooh glaciers: Geogr. J., v. 87, n. 6, p. 496-517.
- , 1966, Evidence from Alaskan glaciers of major climatic changes: Roy. Meteorol. Soc. Proceedings, International Symposium on World Climate from 8000 to 0 B.C., p. 40-53.
- Green, R. E., Jr., and Mackinnon, L., 1956, Determination of the elastic constants of ice single crystals by an ultrasonic pulse method: J. Acoust. Soc. America, v. 28, n. 6, p. 1292.
- Grew, E., and Mellor, M., 1966, High snowfields of the St. Elias Mountains, Yukon Territory, Canada: CRREL Tech. Rept. 177, 18 p.
- Griggs, D., 1939, Creep of rocks: J. Geol., v. 47, n. 3, p. 225-251.
- Gutenberg, B., and Richter, C. F., 1949, Seismicity of the earth and associated phenomena: Princeton Univ. Press, Princeton, N. J., 273 p.
- Hampton, L. D., 1964, Acoustic properties of sediments: Abstract of paper presented at 68th meeting, Acoustical Society of America, J. Acoust. Soc. America, v. 36, n. 10, p. 1993.
- Hansen, W. R., Eckel, E. B., Schaem, III, E., Lyle, R. E., George, W., and Chance, Genie, 1966, The Alaska earthquake, March 27, 1964: Field investigations and reconstruction effort: U. S. Geol. Survey Prof. Paper 541, 111 p.
- Hearmon, R. F. S., 1946, The elastic constants of anisotropic materials: Revs. Mod. Phys., v. 18, n. 1, p. 409-440.
- , 1956, The elastic constants of anisotropic materials, II: Advances in Physics, v. 5, n. 19, p. 323-382.
- Hoinkes, H., 1955, Measurements of ablation and heat balance on Alpine glaciers: J. Glaciol., v. 2, n. 17, p. 497-501.

- Holdsworth, G., 1965, An examination and analysis of the formation of transverse crevasses, Kaskawulsh Glacier, Yukon Territory, Canada: Inst. Polar Studies, The Ohio State Univ., Rept. 16, 91 p.
- Huntington, H. B., 1958, The Elastic Constants of Crystals: Academic Press, New York, 139 p.
- Jakosky, J. J., 1961, Exploration Geophysics: Trija Publ. Co., Newport Beach, Calif., 1195 p.
- Jeffreys, H., and Bullen, K. E., 1948, Seismological Tables: British Assn. for the Advancement of Sci., Gray-Milne Trust, 50 p.
- Jona, Von F., and Scherrer, P., 1952, Die elastischen Konstanten von Eis-Einkristallen: Helvetica Physica Acta, v. 25, Fasc. 1/2, p. 35-54.
- Jones, R., 1952, A method of studying the formation of cracks in a material subjected to stress: British J. Applied Physics, v. 3, p. 229-232.
- Jost, W., 1954, Études glaciologiques sur le Glacier Inferieur de l'Aar: Union Géodésique et Géophysique Internationale, Association Internationale d'Hydrologie Scientifique, Assemblée Générale de Rome, Tom 4, p. 351-355.
- Kamb, W. B., 1959a, Theory of preferred crystal orientation developed by crystallization under stress: J. Geol., v. 67, n. 2, p. 153-170.
- , 1959b, Ice petrofabric observations from Blue Glacier, Washington, in relation to theory and experiment: J. Geophys. Res., v. 64, n. 11, p. 1891-1909.
- , 1964, Glacier geophysics: Science, v. 146, n. 3642, p. 353-365.
- Kanasewich, E. R., 1963, Gravity measurements on the Athabaska Glacier, Alberta, Canada: J. Glaciol., v. 4, n. 35, p. 617-631.
- Keeler, C. M., 1964, Relationship between climate, ablation, and run-off on the Sverdrup Glacier, 1963, Devon Island, N.W.T.: Arctic Inst. of North America Res. Paper No. 27, 80 p.
- King, M. S., 1966, Wave velocities in rocks as a function of changes in overburden pressure and pore fluid saturants: Geophysics, v. 31, n. 1, p. 50-73.

- Kisslinger, C., Mateker, E. J., Jr., and McEvelly, T. V., 1961, SH motion from explosions in soil: J. Geophys. Res., v. 66, n. 10, p. 3487-3496.
- Knopoff, L., 1952, On Rayleigh wave velocities: Bull. Seismol. Soc. America, v. 42, n. 4, p. 307-308.
- and Gilbert, F., 1960, First motions from seismic sources: Bull. Seismol. Soc. America, v. 50, n. 1, p. 117-134.
- Kraut, E. A., 1963, Advances in the theory of anisotropic elastic wave propagation: Rev. Geophys., v. 1, n. 3, p. 401-448.
- Kravtsov, G. S., and Terent'eva, A. G., 1959, Rezul'tati seismicheskikh issledovaniy na visokogornikh lednikakh Tzentral'nogo Altaya v 1957 g.: Glyatziologicheskie Issledovaniya v Period M.G.G., IX Razdel Programmi M.G.G. (Glyatziologiya), n. 1, Izdat. Akad. Nauk SSSR, Moskva, p. 62-68.
- Kravtsov, G. S., 1960, Issledovanie uprugikh svoystv l'da visokogornikh gletcherov tzentral'nogo Altaya: Glyatziologicheskie Issledovaniya, IX Razdel Programmi M.G.G. (Glyatziologiya), n. 5, Izdat. Akad. Nauk SSSR, Moskva, p. 95-108.
- Krinsley, D. B., 1965, Pleistocene geology of the southwest Yukon Territory, Canada: J. Glaciol., v. 5, n. 40, p. 385-397.
- Lamb, Horace, 1945, Hydrodynamics: Dover Publications, New York, 738 p.
- Langway, C. C., Jr., 1958, Bubble pressures in Greenland glacier ice: Symposium of Chamonix, International Association of Scientific Hydrology, Pub. No. 47, p. 336-349.
- La Placa, S., and Post, B., 1960, Thermal expansion of ice: Acta Crystallographica, v. 13, pt. 6, p. 503-505.
- Lawrence, R. W., 1947, A scientific approach to the industrial application of shaped charges: Explosives Engineer, v. 25, p. 171-183.
- Love, A. E. H., 1944, A treatise on the mathematical theory of elasticity: Dover Publications, New York, 643 p.
- McCall, J. G., 1952, The internal structure of a cirque glacier: Report on studies of the englacial movements and temperatures: J. Glaciol., v. 2, n. 12, p. 122-130.

- Marcus, M. G., 1965a, Summer temperature relationships along a transect in the St. Elias Mountains, Alaska and Yukon Territory: Man and the Earth, Series in Earth Sciences, No. 3, Univ. of Colo. Studies, Univ. of Colo. Press, Boulder, p. 15-30.
- , 1965b, Icefield Ranges climatology program, St. Elias Mountains, 1964: Part 1: Data presentation: Arctic Inst. of North America Res. Paper 31-A, 109 p.
- , Rens, F., and Taylor, B. E., 1966, Icefield Ranges climatology program: 1965 data presentation and programming analysis: Arctic Inst. of North America Res. Paper 33, 111 p.
- Meier, M. F., Conel, J. E., Hoerni, J. A., Melbourne, W. G., Pings, C. J., Jr., and Walker, P. T., 1957, Preliminary study of crevasse formation: SIPRE Rept. 38, 80 p.
- Meier, Mark F., 1960, Mode of flow of Saskatchewan Glacier, Alberta, Canada: U. S. Geol. Survey Prof. Paper 351, 70 p.
- Mellor, M., 1964, Snow and ice on the earth's surface: CRREL Cold Reg. Sci. and Eng. Monograph, Part II, Sect. CI, 163 p.
- Miller, M. M., 1958, The role of diastrophism in the regimen of glaciers in the St. Elias district, Alaska: J. Glaciol., v. 3, n. 24, p. 292-297.
- Mothes, H., 1927, Seismische Dickenmessung von Gletschereis: Zeitschrift für Geophysik, Bd. 3, p. 121-134.
- Muller, J. E., 1967, Kluane Lake map-area, Yukon Territory: Geol. Survey Canada, Memoir 340, 137 p.
- Musgrave, M. J. P., 1959, The propagation of elastic waves in crystals and other anisotropic media: Rept. Prog. Phys., v. 22, p. 74-96.
- Nafe, J. E., 1957, Reflection and transmission coefficients at a solid-solid interface of high velocity contrast: Bull. Seismol. Soc. America, v. 47, n. 3, p. 205-219.
- Nicholls, H. R., 1961, In situ determination of the dynamic elastic constants of rock: U. S. Bur. Mines, Rept. Investigations 5888, 13 p.
- Nye, J. F., 1951, The flow of glaciers and ice sheets as a problem in plasticity: Proc. Roy. Soc., Ser. A, v. 207, p. 554-572.

- Nye, J. F., 1957, Physical properties of crystals, their representation by tensors and matrices: Clarendon Press, Oxford, 322 p.
- , 1959, The motion of ice sheets and glaciers: J. Glaciol., v. 3, n. 26, p. 493-507.
- Obert, L., and Duvall, W. I., 1945, The microseismic method of predicting rock failure in underground mining: U. S. Bur. Mines, Rept. Investigations 3803, 14 p.
- , 1957, Microseismic method of determining the stability of underground openings: U. S. Bur. Mines, Bull. 573, 18 p.
- , 1961, Seismic methods of detecting and delineating subsurface subsidence: U. S. Bur. Mines, Rept. Investigations 5882, 28 p.
- Oelsner, C., 1965 (pub. 1967), Seismoakustik, sine neue Messmethode für die Gletschermechanik: Polarforschung, Bd. 6, J. 35, Ht. 1/2, p. 19-26.
- Olhovich, V. A., 1964, The causes of noise in seismic reflection and refraction work: Geophysics, v. 29, n. 6, p. 1015-1030.
- Penny, A. H. A., 1948, A theoretical determination of the elastic constants of ice: Proc. Cambridge Phil. Soc., v. 44, p. 423-439.
- Pflueger, J. C., 1954, Delta-T formula for obtaining average seismic velocity to a dipping reflecting bed: Geophysics, v. 19, n. 2, p. 339-341.
- Phillips, F. C., 1949, An Introduction to Crystallography: Longmans, Green and Co., London, New York, Toronto, 302 p.
- Postma, G. W., 1955, Wave propagation in a stratified medium: Geophysics, v. 20, n. 4, p. 780-806.
- Poulter, T. C., 1950, The Poulter seismic method of geophysical exploration: Geophysics, v. 15, n. 2, p. 181-207.
- Pounder, E. R., 1965, The Physics of Ice: Pergamon Press, Oxford, 151 p.
- Redpath, B. B., 1965, Seismic investigations on glaciers on Axel Heiberg Island, Canadian Arctic Archipelago: Axel Heiberg Island Res. Rept., Geophysics, No. 1, McGill Univ., Montreal, 26 p.

- Renaud, A., and Mercanton, P. L., 1950, Les sondages sismiques de la Commission Helvétique des Glaciers: Publ. du Bureau Central Seismologique International, Serie A, Travaux Scientifiques, Fasc. 17, p. 66-78.
- Rigsby, G. P., 1951, Crystal fabric studies on Emmons Glacier, Mount Rainier, Washington: J. Geol., v. 59, n. 6, p. 590-598.
- , 1960, Crystal orientation in glacier and in experimentally deformed ice: J. Glaciol., v. 3, n. 27, p. 589-606.
- Riznichenko, Yu. V., 1949, O seismicheskoi kvazi-anizotropii: Izvestiya Akademii Nauk SSSR, Seriya Geograficheskaya i Geofizicheskaya, T. 13, n. 6, p. 518-544.
- Robin, G. De Q., 1958, Glaciology III: Seismic shooting and related investigations: Norwegian-British-Swedish Antarctic Expedition, 1949-1952, Scientific Results, v. V, Norsk Polarinstittutt, Oslo, 134 p.
- Robinson, E. S., 1964, Some aspects of subglacial geology and glacial mechanics between the South Pole and the Horlick Mountains: Univ. of Wisconsin Geophysical and Polar Research Center, Res. Rept. 64-7, 86 p.
- Röthlisberger, H., 1955, Studies in glacier physics on the Penny Ice Cap, Baffin Island, 1953. Part III: J. Glaciol., v. 2, n. 18, p. 539-552.
- , 1964, Reflection and transmission coefficients at the interface ice-solid: CREL Res. Rept. 110, 17 p.
- Rudzki, M. P., 1898, Von der Gestalt elastischen Wellen in Gesteinen: II. Studie aus der Theorie der Erdbeben: Gerlands Beiträge zur Geophysik, v. 3, p. 519-540.
- , 1911, Parametrische Darstellung der elastischen Welle in anisotropen Medien: Akademija Umiejtnosci, Krakow: Anzeiger der Akademie der Wissenschaften in Krakau, mathematisch-naturwissenschaftliche Klasse, Reihe A: mathematische Wissenschaften, p. 503-536.
- Russell, D. R., Jacobs, J. A., and Grant, F. S., 1960, Gravity measurements on the Salmon Glacier and adjoining snow field, British Columbia, Canada: Bull. Geol. Soc. America, v. 71, n. 8, p. 1223-1229.
- St. Amand, Pierre, 1957, Geological and geophysical synthesis of the tectonics of portions of British Columbia, the Yukon Territory, and Alaska: Bull. Geol. Soc. America, v. 68, n. 10, p. 1343-1370.

- Sander, Bruno, 1930, Gefüoekunde der Gesteine, mlt besonderer Berücksichtigung der Tektonik: Springer Verlag, Berlin, Vienna, 352 p.
- Sharp, R. P., 1951, Thermal regimen of firn on upper Seward Glacier, Yukon Territory, Canada: *J. Glaciol.*, v. 1, n. 9, p. 476-487.
- Shumekii, P. A., 1964, Principles of Structural Glaciology: Dover Publications, New York, 497 p.
- Simmons, G., and Brace, W. F., 1965, Comparison of static and dynamic measurements of compressibility of rocks: *J. Geophys. Res.*, v. 70, n. 22, p. 5649-5656.
- Slichter, L. B., 1932, The theory of the interpretation of seismic travel-time curves in horizontal structures: *Physics (J. of Applied Physics since 1937)*, v. 3, n. 6, p. 273-295.
- Stoneley, R., 1949, The seismological implications of aeolotropy in continental structure: *Mon. Not. Roy. Astr. Soc., Geophys. Sup.*, v. 5, n. 8, p. 222-232.
- Süsstrunk, A., 1951, Sondage du glacier par la méthode sismique: *La Houille Blanche, Numero Special A*, p. 309-317.
- Thomson, W. T., 1950, Transmission of elastic waves through a stratified solid medium: *J. Applied Physics*, v. 21, n. 2, p. 89-93.
- Thyssen, F., 1967, Die Temperaturabhängigkeit der P-Wellengeschwindigkeit in Gletschern und Inlandeisen: *Zeitschrift für Geophysik*, J. 33, Ht. 2, p. 65-79.
- Tobin, D. G., and Sykes, L. R., 1966, Relationship of hypocenters of earthquakes to the geology of Alaska: *J. Geophys. Res.*, v. 71, n. 6, p. 1659-1667.
- Tocher, Don, 1957, Anisotropy in rocks under simple compression: *Trans. Amer. Geophys. Union*, v. 38, n. 1, p. 89-94.
- Turner, F. J., and Weiss, L. E., 1963, Structural analysis of metamorphic tactionites: McGraw-Hill, New York, 545 p.
- Tushinskii, G. K., 1960, Moshchnost' l'dov El'brusa: *El'brusskaya ekspeditziya Moskovskogo Gosudarstvennogo Universiteta i Institute Prikladnoi Geofizika Akademii Nauk SSSR*, G. K. Tushinskii, Red., Informatzionii Sbornik o Rabotakh po M. G. G., n. 5, p. 6-9.

- Uhrig, L. F., and Van Malla, F. A., 1955, Velocity anisotropy in stratified media: *Geophysics*, v. 20, n. 4, p. 774-779.
- Untersteiner, N., 1955, Some observations on the banding of glacier ice: *J. Glaciol.*, v. 2, n. 17, p. 502-506.
- Voigt, Waldemar, 1928, Lehrbuch der Krlatallphyslk (mit Ausschluss der Kristalloptik): B. G. Teubner, Leipzig, 978 p.
- Walsh, J. B., and Brace, W. F., 1966, Elasticity of rock: a review of some recent theoretical studies: *Rock Mechanics and Engineering Geology*, v. 4, n. 4, p. 283-297.
- Weertman, J., 1957, On the sliding of glaciers: *J. Glaciol.*, v. 3, n. 21, p. 33-38.
- , 1964, The theory of glacier sliding: *J. Glaciol.*, v. 5, n. 39, p. 287-303.
- Westphal, J. A., 1965, In situ acoustic attenuation measurements in glacial ice: *J. Geophys. Res.*, v. 70, n. 8, p. 1849-1853.
- Wheeler, J. O., 1963, Kaskawulsh map-area, Yukon Territory: *Geol. Survey Canada, Map 1134A*.
- White, J. E., and Sengbush, R. L., 1963, Shear waves from explosive sources: *Geophysics*, v. 28, n. 6, p. 1001-1019.
- Wood, F. J., 1966, editor, *The Prince William Sound, Alaska, earthquake of 1964 and aftershocks, Vol. 1.*, U. S. Dept. of Commerce, Coast and Geodetic Survey Publication 10-3, 263 p.